

**Spectroscopic Studies of
Peptidylglycine α -Hydroxylating Monooxygenase.
Toward a Mechanism of Superoxide Channeling**

Shulamit Jaron

B.S., University of Rhode Island, 1994

A dissertation submitted to the faculty of the
OGI School of Science & Engineering
Oregon Health & Science University
in partial fulfillment of the requirements for the degree of
Doctor of Philosophy
in
Biochemistry and Molecular Biology

September 2001

The dissertation "Spectroscopic Studies of Peptidylglycine α -Hydroxylating Monooxygenase: Toward a Mechanism of Superoxide Channeling" by Shulamit Jaron has been examined and approved by the following Examination Committee:

Ninian J. Blackburn, Advisor
Professor

Thomas M. Loehr
Professor

James W. Whittaker
Associate Professor

Svetlana Lutsenko
Assistant Professor
Oregon Health Sciences University

ACKNOWLEDGMENTS

I would like to express my sincere thanks to my dissertation advisor, Professor Ninian J. Blackburn. Ninian always trusted in my ability to organize and direct my own research. He provided guidance at key decision-making points while allowing me to discover how to conduct independent science. He always believed in my results and was willing to listen to and defend my "crazy" ideas. I found that his enthusiasm for new approaches and ideas instilled the excitement and confidence in me needed to accomplish my goals.

I also wish to thank my other dissertation committee members, Professors Thomas Loehr, Jim Whittaker, and Svetlana Lutsenko. Dr. Loehr's amazing teaching skills and cheerful disposition created a comfortable learning atmosphere within the department. He is one of the few instructors I've had who is able to excite his students about any subject. My respect for Dr. Whittaker's immense knowledge pushed me to always work hard. And I especially want to thank Dr. Lutsenko, who helped improve the quality of a dissertation in which she was not vested.

Additionally, I would like to thank all my friends at OGI — Martina, Heather Y., Ash, Jay S., Frank R., Jonathan C., Ameer, Illa, Garnet, and Anna, for making graduate school, and OGI especially, a tolerable experience. I still think it is incredible that such a small institution can attract such intelligent, kind, and fun people.

Finally, I would like to express my deepest gratitude to Corey Cartwright for providing the support, friendship, and love I needed to make it through these crazy years with my mind intact.

This dissertation is dedicated to my parents, Dr. Linda Hufnagel and Dr. Dov Jaron, who have always been my most important role models.

TABLE OF CONTENTS

ACKNOWLEDGMENTS	iii
TABLE OF CONTENTS	iv
LIST OF TABLES	ix
LIST OF FIGURES	xi
LIST OF SCHEMES	xiv
ABSTRACT	xv
CHAPTER 1 INTRODUCTION	1
1.1 The Chemistry of Oxygen and Oxygen Activation by Copper-Containing Enzymes	1
1.1.1 Oxygen Chemistry	1
1.1.2 Cu_nO_2 Complexes	6
1.1.3 Copper Monooxygenases	7
1.1.4 Copper Dioxygenases and Multicopper Oxidases	9
1.2 Electron Transfer	10
1.3 Peptide Amidation	11
1.3.1 Peptidyl α -Amidating Monooxygenase (PAM)	12
1.3.2 Peptidylhydroxyglycine α -Amidating Lyase (PAL)	14
1.3.3 Peptidylglycine α -Hydroxylating Monooxygenase (PHM)	16
1.4 Physical Methods for Studying Copper Centers	26
1.4.1 Atomic Absorption Spectroscopy	26
1.4.2 Ultraviolet and Visible Spectroscopy (UV-vis)	26
1.4.3 Infrared Spectroscopy	27
1.4.4 X-ray Absorption Spectroscopy	31

CHAPTER 2 DOES SUPEROXIDE CHANNEL BETWEEN THE COPPER	
CENTERS IN PEPTIDYLGLYCINE MONOOXYGENASE? A NEW	
MECHANISM BASED ON CARBON MONOXIDE REACTIVITY	
	39
2.1	Introduction 39
2.2	Experimental Procedures 43
2.2.1	Preparation of Medium for Cell Culture 43
2.2.2	Cell Lines and Cell Growth 44
2.2.3	Enzyme Isolation 45
2.2.4	PHM Mutants 45
2.2.5	Copper Reconstitution 45
2.2.6	Copper and Protein Concentration 46
2.2.7	Activity Measurements 46
2.2.8	Measurement of CO Binding Stoichiometry 47
2.2.9	CO Binding to PHM in the Presence of Substrate 48
2.2.10	Isotope Shifts and Reversibility of CO Binding 48
2.2.11	Titration of PHM with N-AcYVG and Subsequent Carbonylation . . 49
2.2.12	IR Spectroscopy 49
2.2.13	X-ray Absorption (XAS) Data Collection and Analysis 50
2.3	Results 51
2.3.1	Stoichiometry of CO Binding to Wild-Type PHM 51
2.3.2	Infrared Analysis of CO Binding to wtPHM 51
2.3.3	¹³ CO Isotope Binding Data 55
2.3.4	Copper Binding, CO Stoichiometry, and Infrared Spectroscopy of the H242A Mutant 55
2.3.5	XAS of PHM-CO 56
2.3.6	CO Binding to PHMcc in the Presence of Substrate 59
2.3.7	Infrared Spectra and Isotope Shifts for CO Binding to PHMcc in the Presence of Substrate 61
2.4	Discussion 61

CHAPTER 3 CHARACTERIZATION OF A HALF-APO DERIVATIVE OF	
PEPTIDYLGLYCINE MONOOXYGENASE. INSIGHT INTO THE	
REACTIVITY OF EACH ACTIVE SITE COPPER 72	
3.1	Introduction 72
3.2	Experimental Procedures 76
3.2.1	Purification of Native PHM 76
3.2.2	Determination of Copper and Protein Concentration 76
3.2.3	Synthesis of the Half-Apo PHM Derivative 76
3.2.4	Measurement of CO Stoichiometry 77
3.2.5	Infrared Spectroscopy of Protein Samples 78
3.2.6	XAS Data Collection and Analysis 78
3.2.7	Activity Measurements and Substrate Turnover 79
3.3	Results 80
3.3.1	Stoichiometry of Copper Binding to Half-Apo PHM 80
3.3.2	Oxygen Activity and Turnover by Half-Apo PHM 80
3.3.3	EXAFS Spectroscopy of Half-Apo PHM and Half-Apo PHM in the Presence of Bound YVG Substrate 82
3.3.4	Stoichiometry of CO Binding to Copper in Half-Apo PHM 88
3.3.5	Infrared Spectroscopy of Half-Apo PHM-CO 88
3.3.6	Infrared Spectroscopy of PHM-YVG-CO 91
3.3.7	EXAFS Spectroscopy of Half-Apo PHM-CO 91
3.4	Discussion
3.4.1	Characterization of the Half-Apo Cu _M -Carbonyl Complex 94
3.4.2	Changes in the Active Site Caused by Substrate Binding 97
 CHAPTER 4 INFRARED AND EXAFS CHARACTERIZATION OF THE	
H172A MUTANT OF PEPTIDYLGLYCINE α-HYDROXYLATING	
MONOOXYGENASE 100	
4.1	Introduction 100
4.2	Experimental Procedures 103
4.2.1	Purification of the Mutant Enzyme 103

4.2.2	Calculation of Copper and Protein Concentrations	105
4.2.3	Specific Activity Measurements	105
4.2.4	HPLC Analysis	106
4.2.5	CO Binding	106
4.2.6	FTIR Analysis	107
4.2.7	X-ray Absorption (XAS) Data Collection and Analysis	107
4.3	Results	107
4.3.1	Copper Binding Stoichiometry	107
4.3.2	Steady-State Activity of H172A and Lack of Rescue by Imidazole	109
4.3.3	FTIR Spectroscopy of CO Binding to H172A With and Without Bound YVG	109
4.3.4	X-ray Absorption Spectroscopy	112
4.4	Discussion	119
4.4.1	Oxidized Enzyme	122
4.4.2	Reduced Enzyme	123
4.4.3	Ligand Binding to H172A	123

**CHAPTER 5 pH-DEPENDANT STRUCTURAL CHANGES OF THE
ACTIVE SITE IN PEPTIDYLGLYCINE α -HYDROXYLATING**

	MONOOXYGENASE (PHM)	128
5.1	Introduction	128
5.2	Experimental Procedures	130
5.2.1	Enzyme Isolation	130
5.2.2	X-ray Absorption Spectroscopy	131
5.3	Results	131
5.3.1	Oxidized PHMcc, pH 9.0	131
5.3.2	Reduced PHMcc, pH 9.0	131
5.3.3	Oxidized PHMcc With and Without Bound Substrate, pH 5.5 . . .	134
5.3.4	Reduced PHMcc With and Without Bound Substrate, pH 5.5 . . .	139
5.3.5	X-ray Absorption Edge	142

5.4	Discussion	146
5.4.1	Structural Dependence on pH	146
5.4.2	Coordination of a New Ligand at Low pH in the Reduced Enzyme	147
5.4.3	Dependence of Methionine Coordination on pH and Peptidylgly Substrate Binding	148
CHAPTER 6 FUTURE DIRECTIONS		149
6.1	Dioxygen Binding at Cu _H	149
6.2	Superoxide Channeling	150
6.2.1	Inhibition by Superoxide Dismutase	150
6.2.2	Addition of Superoxide	150
6.2.3	Spin Trapping Superoxide	151
6.2.4	Freeze Trapping Cu _H -Superoxide Intermediate	151
6.3	Identifying Residues Involved in Superoxide Channeling	151
6.4	NMR Solution Structures	152
LITERATURE CITED		153
BIOGRAPHICAL SKETCH		168

LIST OF TABLES

1.1	Oxidase and Oxygenase Reactions of Many Iron- and Copper-Containing Enzymes	3
2.1	Stoichiometry of Carbon Monoxide Binding to Reduced PHMcc	52
2.2	Infrared Frequencies and Isotope Shifts for Carbonyl Complexes of PHMcc and Other Copper Proteins	54
2.3	Parameters Used to Simulate the EXAFS and Fourier Transform of Reduced Carbonylated PHMcc (PHM-CO)	58
2.4	Stoichiometry of Carbon Monoxide Binding to wtPHMcc in the Presence of the Peptide Substrate N-AcYVG	60
3.1	Copper-to-Protein Stoichiometry of Eight Individual Preparations of Half-Apo PHM and Their Average	81
3.2	First Shell EXAFS Fitting Parameters for a Number of Different Preparations of Half-Apo PHM and Their Derivatives with Bound Substrate and CO	85
3.3	Stoichiometry of CO Binding to Five Individual Preparations of Half-Apo PHM and Their Average	89
4.1	Copper-to-Protein Stoichiometry for Five Independent Preparations of H172A PHMcc	108
4.2	XAS Refinement Results for Oxidized H172A Using EXCURVE 98	114
4.3	Parameters Used to Simulate the EXAFS and Fourier Transform of Reduced H172A	117
4.4	Copper-Carbonyl Infrared Stretching Frequencies for Proteins That Have Tris-Histidine Ligation	125
5.1	EXAFS Parameters for Oxidized and Reduced PHMcc at pH 9.0	133
5.2	EXAFS Parameters of Oxidized PHMcc at pH 5.5	136

5.3	EXAFS Parameters of Oxidized PHMcc with Bound YVG at pH 5.5 . . .	138
5.4	EXAFS Parameters of Reduced PHMcc at pH 5.5	141
5.5	EXAFS Parameters of Reduced PHMcc with Bound YVG at pH 5.5 . . .	144

LIST OF FIGURES

1.1	The two enzymatic steps involved in the amidation of peptide hormones are shown with their respective cofactors	15
1.2	Electron paramagnetic resonance spectra of the bifunctional enzyme PAM	17
1.3	The enzymatic mechanism of PHM	20
1.4	Detailed mechanism proposed for PHM	21
1.5	A representation of the two-domain structure of PHM, as derived from the X-ray crystal structure	22
1.6	The X-ray crystallographic active site	24
1.7	Schematic representation of an infrared spectrometer	30
1.8	Representative Cu(I) K-edge X-ray absorption spectrum	32
1.9	Outgoing and backscattered portions of final-state wave function	33
1.10	Basic storage ring setup	35
1.11	Typical experimental station setup	37
1.12	Each peak in the EXAFS FT spectrum represents a single scattering radius in the sample	38
2.1	Ribbon diagram for the PHMcc crystal structure showing the position of the catalytic copper centers and important active site residues	41
2.2	Fourier transform infrared spectra of the complexes formed in the reaction of carbon monoxide with reduced PHMcc and a H242A site-directed mutant	53
2.3	Fourier transform and EXAFS of reduced wtPHMcc reacted with carbon monoxide	57

2.4	Fourier transform infrared spectra of the complexes formed in the reaction of carbon monoxide with reduced PHMcc in the presence of substrates	62
2.5	Titration of the PHM-CO complex with increasing amounts of N-AcYVG substrate	63
2.6	A proposed mechanism for superoxide channeling between the two copper centers of PHMcc	70
3.1	Overall reaction scheme of the bifunctional enzyme peptidylglycine α -amidase (PAM) broken down into its two constituent activities	74
3.2	HPLC separation of the dansylated substrate d-YVG from product d-YVG-OH following PHM turnover	83
3.3	Experimental and simulated FT and EXAFS for the sample S1199 of half-apo PHM	86
3.4	Experimental and simulated FT and EXAFS for the sample S200 of half-apo PHM treated with 2 equiv per Cu of peptide substrate YVG	87
3.5	Infrared spectra of the carbonylated half-apo enzyme	90
3.6	Infrared spectrum of the carbonylated half-apo enzyme with bound YVG	92
3.7	Experimental and simulated FT and EXAFS for the sample 9500 of half-apo PHM-CO	93
4.1	HPLC separation of the dansylated substrate from product	110
4.2	Infrared spectra of the carbonyl stretching region for copper-carbonyls	111
4.3	EXAFS spectrum and Fourier transform of oxidized H172A	113
4.4	EXAFS spectrum and Fourier transform of reduced H172A	116
4.5	EXAFS spectrum and Fourier transforms of reduced wild-type PHM versus reduced H172A	118
4.6	XANES pre-edge data for H172A and wild-type PHM	120
5.1	X-ray absorption spectra of PHMcc at pH 9.0 collected on BL 7.3	132
5.2	X-ray absorption spectra of oxidized PHMcc at pH 5.5 collected on BL 7.3	135

5.3	X-ray absorption spectra of oxidized PHMcc with bound YVG at pH 5.5 collected on BL 7.3	137
5.4	X-ray absorption spectra of reduced PHMcc at pH 5.5 collected on BL 7.3	140
5.5	X-ray absorption spectra of reduced PHMcc with bound YVG at pH 5.5 collected on BL 9.3	143
5.6	X-ray absorption near edge structure (XANES) of reduced PHMcc at three different pHs	145

LIST OF SCHEMES

4.1	The amidating reaction of peptidyl α -amidating monooxygenase (PAM)	101
4.2	Proposed reaction mechanism for channeling of superoxide between the two coppers in PHM	104
4.3	Proposed proton donation by His172 to bound superoxide, following oxidation of Cu_H	127

ABSTRACT

Spectroscopic Studies of Peptidylglycine α -Hydroxylating Monooxygenase. Toward a Mechanism of Superoxide Channeling

Shulamit Jaron, B.S.

Ph.D., OGI School of Science & Engineering

September 2001

Thesis Advisor: Dr. Ninian J. Blackburn

This dissertation describes the structural characterization of peptidylglycine monooxygenase (PHM). PHM belongs to a unique class of enzymes: the mononuclear dicopper monooxygenases. By investigating the structure and chemistry of oxygen binding to the copper sites in PHM and its active site mutants, we hope to gain an understanding of the mechanism of oxygen activation and electron transfer within this enzyme class.

The present work has used CO to probe the chemistry of dioxygen interaction with the copper centers of PHMcc. The results indicate a stoichiometry of 0.5 CO per Cu and a single band in the FTIR spectrum ($\nu(\text{CO}) = 2093 \text{ cm}^{-1}$). Binding of CO to wild-type PHMcc causes a $0.10 \pm 0.02 \text{ \AA}$ increase in the Cu-S(Met) bond length, which is consistent with replacement of a weakly coordinating solvent by a strong field ligand such as CO at the Cu_M center. When 1 equivalent of N-AcYVG is added to the CO binding assay, the CO:Cu ratio increases towards 1 (average of 0.85), and a second FTIR band appears at 2062 cm^{-1} . The discovery that substrate binding turns on CO- and (by inference) O_2 -binding activity at a second copper center

in PHM has allowed us to suggest a completely new mechanism for oxygen activation and formation of the reactive peroxo intermediate. This mechanism was further investigated by the characterization of both a half-apo derivative (Cu_H deleted) and a carefully selected site-directed mutant (H172A). These enzymes assigned the Cu_M -CO stretching frequency as 2093 cm^{-1} and the Cu_H -CO stretching frequency as $2062\text{--}2075\text{ cm}^{-1}$. The infrared frequency of the CO ligand bound at Cu_M (2093 cm^{-1}) is unaffected by substrate binding, whereas $\nu(\text{CO})$ for the substrate-induced Cu_H -CO complex is extremely sensitive to the nature of the substrate (hippuric acid, 2075 cm^{-1} ; N-AcYVG, 2062 cm^{-1}).

The positions of two active site residues, Met314 and His172, appeared to independently depend on the oxidation state of the copper sites. Two positions were found for each residue: one “copper-on” and one “copper-off”. The “copper-off” position was disordered for both residues at pH 7 but became more structured upon lowering the pH. The full details of these results and their implications in the mechanism of PHM are described.

CHAPTER 1

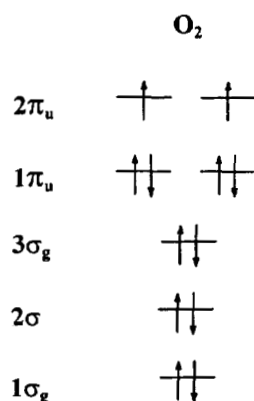
INTRODUCTION

1.1 THE CHEMISTRY OF OXYGEN AND OXYGEN ACTIVATION BY COPPER-CONTAINING ENZYMES

1.1.1 Oxygen Chemistry

Molecular oxygen, utilized for energy by many organisms, is an ideal terminal oxidant. (1) Dioxygen has a high oxidizing potential, which means that its reduction creates a large amount of energy making it available to an organism. (2) The high oxidizing potential of O_2 limits the number and types of reactions that dioxygen takes part in, thus restricting indiscriminant oxidation. (3) Reduction of dioxygen is fairly harmless to the cell because it produces carbon dioxide and water, both innocuous products that are neutral and unreactive [Ingraham and Meyer, 1985].

Dioxygen has a triplet ground state, $^3\Sigma_g^-$. Most organic molecules are singlets, such that reaction with O_2 is a "spin-forbidden" process.



The addition of a single electron to form either $O_2^{\cdot-}$ or HOOH reduces the oxidation barrier because it creates a species that is highly reactive. However, the single electron transfer to oxygen requires a reducing agent that exceeds an

$E^0 = -0.33$ V (at pH 14) to achieve a significant reaction rate. This kinetic barrier results from the triplet ground state of dioxygen and the fact that the lowest orbital available to accept an electron is an antibonding orbital. Therefore, if dioxygen is to be used as a terminal oxidant in biological systems, it must first be activated.

In biological systems, activation of dioxygen is typically accomplished by forming an oxygen complex with a transition metal. Bonding in the metal- O_2 complex involves sigma donation of two O_2 lone pair electrons and back-donation to the π^* orbitals of oxygen from the d_{xz} or d_{yz} orbitals of the metal. Large back-donation of electrons makes the antibonding π -orbitals more like electron pairs. This eliminates the barrier to adding the first electron to dioxygen and relieves the restrictions resulting from its triplet state. Such back-donation of π -electrons into π^* orbitals of dioxygen in the metal-dioxygen complexes weakens and lengthens the O-O bond. Transition metals, such as heme iron, nonheme iron, molybdenum, and copper, are responsible for dioxygen reduction (oxidase activity) and activation for incorporation into a substrate (oxygenase activity). Oxidases reduce dioxygen by either two or four electrons to hydroperoxide or water while oxygenases incorporate either one (monooxygenase) or two (dioxygenase) atoms of oxygen into their substrates. Table 1.1 provides a list of many of the oxidase and oxygenase reactions, the metal utilized to activate dioxygen, and the reaction catalyzed. While there is a large literature on the activation of dioxygen by iron-containing enzymes, the focus of the remainder of Section 1.1 will be on dioxygen activation by copper.

Copper enzymes historically have been classified into three categories, based mainly on their spectroscopy:

Type 1 or "blue copper" enzymes were so named because of their intense blue color, which results from a strong absorption at ~ 600 nm. The frequency of the absorption is due to copper-cysteinate ligation, while the asymmetry of the site creates the intensity. This type of copper also has a band at 450 nm and shows an electron paramagnetic resonance signal. Most are known to possess a high redox potential (0.3–0.8 V) and small electron paramagnetic resonance (EPR) hyperfine splitting. Blue copper centers are usually associated with electron carriers and multicopper oxidases. Examples are azurin and the type 1 site in ascorbic acid oxidase.

Table 1.1
Oxidase and Oxygenase Reactions
of Many Iron- and Copper-Containing Enzymes

Enzyme Type	Reaction Type	Representative Enzyme ^b		Catalytic Reaction ^c	
<i>mononuclear non-heme iron enzymes</i>					
intramolecular dioxygenase	intradiol dioxygenation	protocatechuate 3,4-dioxygenase (PCD) ^d		$\xrightarrow[O_2]{3,4\text{-PCD (Fe}^{III}\text{)}}$	
	extradiol dioxygenation	catechol 2,3-dioxygenase (CTD) ^e		$\xrightarrow[O_2]{2,3\text{-CTD (Fe}^{II}\text{)}}$	
	hydroperoxidation	lipoxygenases (LO) ^f		$\xrightarrow[O_2]{LO (Fe^{III})}$	
	cis-hydroxylation	phthalate dioxygenase (PDO) ^{g,s}		$\xrightarrow[O_2, NADH \rightarrow NAD^+]{PDO (Fe^{II} + \text{Rieske})}$	
external monooxygenase	hydroxylation	ω -hydroxylase (ω H) ^t	RCH_3	$\xrightarrow[O_2, 2Rd_{red} \rightarrow H_2O, 2Rd_{ox}]{\omega H (Fe^{II})}$	RCH_2OH
intermolecular dioxygenase	pterin-dependent hydroxylation	phenylalanine hydroxylase (PAH) ^{h,i}		$\xrightarrow[O_2, H_4\text{biopterin} \rightarrow H_2O, H_2\text{biopterin}]{PAH (Fe^{II})}$	
	α -ketoglutarate-dependent hydroxylation	clavaminic synthase (CS) ^j		$\xrightarrow[O_2, \alpha\text{-KG} \rightarrow CO_2, \text{succinate}]{CS (Fe^{II})}$	
oxidase	α -ketoglutarate-dependent 4e ⁻ oxidation	clavaminic synthase		$\xrightarrow[O_2, \alpha\text{-KG} \rightarrow H_2O, CO_2, \text{succinate}]{CS (Fe^{II})}$	
	4 e ⁻ oxidation	isopenicillin N-synthase (IPNS) ^k		$\xrightarrow[O_2, 2H_2O]{IPNS (Fe^{II})}$	
	H ⁺ abstraction	bleomycin (BLM) ^k		$\xrightarrow[O_1, e^-]{BLM (Fe^{II})}$	
<i>binuclear non-heme iron enzymes</i>					
external monooxygenase	hydroxylation	methane monooxygenase (MMO) ^l	CH_4	$\xrightarrow[O_2, NADH \rightarrow H_2O, NAD^+]{MMO (Fe^{II}Fe^{II})}$	CH_3OH
oxidase	4 x 1e ⁻ oxidation/ 4e ⁻ reduction of O ₂	ribonucleotide diphosphate reductase (RDPR) ^m		$\xrightarrow[O_2, e^- \rightarrow 2H_2O]{RDPR (Fe^{II}Fe^{II})}$	
	2e ⁻ oxidation	Δ^9 desaturase (Δ^9) ⁿ		$\xrightarrow[O_2, AH_2 \rightarrow 2H_2O, A]{\Delta^9 D (Fe^{II}Fe^{II})}$	

Enzyme Type	Reaction Type	Representative Enzyme ^b	Catalytic Reaction ^c
mononuclear copper enzymes^l			
oxidase	2e ⁻ oxidation/ 2e ⁻ reduction of O ₂	amine oxidase (AmO) ✓	
		galactose oxidase (GO) ✓	
reductase	1e ⁻ oxidation of PsAz/ 1e ⁻ reduction of NO ₂ ⁻	nitrite reductase (NiR) ✓	
uncoupled binuclear copper enzymes			
external monooxygenase	hydroxylation	dopamine β-hydroxylase (DBH)	
		peptidylglycine α-hydroxylating monooxygenase (PHM) ^m	
internal monooxygenase	hydroxylation & 2e ⁻ oxidation	tyrosinase	
		trinuclear copper enzymes	
oxidase	4 x 1e ⁻ oxidation/ 4e ⁻ reduction of O ₂	ascorbate oxidase (AO) ✓	
		ceruloplasmin (CEP) ⁿ ✓	
		laccase (LC)	
external monooxygenase	hydroxylation	copper methane monooxygenase (MMO) ^o	
copper-heme enzymes			
oxidase	4 x 1e ⁻ oxdn of cyt c/ 4e ⁻ redn of O ₂	cytochrome c oxidase ✓	

Originally published as Table 12 in:

Holm, R. H., Kennepohl, P., and Solomon, E. I. (1996) Structural and functional aspects of metal sites in biology. *Chem. Rev.* **96**, 2239-2314.

Used here with permission of the American Chemical Society.

Type 2 or “nonblue copper” (sometimes called “normal” copper) enzymes have a weak absorption in the visible region, between 600 and 700 nm, and carry out O₂ reduction or redox chemistry at these sites. Normal copper proteins possess normal extinction coefficients and EPR parameters, and their coordination geometry is usually square planar. The redox behavior of the copper is variable between enzymes. Examples are DβM, the colorless anion binding site in multicopper oxidases, galactose oxidase, amine oxidases, and superoxide dismutase.

Type 3 or “silent copper” enzymes possess a dinuclear copper center, where the coppers are close enough to be spin-paired and hence have no EPR signal. An absorption band at 330 nm is usually associated with the type 3 centers. As in the type 2 enzymes, the redox behavior of the type 3 copper center varies between enzymes. These enzymes are represented by any coupled dinuclear center, such as in hemocyanin and tyrosinase, which can take part in both dioxygen transport and activation [Jameson, 1981].

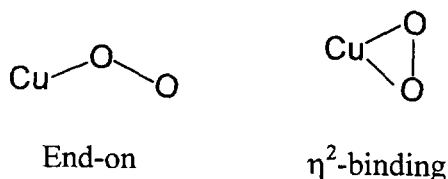
The activation of dioxygen by a copper enzyme is highly dependent on the identity and structural geometry of the protein residues ligating the copper. In general, the rate of oxidation of the copper complex increases as the redox potential of the Cu(II)/Cu(I) couple decreases. For example, complexes with π-acceptor ligands are much less reactive than complexes with O-donor group ligands [Zuberbuhler, 1983]. This is because the more basic a ligand, the higher the electron density at the central atom, making electron transfer to O₂ easier. The reactivity of a Cu(I) complex with O₂ is also dependent on steric factors, such that easy transition to a “cupric-like” state is important for biological reactivity. Even the most basic ligands will form inert complexes if the steric factors create a complex that is inaccessible to O₂ binding [Zuberbuhler, 1983].

These notions have been emphasized through the structural and spectroscopic characterization of copper–oxygen adducts.

1.1.2 Cu_nO_2 Complexes

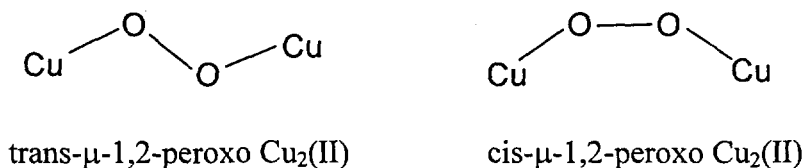
There are two basic types of copper sites which activate dioxygen for insertion into a substrate: mononuclear and dinuclear. Binding of dioxygen at each of these copper sites happens in a few very specific arrangements.

Mononuclear CuO_2 complexes show either end-on or η^2 -binding, as shown below.

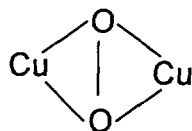


Formation of the $\text{Cu}-\text{O}_2$ adduct causes the activation of the dioxygen by the donation of one electron from copper to oxygen, forming a Cu(II) -superoxo species. The formation of superoxide, however, is restricted by the low redox potential of the $\text{O}_2/\text{O}_2^{\cdot-}$ couple (-0.33 V) [Zuberbuhler, 1983]. This limitation can be overcome if this complex reacts readily with another copper(I) ion to form a μ -peroxo dinuclear copper(II) complex.

Dinuclear Cu_2O_2 complexes bind O_2 between both copper atoms, which avoids the formation of free $\text{O}_2^{\cdot-}$. Each type of dinuclear complex is also easily distinguishable from each other, based on their absorption spectroscopy. The μ -1,2-peroxo dicopper(II) complex has an intense purple color with strong UV-vis absorptions at 440, 525, and 590 nm and an additional d-d band at 1035 nm [Jacobson et al., 1988; Karlin et al., 1987; Pate et al., 1987].



The side-on μ - η^2 : η^2 -peroxo dicopper(II) complex absorbs at 349 and 551 nm and has a particularly low value of the O-O stretch at 741 cm^{-1} (resonance Raman). Spectroscopy of oxyhemocyanin matches these values, suggesting this type of structure for oxygen binding [Kitajima et al., 1989].



$\mu\text{-}\eta^2\text{:}\eta^2\text{-Peroxo Cu}_2(\text{II})$

There are also other Cu_2O_2 complexes, which show spectroscopy that does not match with the above structures. The exact structure of these complexes is not yet identified [Solomon et al., 1993].

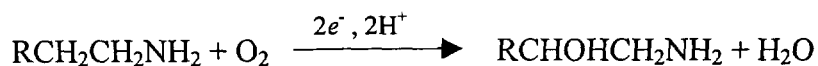
1.1.3 Copper Monooxygenases

Copper oxygenases are responsible for incorporating one atom of oxygen from molecular oxygen into a peptide product. These enzymes incorporate either one or two atoms of oxygen and are therefore known as either monooxygenases or dioxygenases, respectively [Ingraham and Meyer, 1985]. Only four types of prosthetic groups are associated with monooxygenases: copper, nonheme iron, heme iron, and flavin. This section will focus on the structure of and oxygen activation by copper monooxygenases.

1.1.3.1 Tyrosinase. Tyrosinase (Ty, EC 1.14.18.1) reversibly binds dioxygen at a type 3 copper site, which is similar in structure (although not in function) to the active site of hemocyanin, an O_2 carrier. Activation of O_2 by this enzyme occurs via the bridging of dioxygen between two coppers in a coupled binuclear metal active site. Ty is responsible for the conversion of monophenols to *o*-diphenols and diphenols to *o*-quinones by incorporating one atom of oxygen derived from O_2 into the phenolic substrate [Solomon et al., 1996]. This activity occurs in the pathway for the production of melanin pigment in both plant and animal cells. In mammals, Ty is found specifically in melanocytes. The active site of the resting enzyme consists of two cupric centers that are antiferromagnetically coupled. Oxytyrosinase is produced by the reduction of the resting form, followed by the binding of O_2 . In deoxy-Ty-Cu(I), the two copper atoms are about 3.5 Å apart, and each is coordinated by the N_ϵ atoms of three histidine residues [Woolery et al., 1984;

Longa et al., 1996]. Binding and activation of O₂ occurs via electron transfer from both Cu(I) ions to dioxygen, resulting in a bound peroxide dianion which bridges the two coppers as a μ -peroxo. This copper bridge exhibits an intense absorption band at 350 nm [Eickman et al., 1979], which is indicative of a very strong σ -donor ligand to the coppers. There is also an exceedingly low O–O stretching frequency of 750 cm⁻¹ [Freedman et al., 1976] that indicates an extremely weak O–O bond, due to the shift in electron density into the σ^* orbital of the peroxide, which activates the O₂ for cleavage [Ross and Solomon, 1991].

1.1.3.2 Dopamine- β -monooxygenase. A second copper monooxygenase, dopamine β -hydroxylase (D β H, EC 1.14.17.1), activates O₂ at a mononuclear copper site as an end-on Cu–O₂-bound species. D β H is responsible for the stereospecific hydroxylation of dopamine, creating norepinephrine, which is part of the metabolic pathway producing epinephrine from tyrosine (tyrosine to dopa to dopamine to norepinephrine to epinephrine) [Stewart and Klinman, 1988].



The active site of the enzyme is composed of two coppers that are redox active [Ash et al., 1984; Stewart and Klinman, 1988] and found to be typical “type 2” copper centers in EPR studies [Walker et al., 1977; Abudu et al., 1998]. The two coppers are thought to be mononuclear [Blackburn et al., 1988] and chemically inequivalent with only one copper available for small molecule binding [Blackburn et al., 1990; Pettingill et al., 1991; Reedy and Blackburn, 1994]. Based on this evidence, it was suggested that one copper site, Cu_M, acts as the O₂ binding site while the other copper, Cu_H, is an electron transfer site [Brenner et al., 1989]. The mechanism proceeds through a redox process, where the copper sites are first reduced to Cu(I) by ascorbate followed by the binding of dioxygen and hydroxylation of substrate. Activation of dioxygen occurs via the two-electron reduction of O₂ bound at the Cu_B(I) site to form a high-energy Cu_B(II)–O–O–H species. Presumably, the copper–peroxo species is responsible for the H atom abstraction from the benzylic

position of the substrate, coupled with the homolytic cleavage of the O–O bond, resulting in Cu(II)–O^{*}, a substrate-derived radical species, and water [Ahn and Klinman, 1983; Fitzpatrick et al., 1985; Miller and Klinman, 1985; Tian et al., 1994].

1.1.3.3 Peptidylglycine α -amidating monooxygenase. Peptidylglycine α -amidating monooxygenase (PAM, EC 1.14.17.3) appears to activate dioxygen in a similar way to D β H. These enzymes share 28% identity, including a conserved catalytic domain consisting of two mononuclear copper sites [Southan and Kruse, 1989]. A full description of this enzyme is provided in Section 1.3.1.


1.1.4 Copper Dioxygenases and Multicopper Oxidases

Two other important classes of copper enzymes that activate oxygen are the copper dioxygenases and the multicopper oxidases. Copper dioxygenases are responsible for incorporating both atoms of oxygen from dioxygen into a substrate. One example of a dioxygenase is quercetinase, which is responsible for the cleavage of quercetin to produce 2-protocatechuoyl phloroglucinol and carbon monoxide in fungi [Balogh-Hergovich et al., 1991]. Copper may serve to activate the substrate, allowing O₂ attack to give an organic peroxide, which then cleaves to give a product [Karlin et al., 1993]. Multicopper oxidases are a class of enzymes that couple the 4-electron reduction of dioxygen to water with the oxidation of substrate. These include laccases, ascorbate oxidase, and ceruloplasmin. These enzymes possess a type 1 copper site, used for electron transfer, and a type 2/type 3 trinuclear cluster as the minimal functional unit [Solomon et al., 1996]. Electrons are fed by ascorbate to the type 1 copper, which passes electrons through a protein pathway to the trinuclear center where dioxygen reduction occurs. In both dioxygenases and multicopper oxidases, the mode of interaction with oxygen is similar to that in the monooxygenases, although the spectroscopy may be very different.

1.2 ELECTRON TRANSFER

Any discussion concerning dioxygen activation is not complete without considering electron transfer. Four electrons are needed to reduce O_2 to H_2O ; in the system described herein, two of the electrons are derived from the peptide substrate. However, two more electrons are needed, and these are obtained from an exogenous reductant. In many enzymes, electron transfer must occur *intramolecularly* before catalysis can occur; for example, a transfer between two sites in a single molecule or an exchange between two molecules that are covalently bonded. The donor and acceptor sites may be quite close, or they may be separated by many angstroms of protein matter. *Intermolecular* reactions (the electron exchange between two molecules not covalently linked) also occur and depend on the change in redox potential, the distance between the donor and acceptor, and their relative orientation [Stryer, 1995]. However, these reactions will not be considered here.

Intramolecular electron transfer depends on the distance and driving force between donor and acceptor sites; the rate of transfer decreases exponentially as the distance increases [Isied et al., 1992]. For low driving force reactions, the rate is determined by both the electronic effects and the reorganization energy of the donor and acceptor sites, while the rate of transfer in high driving force reactions is governed primarily by electronic effects. The rate of electron transfer can be described by the following equation:

$$k_{et} = 10^{13} \exp[-\beta(d - d_0)] \exp\left[-\left(\frac{(\lambda + \Delta G_0)^2}{4\lambda RT}\right)\right]$$


Electronic interaction
between donor and
acceptor

In the first part of this equation the electronic factor, β , is related to the magnitude of the interaction, d is the center-to-center distance between the donor and acceptor, and d_0 is the close contact separation between these sites. The second part of the equation takes into account the reorganization energy, λ , which has components of both the

inner sphere and outer sphere reorganization energy, and the driving force of the reaction, ΔG_0 [Marcus and Sutin, 1985]. There are two types of electron transfer that occur in protein systems: through-bond and through-space. Through-space electron transfer does not involve the orbitals of the bridging peptide between the donor and acceptor and generally refers to transfer through solvent. This type of transfer is usually limited to short distances where there is little reorganization and/or a highly structured solvent [Sharp, 1998]. On the other hand, through-bond electron transfer utilizes the orbitals of the bridging group to assist in carrying the charge transfer, which can support long-range electron transfer. In many systems, a combination of the two transfer methods are utilized.

Protein-bound metal ions that are involved in electron transfer usually do so at low driving force and have been set up to optimize the transfer using other factors. These factors include: (1) metal ligands that reduce the central charge on the metal (e.g., sulfur, imidazole, and porphyrin); (2) a ligand geometry that is induced by the protein fold, which disallows ligand rearrangement on change of metal charge; (3) metal ions are insulated from the solvent so that reactions with small molecules cannot occur; (4) the distance for electron transfer is generally between 10 and 20 Å [Williams, 1990].

1.3 PEPTIDE AMIDATION

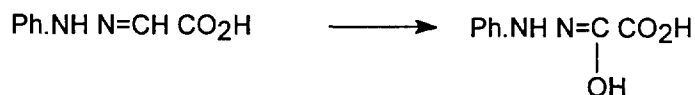
Investigations into the structure/function relationship in copper-containing oxygenases have led to an understanding of oxygen activation and electron transfer in these enzymes. In this thesis, I have undertaken the spectroscopic study of the enzyme peptidylglycine α -hydroxylating monooxygenase (PHM), one half of the mammalian enzyme peptidyl α -amidating monooxygenase (PAM), to help gain an understanding of the nature of electron donation by the active site coppers.

The bifunctional enzyme, PAM, is responsible for the C-terminal amidation of glycine extended peptides. A wide variety of amidated hormones are distributed throughout neural tissue [Eipper and Mains, 1988; Braas et al., 1989] making the understanding of the biochemical activity and mechanism of this enzyme important.

1.3.1 Peptidyl α -Amidating Monooxygenase (PAM)

C-terminal amidation of mammalian peptide hormones was first documented 50 years ago [Acher and Chauvet, 1953; du Vigneaud et al., 1953]. Since that time, this modification has been found in a large percentage (at least 50%) of the known peptide hormones, and its importance has been linked to the biological activity and/or stability of the hormone [Rittel et al., 1976; Pratt et al., 1989]. For some of these hormones, the amidation is absolutely necessary for biological activity; for example, in oxytocin, gastrin, and calcitonin [Morley, 1968; Rittel et al., 1976]. The amidation reaction was discovered to be a post-translational modification that depended on the presence of O₂, copper, and a reducing agent [Eipper et al., 1983; Pratt et al., 1989]. In the 1980s, the protein responsible for α -amidation was purified from a variety of sources; each individual protein had a molecular weight in the range of 42 to 92 kDa [Emeson, 1984; Wand et al., 1985a,b; Mackin et al., 1987]. Although peptides have been found with an α -amide moiety derived from each of the 20 amino acids, amidation is most common for neutral amino acid residues. In particular, the amidating enzyme preferentially acts upon C-terminal glycine and alanine residues [Bradbury and Smyth, 1983; Landymore-Lim et al., 1983; Tamburini et al., 1988, 1990]. Incorporation of ¹⁵N into the C-terminal glycine residue of the tripeptide D-tyrosylvalylglycine by Pratt et al. [1989] demonstrated that the α -amide moiety was derived from the terminal glycine residue of the peptide.

The oxidative nature of the amidating enzyme was later proven when a hydroxylated intermediate in the reaction was trapped [Bradbury and Smyth, 1987]. It was found that the enzyme could catalyze the conversion of glyoxalic acid phenylhydrazone to oxalic acid phenylhydrazide by the replacement of the hydrogen on the α -carbon with a hydroxyl group.



This led to the proposal that the amidating mechanism first involved the hydroxylation of the glycine-extended precursor, which was later substantiated by the observation that an exogenous α -hydroxyglycine peptide can be amidated by the same enzyme

[Young and Tamburini, 1989]. In the first step, the hydroxylation of the carbon atom was found to be stereospecific, with the addition of -OH and then subsequent amidation occurring at the site of the *pro-S* hydrogen only [Ramer et al., 1988; Ping et al., 1992].

Throughout this time, multiple forms of the amidating enzyme were being discovered, although their individual importance was unclear [Beaudry and Bertelsen, 1989; Gilligan et al., 1989; Stoffers et al., 1989]. In 1990, the isolation of a pituitary enzyme, α -hydroxyglycine amidating dealkylase (HGAD), that catalyzed the conversion of α -hydroxybenzoylglycine to benzamide was reported [Katopodis et al., 1990]. When HGAD and PAM were purified separately, each fraction exhibited low amidation activity, but, when recombined, full PAM activity was restored, suggesting that more than one enzyme was involved in the amidation reaction. Katopodis et al. [1990] proposed that the monooxygenase domain and the dealkylating domain might initially be produced as a single enzyme, which undergoes tissue-specific endoproteolytic cleavage to produce two soluble enzymes. Further support for this idea resulted from the observation that a hydroxylated peptide produced by the monooxygenase enzyme could be amidated by the dealkylating enzyme, even when the two enzymes were purified separately [Kato et al., 1990; Katopodis et al., 1990; Takahashi et al., 1990]. The first enzyme was given the name peptidylglycine α -hydroxylating monooxygenase (PHM) because of its apparent substrate hydroxylation from one atom of dioxygen, while the second enzyme became peptidylhydroxyglycine α -amidating lyase (PAL) due to its ability to cleave the N-C peptide bond. In bovine neurointermediate pituitary, these enzymes are generated by endoproteolytic cleavage of a 108-kDa PAM precursor [Perkins et al., 1990]. However, the bifunctional enzyme is also found as a single, 75-kDa protein in rat medullary thyroid carcinoma cells and adult rat atrium (where it is membrane associated), which suggests that the need for one enzyme with two activities or two separate enzymes may be tissue specific [Husten and Eipper, 1991; Merkler and Young, 1991]. Additionally, no bifunctional PAM protein has been identified in *Drosophila melanogaster* or in sea anemone although separate genes encoding PHM and PAL have been found [Hauser et al., 1997; Kolhekar et al., 1997b]. This suggests that the two proteins were

originally separate enzymes which were evolutionarily joined together, perhaps explaining the existence of both monofunctional and bifunctional enzymes. The mechanism of peptide amidation, proceeding through a hydroxylated intermediate, is shown in Fig. 1.1. PHM and PAL are shown separately with their necessary individual cofactors.

1.3.2 Peptidylhydroxyglycine α -Amidating Lyase (PAL)

Amidation of the hydroxylated intermediate occurs via the N-C bond cleavage of the terminal glycine residue by the PAL (EC 4.3.2.5) enzyme. The pH optimum for PAL with the substrate α -N-acetyl-Tyr-Val- α -hydroxyglycine is approximately 5 and the K_m of PAL for this substrate is $38 \pm 13 \mu\text{M}$ [Eipper et al., 1991]. The metal chelator EDTA inhibits the activity of PAL, while other chelators (*o*-phenanthroline and diethyl dithiocarbamate) have little effect, suggesting the involvement of a metal [Young and Tamburini, 1989; Eipper et al., 1991; Merkler et al., 1993]. PAL does not appear to be dependent on the binding of copper, although the need for other metals, such as zinc, has not been ruled out [Eipper et al., 1991; Kulathila et al., 1994]. Because PAL activity does not depend on the binding of copper, Kulathila et al. [1994] suggested that inhibition by EDTA results from the binding of EDTA to PAL. However, reconstitution with Zn(II) restored at least 10% of the activity, indicating that PAL is likely a Zn(II)-dependent metalloenzyme [Bell et al., 1997]. An extended X-ray absorption fine structure (EXAFS) of the Zn(II)-bound enzyme revealed that the metal was ligated to the protein by five first-shell O/N ligands at 1.98 Å, at least two of which were histidine residues [Bell et al., 1997]. Bell et al. [1997] proposed that Zn(II) might play either a catalytic role or a structural role in PAL activity. The elimination of PAL activity by the removal of zinc and the similarity of the Zn environment in PAL to other catalytic zinc enzymes suggests a catalytic role for zinc in the lyase reaction. However, the inability to restore full activity to the enzyme by addition of excess zinc points to the possibility that the metal may also play an essential structural role.

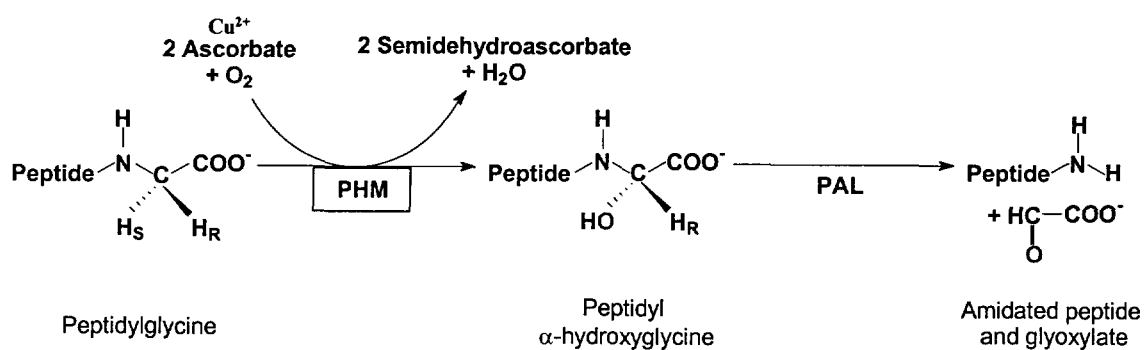


Fig. 1.1 The two enzymatic steps involved in the amidation of peptide hormones are shown with their respective cofactors. The hydroxylation step is catalyzed by PHM and the cleavage step is catalyzed by PAL. Both enzymes together constitute the bifunctional enzyme, PAM.

Originally published as Figure 1 in:

Prigge, S. T., Kolhekar, A. S., Eipper, B. A., Mains, R. E., and Amzel, M. (1997) Amidation of bioactive peptides: the structure of peptidylglycine α -hydroxylating monooxygenase. *Science* **278**, 1300–1305.

Used here with permission of the American Association for the Advancement of Science.

1.3.3 Peptidylglycine α -Hydroxylating Monooxygenase (PHM)

The first step in the amidation of peptide hormones is the hydroxylation of the α -carbon of the C-terminal glycine that occurs through the removal of the *pro*-S hydrogen on this carbon. In tissues where the two enzymes involved in amidation are found separately, the enzyme PHM (EC 1.4.17.3) carries out this reaction. PHM shares a ~30% homology with another type 2 copper protein, D β M, which includes an identical active site structure [Southan and Kruse, 1989; Blackburn et al., 1991; Boswell et al., 1996]. Both enzymes have the same requirement for copper, which goes through redox cycling during catalytic activity, to produce an hydroxylated product and water [Brenner and Klinman, 1989; Merkler et al., 1992; Tian et al., 1994]. Additionally, each copper is mononuclear and separated from the other by no less than 10 Å of solvent [Prigge et al., 1997].

PHM is copper, O₂, and ascorbate dependent. The rate-limiting step for the PHM-catalyzed hydroxylation of the peptide precursor was found to be the cleavage of the C _{α} -H bond. Replacement of the α -hydrogens on the terminal glycine with deuterium caused a large primary isotope effect on the rate of reaction, which would be expected for the limiting step of the reaction [Kizer et al., 1986]. Following C-H bond cleavage, a hydroxyl group is inserted on the α -carbon. Isotopic labeling of molecular oxygen with ¹⁸O provided evidence that the oxygen atom of the -OH group is derived from O₂ [Zabriskie et al., 1991; Merkler et al., 1992; Noguchi et al., 1992]. Hydroxylation of the peptide precursor requires the reduction of a single molecule of O₂ concomitant with the oxidation of one molecule of ascorbate. Thus, one molecule of the peptide substrate will in turn produce one molecule of the hydroxylated intermediate, followed by the formation of one molecule of the amidated product, when PAL is present [Merkler et al., 1992]. Enzyme-bound copper is critical to the activity of PHM—it is responsible for the reduction of oxygen and concomitant oxidation of peptidyl-Gly to peptidyl- α -hydroxyglycine during redox cycling [Freeman et al., 1993]. The maximum catalytic activity of PHM is achieved when two coppers are bound [Kulathila et al., 1994]. EPR spectroscopic studies showed that these were type 2 coppers (Fig. 1.2) [Merkler et al., 1993]. Each copper cycles through the Cu(II) and Cu(I) redox states during catalytic activity. PHM-

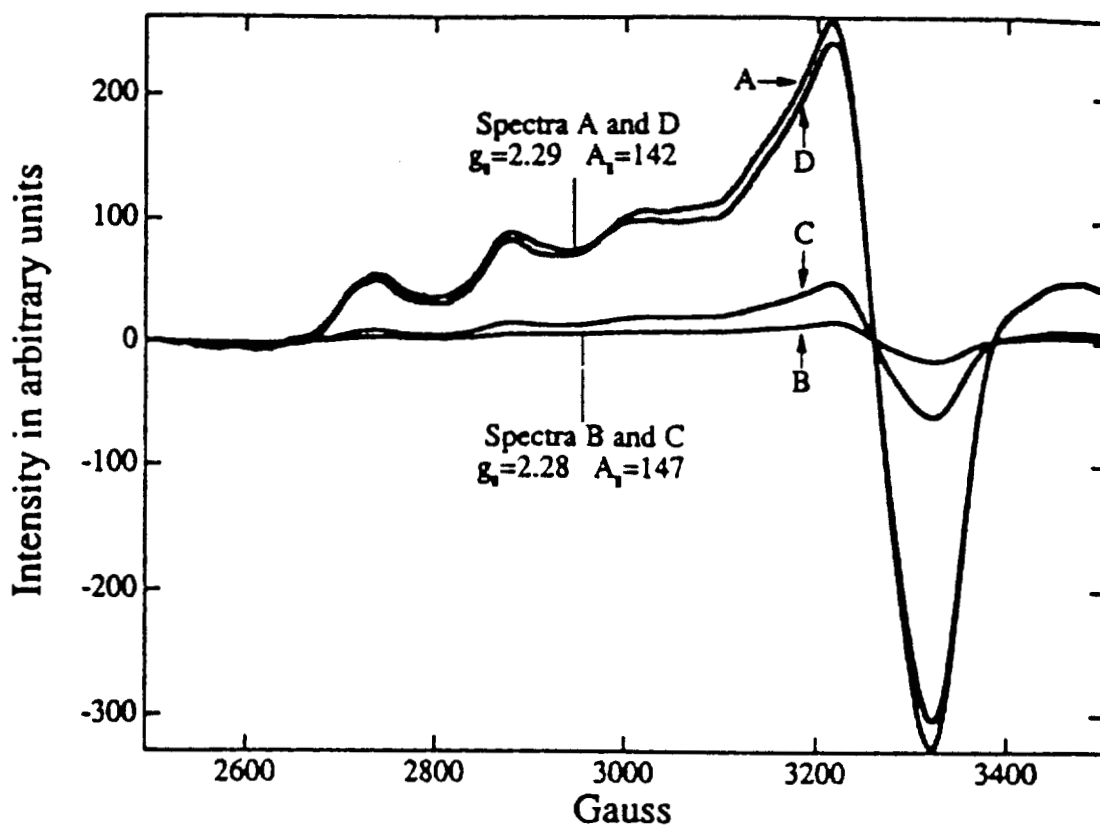


Fig. 1.2 Electron paramagnetic resonance spectra of the bifunctional enzyme PAM in the following conditions: (A) anaerobic oxidized; (B) anaerobic fully reduced; (C) aerobic reduced; (D) aerobic reduced with *N*-dansyl-TyrValGly added (caused enzyme turnover).

Originally published as Figure 1 in:

Freeman, J. C., Villabranca, J. J., and Merkler, D. J. (1993) Redox cycling of enzyme-bound copper during peptide amidation. *J. Am. Chem. Soc.* **115**, 4923-4924.

Used here with permission of the American Chemical Society.

[Cu(II)]₂ is considered the resting form of the enzyme, which can be reduced to PHM-[Cu(I)]₂ by the biological reductant, ascorbate. However, the bound Cu(I) is only reoxidized to Cu(II) in the presence of both peptide substrate and O₂ [Stewart and Klinman, 1987; Freeman et al., 1993]. The ligand environments of the bound coppers were originally described by mutagenesis, EPR, and EXAFS. In the oxidized/resting enzyme (Cu(II) form), the copper was found in a tetragonal environment with 2–3 coordinated His ligands and 1–2 O/N ligands [Eipper et al., 1995]. Mutation of ten conserved His residues revealed that five of these residues (H107, H108, H172, H242, H244) were essential to enzyme activity without having a significant effect on the K_m of peptidylglycine substrate binding compared to wild-type PHM ($K_m = 18 \mu\text{M}$ for $\alpha\text{-N-acetyl-TyrValGly}$) [Husten et al., 1993; Yonekura et al., 1996]. Alternatively, a Met314 to Ile mutant not only was enzymatically inactive, but it was also unable to bind to a peptidylglycine substrate affinity resin. This suggested that Met314 was likely involved in peptide substrate binding to the wild-type enzyme [Eipper et al., 1995]. Later, EXAFS studies helped identify the Met314 residue as an important copper (I) ligand in PHM [Boswell et al., 1996]. Interestingly, mutation of an active site residue not involved in copper binding, Tyr79, caused a 4-fold increase in the K_m of peptidylglycine substrate binding [Eipper et al., 1995]. In their paper, Tian et al. [1994] suggested that in D β M, an active site Tyr forms a Cu(II)-O...Tyr radical pair when the residue donates an H atom to the activated Cu_M-peroxo intermediate. A similar reaction might occur in PHM; however, this is speculative and no function for the Tyr79 residue has yet been identified.

1.3.3.1 Reaction mechanism of PHM. Investigation into the reactivity of PHM with CO, an O₂ analog, provided evidence that the active site coppers in the enzyme were inequivalent; only one of the two coppers was able to bind CO [Boswell et al., 1996]. The value of the intraligand stretching frequency for the copper-bound CO (2093 cm⁻¹) suggested that carbonyl coordination must take place at a copper center with a poor electron donor such as the Met314 at Cu_M. Similar results were seen for D β M [Blackburn et al., 1990; Pettingill et al., 1991], which led to an activity model where one copper, Cu_M, was involved in oxygen binding and activation

and the second copper, Cu_H , was responsible for electron transfer; this is assumed to also be true for PHM [Stewart and Klinman, 1987; Pettingill et al., 1991]. Kinetic investigations into the mechanism of PHM activity have shown that substrate binding (ascorbate, peptidylglycine, and molecular oxygen) is ordered (Fig. 1.3). The first step is the binding of two molecules of ascorbate, which reduce the two enzyme-bound coppers from Cu(II) to Cu(I) , releasing two molecules of semidehydroascorbate [Merkler et al., 1992]. The subsequent binding of peptidylglycine substrate and oxygen is equilibrium ordered, with the peptide substrate binding first, followed by O_2 [Francisco et al., 1998]. Eventually, a $\text{Cu}_M(\text{II})\text{-O-O-H}$ species is proposed to be formed, identical to the Cu -peroxo species formed in $\text{D}\beta\text{M}$. In $\text{D}\beta\text{M}$, this species is thought to be responsible for the H-atom abstraction at the $\alpha\text{-C}$ position on the peptidylglycine substrate causing the homolytic cleavage of the O-O bond to generate Cu(II)-O^\bullet (a substrate-derived radical species) and water [Miller and Klinman, 1985; Wimalasena and May, 1987; Tian et al., 1994]. Radical recombination then occurs, resulting in the formation of a Cu -bound alkoxide, which is then hydrolyzed and released from the active site (Fig. 1.4). A similar mechanism for O-O bond cleavage is thought to occur in PHM. However, how an electron transfers from Cu_H to Cu_M to produce the $\text{Cu}_M(\text{II})\text{-peroxo}$ species is *unknown*. Two significantly different mechanisms have been proposed in the last two years, one of which resulted from this work. The other, based on the X-ray crystal structure of PHMcc in various forms, is described in Section 1.3.3.2.

Kinetic studies on the expression of truncated PHM proteins defined the catalytic core of the enzyme (PHMcc)—the shortest protein fragment needed for efficient folding and full wild-type PHM activity—as consisting of residues 42–356; it was expressed in high levels in CHO (Chinese hamster ovary) cells and is currently the expression system of choice for studying PHM [Kolhekar et al., 1997a].

1.3.3.2 PHM structure. Publication of the X-ray crystal structure of oxidized PHMcc revealed, in detail, the active site structure where both coppers are bound [Prigge et al., 1997]. The overall structure of the enzyme is composed of two domains, each a nine-stranded β -sandwich (Fig. 1.5). There is a linker loop, which

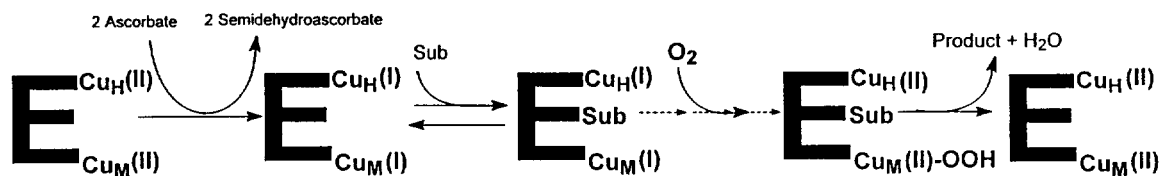


Fig. 1.3 The enzymatic mechanism of PHM. Enzyme-bound copper is initially reduced by bound ascorbate. Peptide substrate and oxygen bind in an ordered fashion. A Cu_M-peroxide is formed by the oxidation of both copper ions. Finally, the product is released.

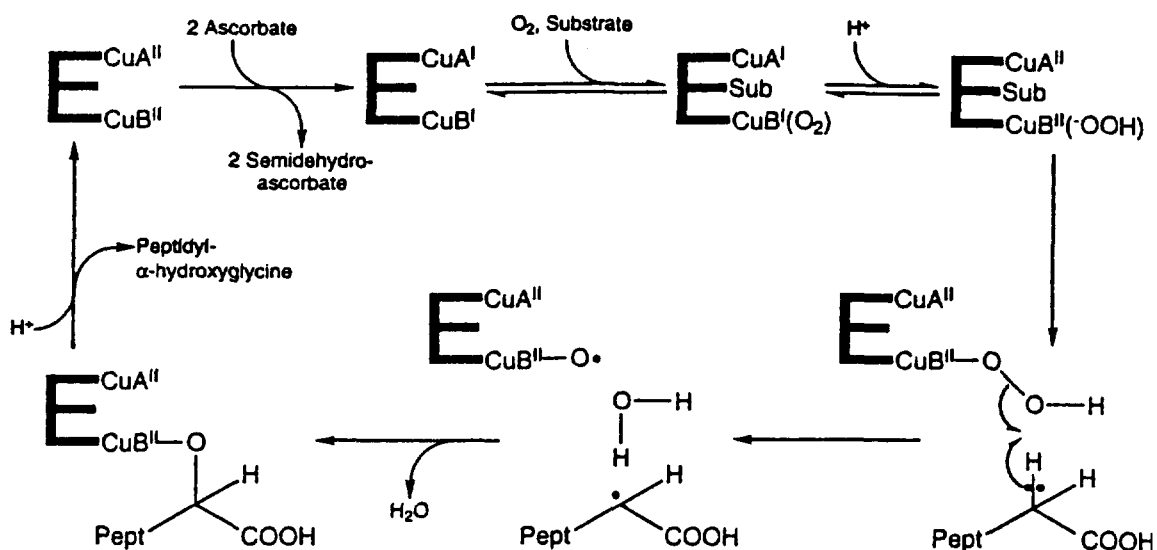


Fig. 1.4 Detailed mechanism proposed for PHM. Molecular oxygen binds to reduced PHM and peptide substrate binds nearby. Both coppers oxidize to form the bound peroxide. The Cu_M -hydroperoxide undergoes heterolytic cleavage of the $O-O$ bond. The *pro-S* hydrogen of the α -carbon is abstracted, forming a substrate radical. Radical recombination forms a Cu^{2+} -alkoxide complex, and the product is formed through slow dissociation.

Originally published as Figure 5 in:

Prigge, S. T., Kolhekar, A. S., Eipper, B. A., Mains, R. E., and Amzel, L. M. (1997) Amidation of bioactive peptides: the structure of peptidylglycine α -hydroxylating monooxygenase. *Science* **278**, 1300–1305.

Used here with permission of The American Association for the Advancement of Science.

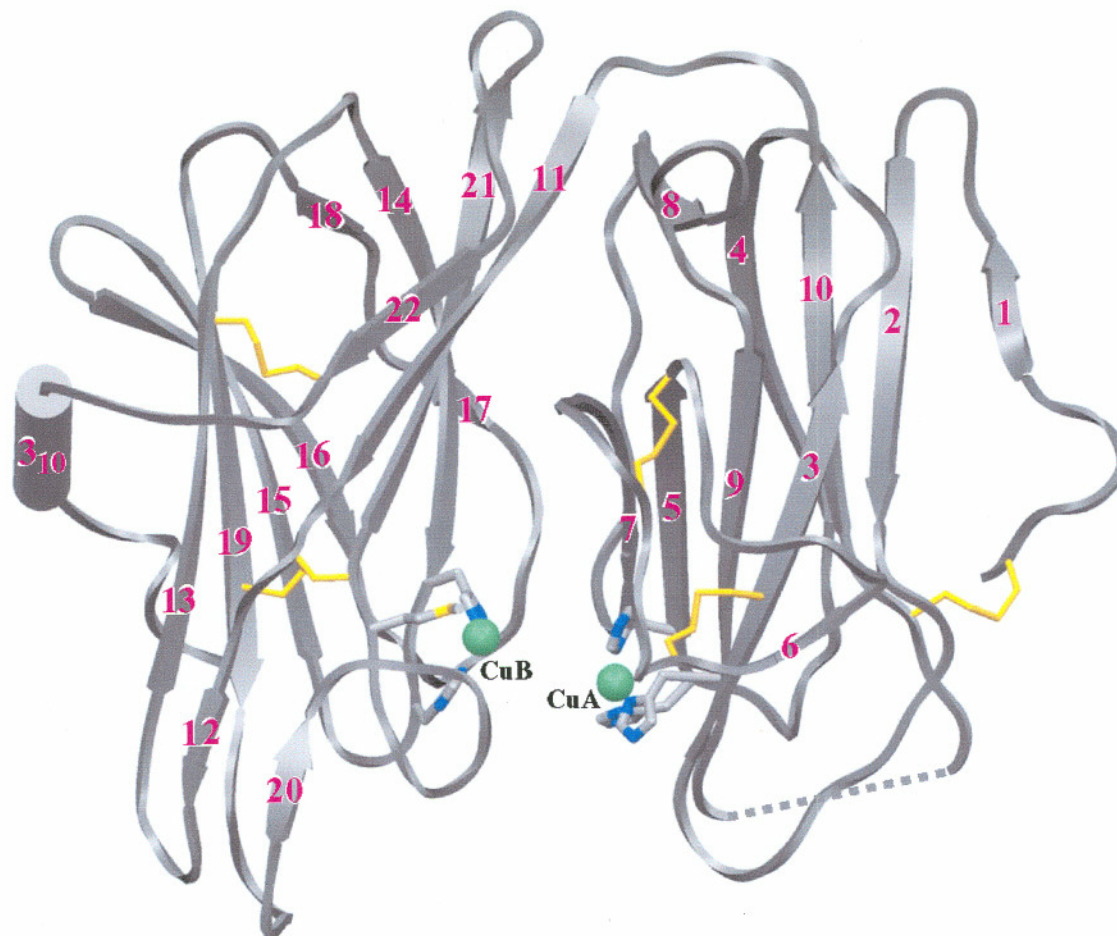


Fig. 1.5 A representation of the two-domain structure of PHM, as derived from the X-ray crystal structure.

Originally published as Figure 2 in:

Prigge, S. T., Kolhekar, A. S., Eipper, B. A., Mains, R. E., and Amzel, L. M. (1997) Amidation of bioactive peptides: the structure of peptidylglycine α -hydroxylating monooxygenase. *Science* **278**, 1300–1305.

Used here with permission of the American Association for the Advancement of Science.

connects the two domains, and the cleft that this creates is fully accessible to solvent. Each domain binds a single copper, with domain I ligating Cu_H through His107, His108, and His172 and domain II ligating Cu_M through His242, His244, and Met314. The coppers are found at the base of each domain, facing the interdomain space, and are separated by 11 Å of solvent and 240 Å of through-bond distance. The three His ligands at Cu_H assume a square pyramidal geometry, with two additional coordination positions unoccupied. The coordination environment at Cu_M is tetrahedral, with a fourth ligand coming from solvent. Fig. 1.6 depicts the structural environment of each copper as derived from X-ray crystallography. In addition, Prigge et al. [1999] reported the structure of oxidized PHM with bound *N*- α -acetyl-3,5-diiodotyrosylglycine. The peptidylglycine substrate is anchored to the enzyme by Arg240, Tyr318, and Asn316, which hold the peptide facing Cu_M in the interdomain cleft. Of these residues, Arg240 is the only one not found on a β -strand associated with Cu_M ; in fact, the side chain of Arg240 is pointed into the solvent equidistant between both active site coppers (Fig. 1.6). The crystal structure raised the question of how electrons are transferred from Cu_H to Cu_M due to the long distance between the coppers, both through-bond and through-solvent. Suggested possibilities included interdomain motion that might bring the two coppers in close proximity or electron transfer through water.

A second set of crystal structures, published by the same group, began to address this issue [Prigge et al., 1999]. The active sites of three structures were examined in detail: oxidized PHMcc, oxidized PHMcc + peptidylglycine substrate (Ac-DiI-YG, ox-PHM-sub), and reduced PHMcc. All three structures were similar, with the only difference being the position of two residues close to the Cu_H site, Gln170 and His108 (a Cu_H ligand). In the oxidized form, a water molecule bridges these two residues, while in the reduced form they form a hydrogen bond. Neither interaction was seen in the ox-PHM-sub form; however, in this structure a water molecule bridges the Gln170 and the carboxylate oxygen of the bound substrate. From these structures, it was inferred that the reduced PHMcc-substrate formed both a hydrogen bond between Gln170 and His108 and a bridging water molecule between Gln170 and the peptide substrate. The substrate-bound structure showed the *pro*-S

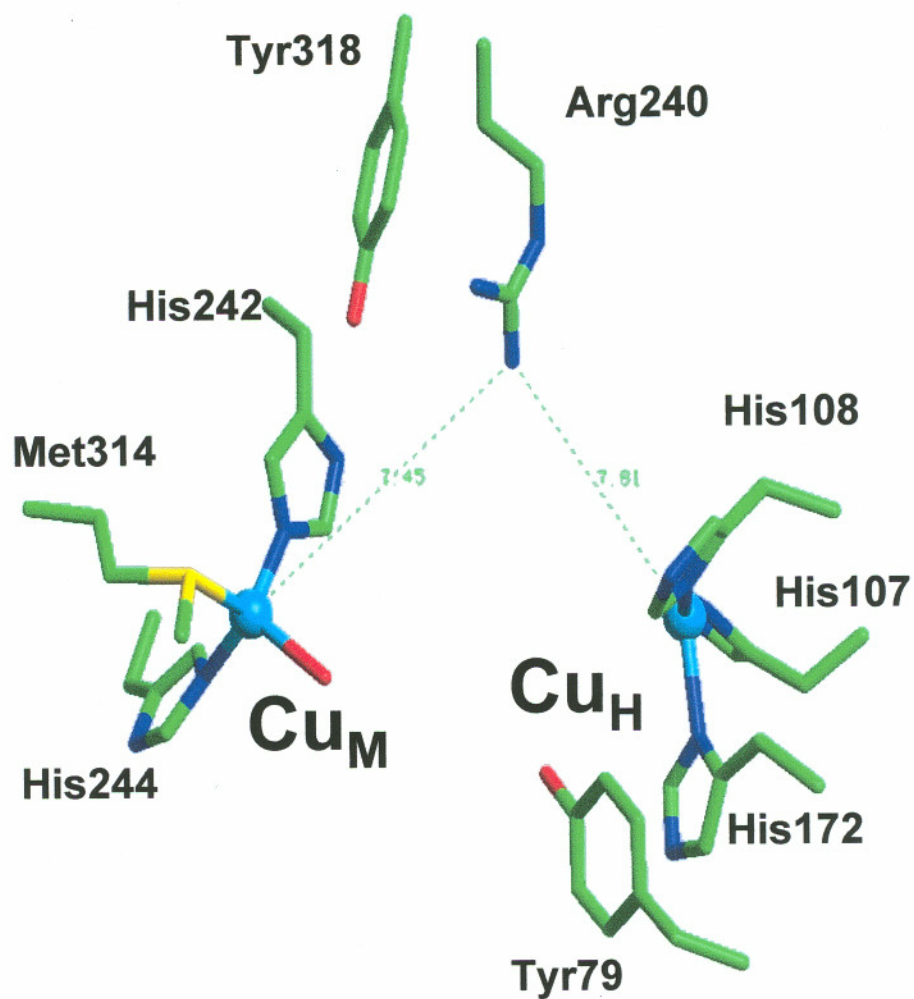


Fig. 1.6 The X-ray crystallographic active site. The coordination geometry at each copper is shown. Three additional conserved active site residues are shown (Tyr318, Arg240, Tyr79) [Prigge et al., 1997]. This figure was made using Insight II.

hydrogen of the glycyl α -carbon pointing toward the Cu_M -bound water molecule, aligning the atoms involved in the hydroxylation reaction. An electron could then transfer from the Cu_H to His108, through the H-bond to Gln170 and the bridging water molecule to the bound peptide substrate. Finally, the electron would have a 3.6 Å through-space hop to the Cu_M -bound oxygen molecule. In this fashion, the bridge created by the binding of substrate reduces the electron transfer pathway between Cu_H and Cu_M to ~ 20 Å, which is a reasonable distance for known electron transfer pathways in proteins. Additionally, the substrate-bound PHM crystal retains the ability to hydroxylate substrates, although at a very diminished rate ($\sim 2,700$ times slower than the solution rate). This final piece of data suggested that movement of the domains to bring the coppers close together was not necessary for turnover of PHM. Competent electron transfer through-bond requires that there be either (a) very little structural change accompanying redox or (b) some type of gating mechanism which minimizes the amount of structural change possible. Although crystallographic data suggest there is little ligand movement at the copper sites during redox activity, EXAFS tells a very different story.

EXAFS analyses of the structures of oxidized and reduced PHMcc suggest that there are major environmental changes which accompany redox cycling [Blackburn et al., 2000]. Copper coordination in the oxidized enzyme was similar to that seen in the crystal, although there were some important differences. The solution structure found that the Cu_M coordination geometry in the Cu(II) form assumes a distorted tetrahedral configuration with the Cu-S(Met) ligand, forming a weak bond at > 2.4 Å. Both coppers in the oxidized form are thought to be 4- or 5-coordinate tetragonal. Reduction of the coppers causes the Met ligand to coordinate, forming a 2.24 Å Cu-S(Met) bond and a 3- or 4-coordinate trigonal or tetrahedral Cu_M (I) site. The Cu_H site appears to become 2- or 3-coordinate (with a third histidine weakly bound and undetectable by EXAFS) upon reduction, due to the loss of ligated solvent molecules. These data contradict crystallography on the enzyme and suggest that the reorganization energy may be too large for electrons to tunnel in PHM.

The following section describes the spectroscopic techniques utilized in this thesis to study the active site coppers in PHM.

1.4 PHYSICAL METHODS FOR STUDYING COPPER CENTERS

1.4.1 Atomic Absorption Spectroscopy

Atomic absorption is defined as the absorption of energy that causes a transition of an electron from the ground state of the atom to the lowest excited state. This method has mainly been used to quantify the concentration of a metal in a protein solution. The most common form of instrumentation uses a flame to atomize the molecule and a source of energy other than the flame to excite the ground-state electrons. The source is usually at a fixed wavelength, which corresponds to the spectral resonance line of the ion being studied. Detection of the transmitted energy quantifies the number of absorbing atoms in the sample [Christian and Feldman, 1979].

1.4.2 Ultraviolet and Visible Spectroscopy (UV-vis)

UV-vis is used for qualitative measurements of proteins and to follow enzymatic reactions. This method evaluates the electronic transitions and rearrangement of the outer-shell electrons in a molecule. These transitions are measured as an absorption spectrum, plotted as the absorbance versus the wavelength of irradiation. Absorption of UV energy causes the promotion of an electron from either the n (nonbonding) or π (bonding) orbital to the π^* antibonding orbital. Another set of transitions occurs between the d -shells in transition metals and is detectable in the visible region. There are also absorptions called charge transfer transitions that occur when an electron is transferred from one atom to another. Many metal-containing enzymes, especially those that do redox chemistry and/or electron transfer, have strong charge transfer bands. These bands change depending on the metal oxidation or bound ligand, allowing the study of the catalytic cycle of an enzyme [Campbell and Dwek, 1984].

Using this method depends on the application of the Beer-Lambert law which states: *the fraction of light absorbed by a transparent medium is independent of the incident light intensity, and each successive layer of the medium absorbs an equal*

fraction of the light passing through it. The law can be expressed in the following relationship:

$$A = \epsilon cl$$

where c is the concentration in terms of molarity, l is the path length of the sample cell in centimeters, and ϵ is the molar absorption coefficient. This equation is often used to determine the concentration in protein samples directly from the absorption at a particular wavelength.

For the purpose of this dissertation, UV-vis spectroscopy was used mainly as a tool to determine the concentration of protein samples from their absorption at 280 nm. At this wavelength, the absorption from peptide bonds is very strong; by establishing the molar absorption coefficient for a particular protein, the concentration is easily calculated from the Beer-Lambert equation.

1.4.3 Infrared Spectroscopy

Detection of organic functional groups in a molecule can be accomplished by measuring the vibrational levels within the electronic ground state of a molecule. These vibrations generally occur in the infrared energy region, $\sim 400\text{--}4000\text{ cm}^{-1}$, and are due to the vibrational motion of a bond within the molecule.

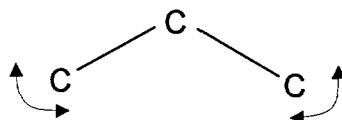
Molecular vibrations are responsible for oscillations of electric charge, the strongest of which is the oscillating dipole. Absorption of energy in the infrared region occurs when the wave number (energy) of the incident radiation is equal to the quantum of energy of the oscillator. Each molecule of N atoms has $3N$ degrees of freedom, and of these there are $3N-6$ vibrational motions that might absorb in the infrared region. There are two types of vibrational motion associated with each bond: a bend and a stretch.



Stretch (symmetric or in phase)



Stretch (asymmetric or out of phase)



Bend

Stretches occur when the two bonded atoms move in such a way as to cause a lengthening or shortening of their bond. Stretches can be further described as symmetric or asymmetric, depending on whether the changes are in or out of phase. A bending vibration is one in which the angle between two bonds changes; bends can be broken down into different forms: wagging, rocking, or twisting. There must be a dipole change for a vibration to be IR active; therefore, infrared spectroscopy is able to detect asymmetric movements. The amount of change in the dipole during the vibration is proportional to the intensity of the IR absorption. The complementary spectroscopy, Raman, detects changes in the molecular polarizability of a bond caused by ultraviolet or visible light [Gans, 1980; Kennedy, 1990; Ebsworth et al., 1991].

In this thesis, I have used infrared spectroscopy to investigate the vibrations of a diatomic molecule, CO; therefore I will focus on the stretching vibration of this molecule that is detectable in the IR spectrum.

1.4.3.1 Infrared spectra of diatomic molecules. The frequency of the vibration depends on the masses of the two atoms and the strength of their bond. This can be expressed with the following equation:

$$\nu = \frac{1}{2\pi} \sqrt{\frac{k}{m_1 m_2 / (m_1 + m_2)}} \text{ Hz}$$

where ν is the frequency, m_1 and m_2 are the mass of the atoms, and k is the force constant.

1.4.3.2 Infrared spectrometers. The Fourier transform infrared (FTIR) spectrometer (interferometer) is the most widely used instrument to measure an IR spectrum and is the type of spectrometer used for experiments described here. A diagram of a basic interferometer is shown in Fig. 1.7. The instrument consists of five basic parts: (1) a source, (2) a beam-splitter, (3) a fixed mirror, (4) a moving mirror, and (5) a detector. The source (a tungsten-halogen lamp) emits radiant energy in the infrared region, which is collimated and directed at the beam-splitter (potassium bromide, KBr). The beam-splitter sends half of the beam toward the fixed mirror and the other half toward the moving mirror, which is used to introduce a varying path difference. The beams are recombined at the beam-splitter before being directed at the sample. If the two path lengths are the same, then the two beams will recombine constructively for all frequencies in the original beam. If, however, the path length differs, the beams will be out of phase, causing some frequencies to interfere destructively. The amplitude of the recombined signal will depend on the frequency and distance the mirror has moved for different path lengths. The recombined beam passes through a sample and is collected by a detector [liquid nitrogen cooled mercury cadmium telluride (MCT)]. Frequencies that are transmitted through the sample are only detected when the two beams are not fully out of phase. This results in an interferogram, which is a plot of the amplitude of the transmitted frequencies versus time (or distance the mirror moves). A computer can then create a Fourier transform from the resulting interferogram, which is printed as an IR spectrum that we can interpret. To create the interferogram, the two recombined beams must be exactly superimposed, and therefore the path difference for all parts of the beam must be the same. This can be achieved by limiting the size of the returning beam with an aperture called a J-stop.

Samples can be either solid or liquid, although all protein samples examined in this study are liquid. Liquid samples are placed in a calcium fluoride cell and

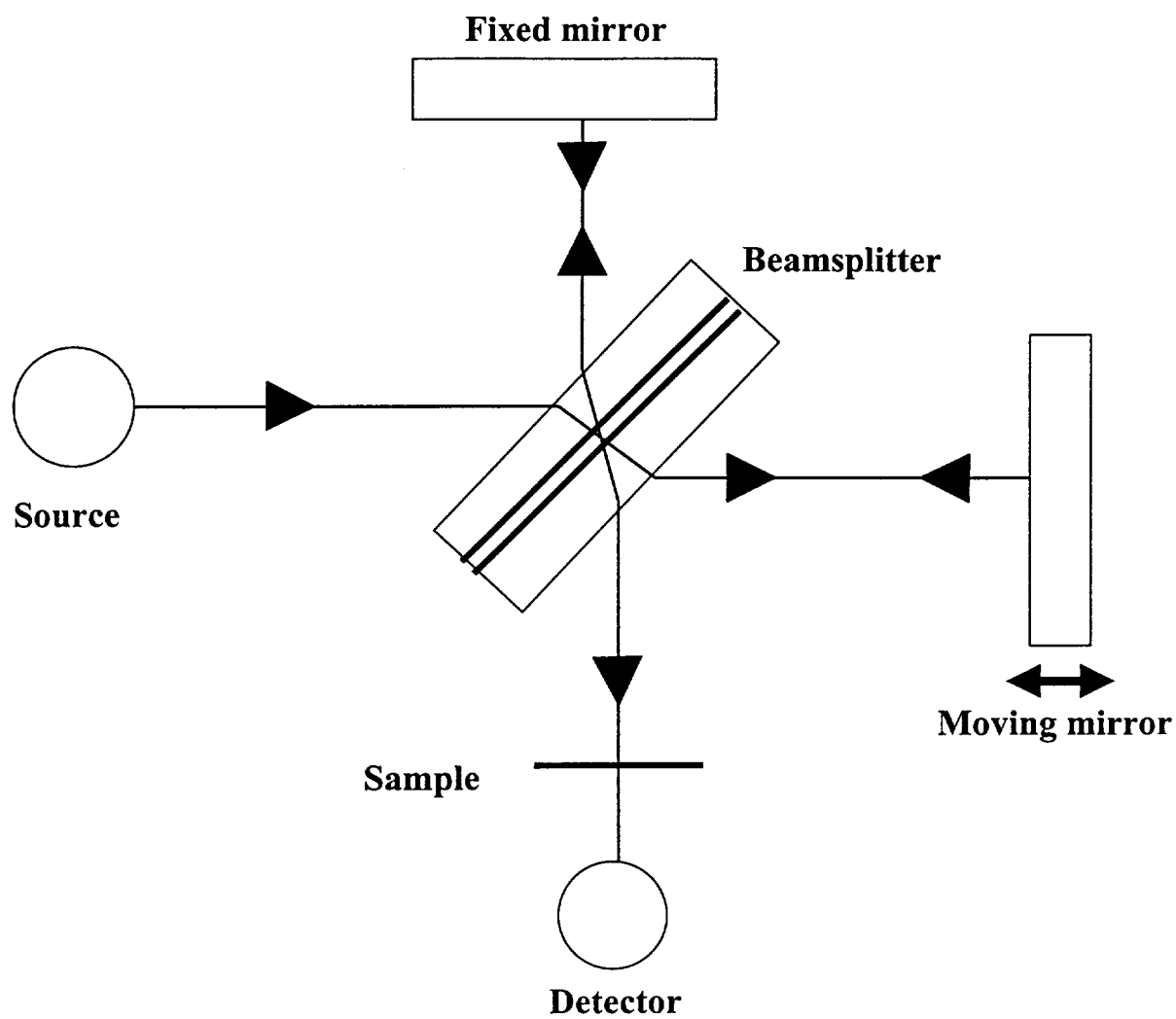


Fig. 1.7 Schematic representation of an infrared spectrometer.

examined by transmission. Calcium fluoride is inert with respect to biological samples, although it can only be used to measure spectra above 1050 cm^{-1} .

Interferometers are able to measure all source wavelengths simultaneously, have a fairly low signal-to-noise ratio which is constant during the scan, have a very accurate and stable reference for wave number calibration (a helium neon laser), and have no discontinuities in the spectrum.

1.4.4 X-ray Absorption Spectroscopy

X-ray absorption spectroscopy (XAS) is a very powerful tool used to determine the structural environment around a particular atom. This technique is selective for a particular element, enabling individual heavy ions to be probed. There are two regions in a typical XAS spectrum: the X-ray absorption near edge structure (XANES) and EXAFS (Fig. 1.8). The absorption edge in the XANES region is a result of the promotion of a 1s core electron to an unoccupied "bound" orbital of the metal (K-edge). There are also L-edge transitions, which involve the promotion of a second-shell electron. The energy needed to excite the electron depends on the atom and a more positively charged nucleus will require more energy to remove the electron. The shape and position of the absorption edge provides information about the oxidation state, the coordination number, and the site symmetry of the absorbing atom.

1.4.4.1 EXAFS. The EXAFS region contributes to the detailed picture of the local environment surrounding the absorbing atom to approximately 5 \AA . The X-ray energy being absorbed by the central atom (metal) may excite some electrons with enough energy to be ejected into the continuum. This electron can then be scattered by neighboring atoms (ligands) such that some of the backscattered waves arrive back at the central atom (Fig. 1.9). The resulting EXAFS spectrum is made up of sinusoidal oscillations, which describe the interference pattern between the outgoing and backscattered waves. It gives such information as types of ligands and their radial distance from the absorber, coordination number, and the existence of metal

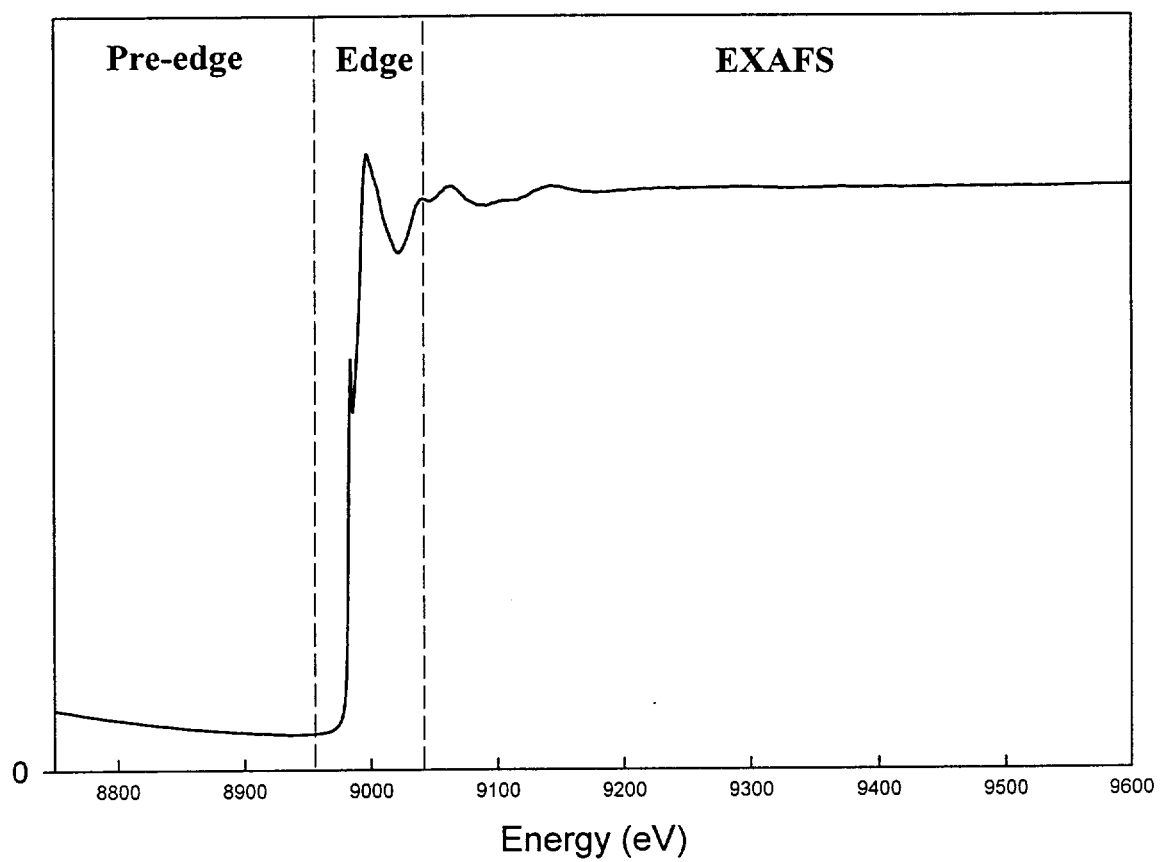


Fig. 1.8 Representative Cu(I) K-edge X-ray absorption spectrum.

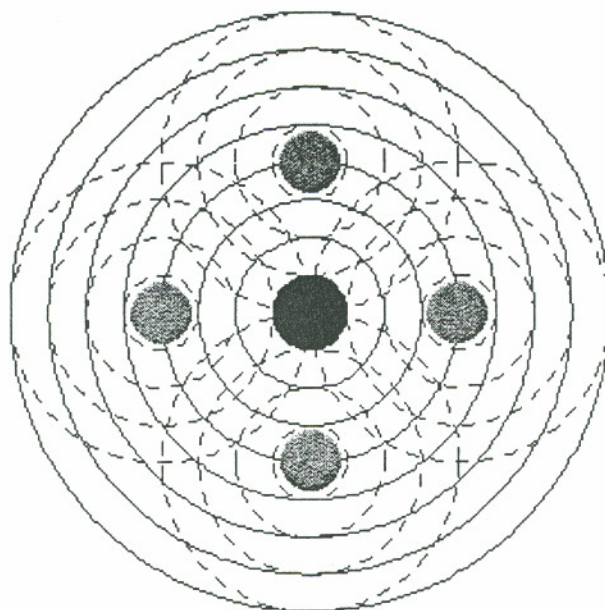


Fig. 1.9 Outgoing and backscattered portions of final-state wave function.

Originally published as Figure 4 in:

Bunker, G. (1997) <http://gbxafs.iit.edu/training/tutorials.html>

Used here with permission of Grant Bunker, Ph.D., Associate Professor of Physics, Illinois Institute of Technology, 3101 S. Dearborn, Chicago, IL 60616.

clusters. The function that describes the oscillatory part of the absorption and is used in simulating the EXAFS spectrum is:

$$\chi(k) = \frac{1}{k} \sum_s N_s \underbrace{\frac{f_s(\pi, k)}{R_{as}^2}}_{\text{Back-scattering amplitude}} \exp(-2\sigma_{as}^2 k^2) \sin \underbrace{[2kR_{as} + \alpha_{as}(k)]}_{\substack{\text{Frequency} \\ \text{Phase}}}$$

where k is the photoelectron wave number, N_s is the number of scatterer-type atoms at a mean distance of R from the absorber atom [Gurman, 1990]. The electron scattering strength of the ligands is described by $f_s(\pi, k)$ and depends on the atomic number of the scattering atom. The Debye-Waller factor ($-2\sigma_{as}^2 k^2$), a thermal disorder term, is dependent on the mean square variation in R . The resulting spectrum is an average of the environments of all atoms of a single type in a molecule or sample.

1.4.4.2 Synchrotron radiation. XAS requires a source of X-rays, usually obtained at a synchrotron facility. All the EXAFS data presented here were collected at the Stanford Synchrotron Radiation Laboratory. Synchrotron radiation is a tunable source of energy that can be adjusted to select the correct edge energy, depending on the central absorber being studied. Typically, electrons are accelerated and stored at high energy in a storage ring. The electrons can be maintained in the storage ring for hours as long as they are kept under high vacuum. Fig. 1.10 shows a diagram of a standard storage ring. The synchrotron (or LINAC) produces electrons, which are injected into the storage ring where they move at a constant velocity. Periodically, the electron encounters a dipole magnet, which accelerates the electron in an arc. Each of these bending magnets produces a continuous spectrum of radiation at a tangent to the arc, which passes through collimation slits. The column of radiation is directed onto a monochromator that focuses the X-rays to the frequency of interest. The monochromator is composed of two identical single crystals that can be tuned by rotation of the crystals to change the angle between them. The column of energy then passes through another set of slits intended to reduce the size of the beam. It then

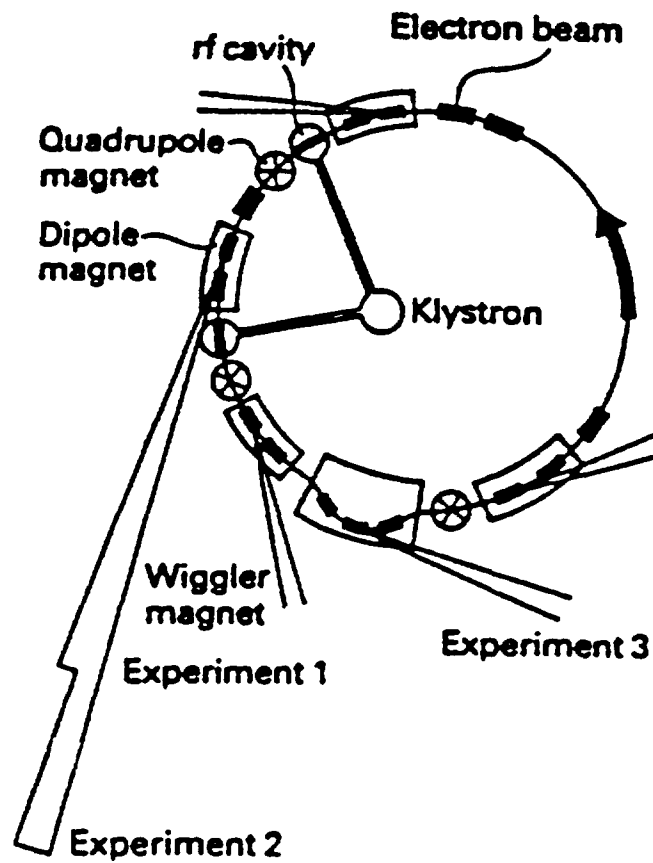


Fig. 1.10 Basic storage ring setup. Electrons are accelerated around the ring using various types of magnets. Both dipole magnets and Wiggler magnets produce energy at a tangent, which is collected and used for X-ray experiments.

travels through an ionization chamber where I_0 is detected and travels on to the sample. Fluorescence is collected at a 45° angle, and the energy that is transmitted (I_1) is detected in a second ionization chamber. A typical setup for the experimental station used herein is shown in Fig. 1.11.

1.4.4.3 Fourier transform. Analysis of the data can either be performed through “real space” analysis, using the Fourier transform, or k space analysis, using the EXAFS spectrum directly. In either case, the data collected (XAS spectrum) are first energy calibrated, using a single point calibration (in the case of copper, a copper foil) converted to k -scale. Then the spectrum can be background subtracted to remove a sloped background, and finally the EXAFS are extracted using a spline subtraction, which fits a smooth curve underneath the post-edge oscillations. The background-subtracted spectrum is weighted by k^3 to counteract the decrease in the amplitude of $\chi(k)$ with increasing k and finally Fourier transformed with respect to $\exp(-2ikr)$:

$$\text{F.T.} = \frac{1}{\sqrt{2\pi}} \int_{k_{\min}}^{k_{\max}} \chi(k) \exp[-i(2kR + \phi k)] dk$$

The resulting spectrum is a function with peaks at different $r(\text{\AA})$ values corresponding to each shell of atoms surrounding the absorbing atom (or the metal–ligand distances) (Fig. 1.12) [Lee, 1981; Stern, 1988; Gurman, 1990].

X-ray crystallography has traditionally been used to determine three-dimensional structures of macromolecules. Due to the large number of atoms per unit cell, however, the resolution in protein crystallography is low compared to small molecules. EXAFS, on the other hand, has an accuracy of $\sim 0.02 \text{ \AA}$ at small distances, making this technique ideal for determining the active site structures of large biological molecules. In addition, EXAFS samples are generally frozen solutions, allowing the trapping of dynamic structures.

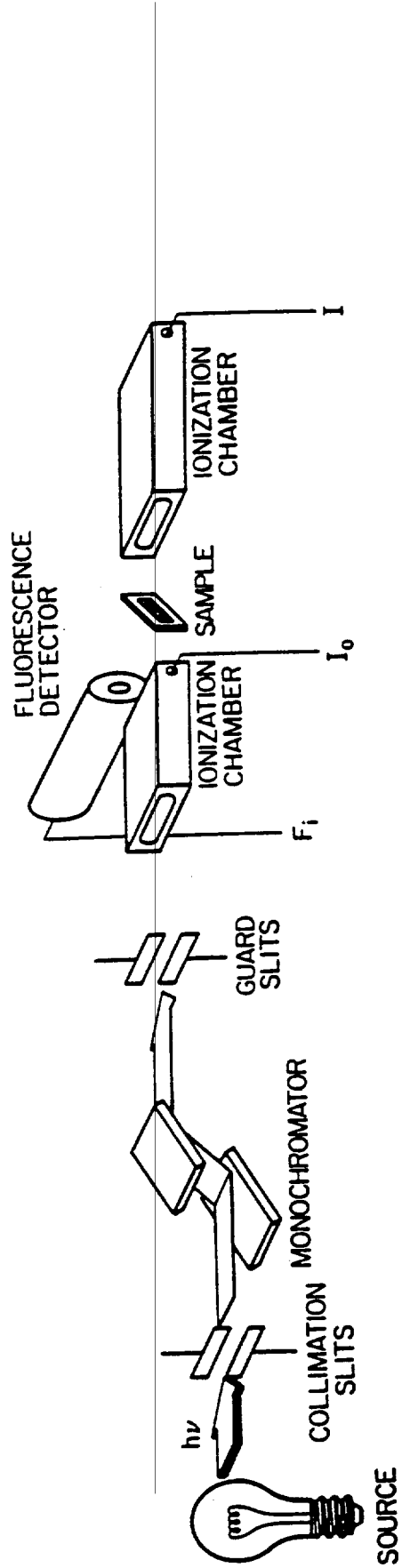


Fig. 1.11 Typical experimental station setup. The entire experiment is set up behind a wall of lead to protect the scientist from X-ray radiation. Data is sent from the fluorescence detector to a computer, where it can be visualized.

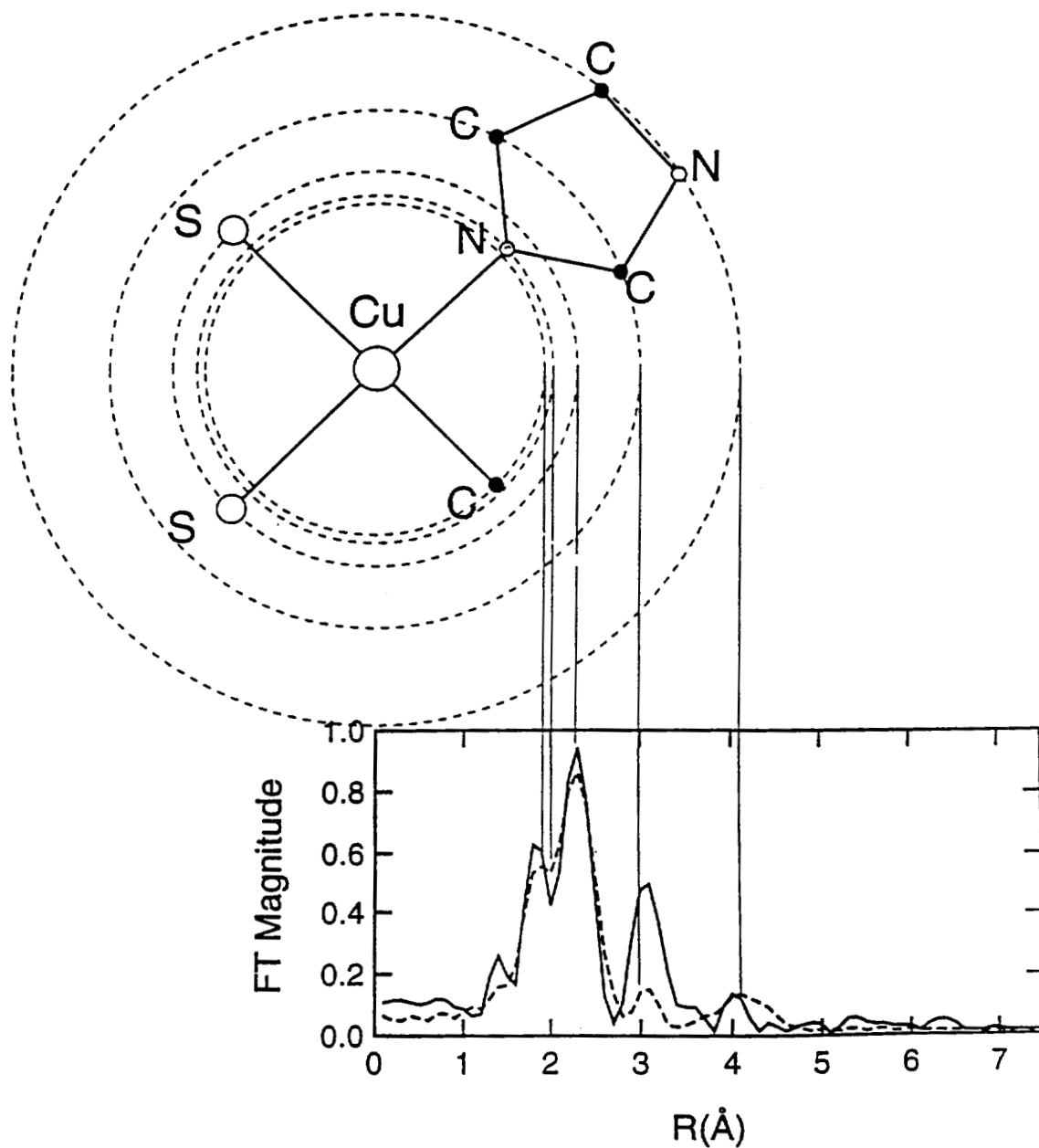


Fig. 1.12 Each peak in the EXAFS FT spectrum represents a single scattering radius in the sample. In this example, the first peak at 1.8 Å is derived from a mixture of the single carbon atom and the imidazole nitrogen atom.

CHAPTER 2
DOES SUPEROXIDE CHANNEL BETWEEN THE COPPER CENTERS
IN PEPTIDYLGLYCINE MONOOXYGENASE?
A NEW MECHANISM BASED ON CARBON MONOXIDE REACTIVITY*

2.1 INTRODUCTION

Many neuropeptides and peptide hormones are activated by post-translational C-terminal amidation in a reaction that is carried out by the enzyme peptidyl- α -amidating monooxygenase (PAM, EC 1.14.17.3) [Vale et al., 1981; Eipper et al., 1983, 1992]. PAM is a bifunctional enzyme which consists of two domains—the peptidyl- α -hydroxylating monooxygenase (PHM) and the peptidyl- α -hydroxyglycine lyase (PAL)—with separate enzymatic activities [Katopodis et al., 1990; Husten and Eipper, 1991; Miller et al., 1992; Husten et al., 1993]. The PHM domain catalyzes the first step of the reaction, in which the terminal glycine residue of a peptide is hydroxylated at the C $_{\alpha}$ position, in a copper, ascorbate, and molecular oxygen-dependent monooxygenation. The hydroxylated peptide is then cleaved through N-C bond fission by the PAL domain to form the amidated peptide in what is believed to be a Zn-dependent process [Bell et al., 1997]. The two enzyme activities are encoded by a single-copy gene and can either be expressed as a single unit or as independent proteins [Stoffers et al., 1991]. PHM shares similar cofactor requirements and a 30% homology in its amino acid sequence with another monooxygenase, dopamine- β -monooxygenase (D β M) [Southan and Kruse, 1989]. Although their substrate

* Originally published in this or similar form in *Biochemistry* and used with permission of the American Chemical Society:

Jaron, S., and Blackburn, N. J. (1999) Does superoxide channel between the copper centers in peptidylglycine monooxygenase? A new mechanism based on carbon monoxide reactivity. *Biochemistry* 38, 15086–15096.

specificity is quite different, both PHM and D β M appear to share a number of mechanistic features [Klinman, 1996; Francisco et al., 1998], and they each contain two mononuclear coppers at their active sites which undergo redox cycling through Cu(II) and Cu(I) forms [Freeman et al., 1993; Kulathila et al., 1994; Boswell et al., 1996].

Spectroscopic studies (and in particular XAS) provided the first structural model of the active site of both the oxidized and reduced forms of PAM [Eipper et al., 1995; Boswell et al., 1996]. EXAFS data were used to show that all five conserved histidines between the amino acid sequence of PHM and D β M (H107, H108, H172, H242, and H244) and one conserved methionine (M314) were ligands to the copper centers [Eipper et al., 1995; Boswell et al., 1996]. Mutations to any one of these ligands produced an inactive enzyme [Eipper et al., 1995; Yonekura et al., 1996; Kolhekar et al., 1997a]. Further analysis of the EXAFS data suggested a copper coordination in the oxidized enzyme composed of two inequivalent mononuclear Cu(II) sites, designated Cu_H and Cu_M, with a Cu_H(His)₃O...Cu_M(His)₂O₂ ligand distribution. Reduction led to dissociation of the bound solvent and the additional coordination of S from the methionine ligand at the Cu_M center [Boswell et al., 1996]. Proteolytic cleavage using endo lys-C was subsequently used to split the enzyme into two subdomains, each containing one copper center with proposed ligand sets [H107, H108, and H172] and [H242, H244, and M314], respectively [Kolhekar et al., 1997a].

These findings have been fully confirmed by the recent X-ray crystal structure of a truncated version of PHM, extending from residues 16 to 356 and designated PHM catalytic core (PHMcc) [Prigge et al., 1997]. The overall structure consists of two 150 residue domains, each a nine-stranded β -sandwich. Each domain binds a single catalytic copper, orienting it into the interdomain space which is completely accessible to solvent. Cu_H is bound to three histidines (H107, H108, and H172) from domain I in approximately T-shaped geometry, while Cu_M is located 11 Å distant, ligated by a solvent molecule, two histidines, and a methionine from domain II (H242, H244, and M314), in pseudo-tetrahedral geometry (Fig. 2.1).

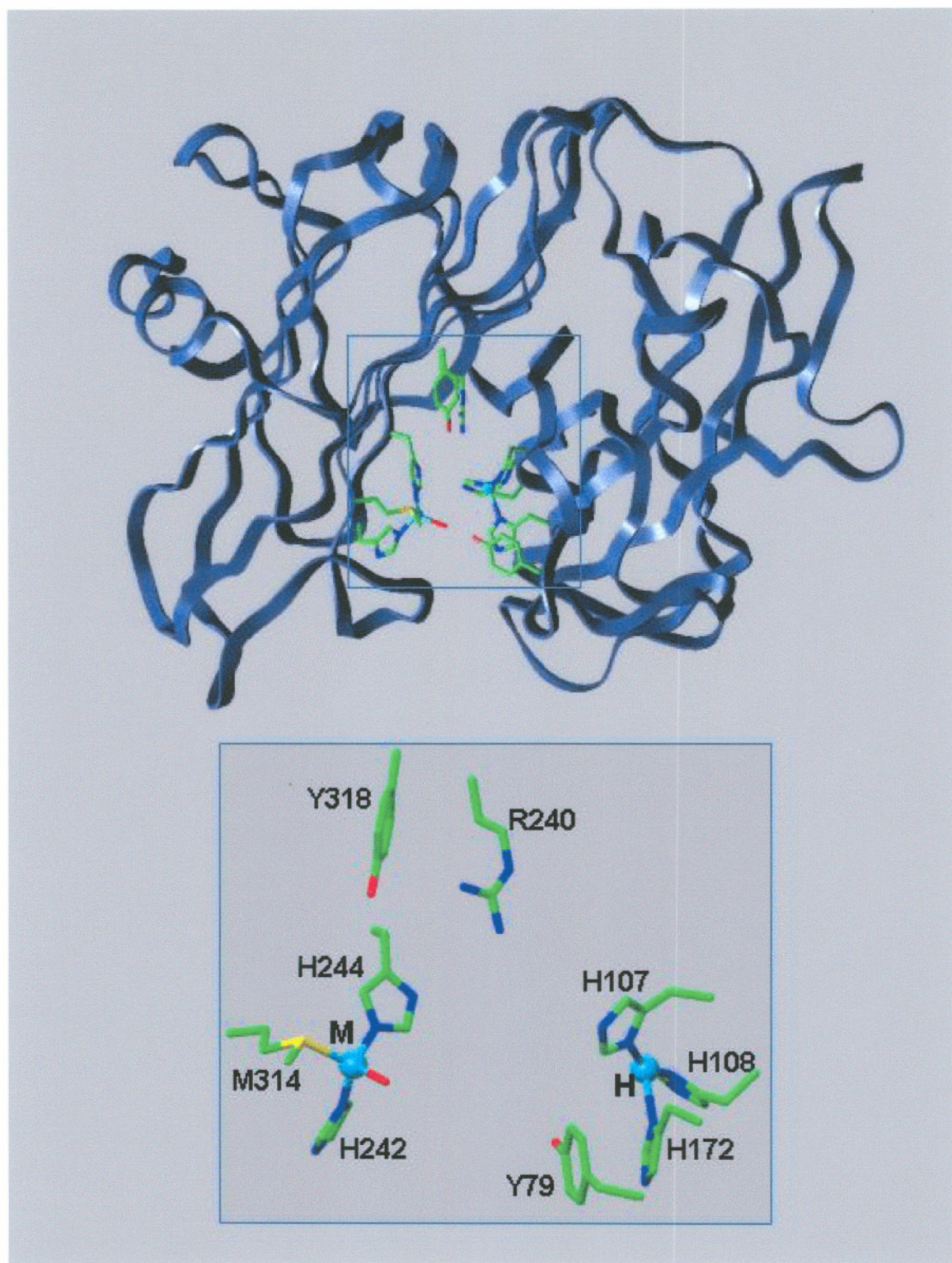


Fig. 2.1 Ribbon diagram for the PHMcc crystal structure showing the position of the catalytic copper centers and important active site residues. The inset shows an exploded view of the active site. Taken from the 1PHM data set of PDB coordinates at 1.9 Å resolution [Reedy and Blackburn, 1994].

The crystal structure of PHM has allowed an intimate look at its active site, which has generated a proposal for the mechanism of catalytic events [Prigge et al., 1997; Francisco et al., 1998]. In this mechanism, Cu^{2+} is first reduced to Cu^{1+} in two one-electron transfers to form the catalytically active dicopper(I) form. The subsequent binding of peptidyl-gly and molecular oxygen is equilibrium-ordered, which implies that the peptide substrate must bind prior to oxygen binding to ensure catalytic competence [Francisco et al., 1998]. The crystal structure shows the peptidyl-gly to be held in place by electrostatic interactions between the negatively charged C-terminal peptide carboxylate oxygens and the positively charged guanidinium group of R240 with an additional H-bond to the hydroxyl of the conserved Y318. This peptide-binding site is in domain II and is close to the oxygen-binding site at Cu_M (as previously suggested from XAS and CO binding data on a Cu_H depleted form of $D\beta M$ [Reedy and Blackburn, 1994]) with the pro-S $\text{C}_\alpha\text{-H}$ pointing directly at the solvent site on Cu_M . Thus, the crystal structure lends strong support to a mechanism involving the formation of a hydroperoxide intermediate at Cu_M , followed by rapid hydroxylation of the peptide substrate which is perfectly aligned within the active site pocket. However, the structure gives no clue to how such an intermediate can be formed, since the copper centers are 11 Å apart and no through-bond electron transfer pathway exists between them. The poor efficiency of electron transfer through disordered water [Gray and Winkler, 1996] brings into question the previously accepted premise [Reedy and Blackburn, 1994; Boswell et al., 1996; Prigge et al., 1997] that O_2 binding occurs at Cu_M and that its subsequent two-electron reduction (to form the hydroperoxide) involves long-range electron transfer between Cu_H and Cu_M [Klinman, 1996]. Some other mechanism for O_2 binding and reduction seems more likely.

Here we explore new mechanisms for O_2 binding and reduction in PHMcc via studies of CO binding to the reduced enzyme. CO has been used extensively as a model for oxygen binding to iron and copper proteins, since both ligands have empty π antibonding orbitals that are available for interactions with filled metal d-orbitals. CO and O_2 are also both neutral diatomic molecules with similar stereochemical binding requirements. Our results show that, in the absence of substrate, CO does

indeed bind to Cu_M as has previously been observed for bifunctional PAM and D β M [Blackburn et al., 1990; Pettingill et al., 1991; Boswell et al., 1996]. However, we find that substrate binding to the enzyme turns on previously undetected CO reactivity at Cu_H . This result suggests a completely new and unprecedented mechanism for electron/proton transfer between the two metal centers involving initial reaction of dioxygen at Cu_H^I to form superoxide, followed by superoxide channeling between the two copper centers and subsequent reaction of HO_2^\bullet at Cu_M^I to form the reactive hydroperoxy intermediate.

2.2 EXPERIMENTAL PROCEDURES

2.2.1 Preparation of Medium for Cell Culture

Minimal medium was prepared as follows. To 1 L of deionized (Nano-pure) water was added 1 packet α -MEM (Minimal Essential Medium), 1.23 g of Hepes, 1.35 g of glucose, 0.12 g of penicillin G, 0.2 g of streptomycin sulfate, and 0.6 g of glutamine. The pH was adjusted to 7.35, and the solution stirred for 30 min, after which 2.2 g of sodium bicarbonate was added. For serum-containing medium, 100 mL of dialyzed calf serum (Hyclone) was added to 900 mL of medium, and the solution was sterile filtered into 1 L glass or polycarbonate bottles. The medium was stored sterile at 4°C.

DMEM/F12 [Dubelco's Modified Eagle Medium, Nutrient Mixture F-12 (Ham)] medium was prepared as above, except that a 1 L packet of DMEM/F12 was used instead of α -MEM. Serum-containing medium was prepared by adding 100 mL of fetal clone II (Hyclone) to 900 mL of medium, followed by sterile filtration into glass bottles. The medium was stored sterile at 4°C.

Complete serum-free medium (CSFM) was prepared as above, except that the dialyzed calf serum or fetal clone II was omitted and 2.5 mg of insulin and 0.5 mg of transferrin were added per liter of medium. The solution was sterile filtered and stored at 4°C.

2.2.2 Cell Lines and Cell Growth

The cell lines used to express and purify PHMcc were constructed and kindly provided to us by Drs. Richard E. Mains and Betty A. Eipper (Department of Neuroscience, The Johns Hopkins School of Medicine). The pCIS.PHMcc vector carrying the PHMcc gene was constructed and stably transfected into a Chinese hamster ovary (CHO) cell line DG44 (dhfr-) (created by Dr. L. A. Chasin, Columbia University). Full details are described by Eipper and coworkers [Kolhekar et al., 1997a]. Frozen cells were thawed and grown initially on minimal medium (α -MEM, GIBCO), containing 10% dialyzed calf serum in order to ensure positive selection for cells that retained high copy numbers of the pCIS.PHMcc vector. After the first passage, the medium was changed to DMEM/F12 (GIBCO) containing 10% fetal clone II (Hyclone), which produced more rapid cell growth and higher rates of division than the minimal medium. Cell mass was amplified in NUNC triple flasks until a confluent area of 0.3–0.4 m² was achieved. At this point, the cells were trypsinized, resuspended in 75 mL of the DMEM/F12/fetal clone II serum-containing medium, and inoculated into a Cellmax 100 1.1 m² hollow-fiber bioreactor (Spectrum). In this system, the cell mass grows on the outside of hollow fibre capillaries through which oxygen-rich medium flows. Since the hollow fibers have a 4 kDa molecular weight cutoff, the secreted proteins, including PHMcc, concentrate in the extra capillary space and can be harvested daily.

The cell mass was grown for approximately 10 days on the serum-containing DMEM/F12/fetal clone II medium. The volume of medium circulated through the bioreactor was 1 L, and the medium was changed when the glucose level dropped below 50% and/or the pH dropped below 6.6. At 3 day intervals, the medium within the extra capillary space (in contact with the growing cell mass) was drained, and fresh DMEM/F12/fetal clone II-containing medium was introduced. After 10 days, the serum was eliminated from the medium, and the cells were switched to growth on CSFM. The extra capillary medium (~60 mL) was harvested daily, but the initial 4–5 days of harvested medium was discarded, because activity levels typically rose sharply after about 1 week of operation. The bioreactor consumed 1 L of CSFM/day, and the average daily PHMcc production was approximately 7–10 mg.

2.2.3 Enzyme Isolation

In a typical enzyme isolation, 7 days of bioreactor harvest were combined. Ammonium sulfate was added to 50% saturation, and the solution stirred for about 1 h. The precipitate was centrifuged and redissolved with gentle shaking in 10 mL of 50 mM potassium phosphate buffer (pH 7.5), containing 0.001% Triton X-100. The sample was then centrifuged to remove any undissolved particulates, filtered through a 0.8 μ m sterile filter, and applied to a 26/60 Hiload Superdex 75 prep grade gel filtration column (Pharmacia) at a flow rate of 2.5 mL/min. The active fractions were pooled, concentrated, and dialyzed against a buffer containing 100 mM potassium phosphate and 500 mM ammonium sulfate. This sample was then applied to a hydrophobic interaction column (Phenyl Superose HR10/10, Pharmacia) previously equilibrated with the same buffer. The column was washed with starting buffer until the baseline had returned to zero and was then eluted with 50 mM potassium phosphate (pH 7.5), containing no ammonium sulfate at a flow rate of 0.5 mL/min. The single peak was concentrated and found to be greater than 95% pure by SDS-PAGE. Typical yields of pure PHMcc were about 50 mg, starting from 7 days of bioreactor harvest.

2.2.4 PHM Mutants

Cell lines carrying specific site mutations of PHMcc (M314I and H242A) were constructed and kindly provided to us by Drs. Aparna S. Kolhekar, Richard E. Mains, and Betty A. Eipper. Full details of the construction and properties of these mutants have been reported previously [Eipper et al., 1995; Kolhekar et al., 1997a].

2.2.5 Copper Reconstitution

As isolated, PHM contained only ~ 0.3 Cu/protein. Following purification, the protein was dialyzed for 2 days in 0.05 M potassium phosphate containing 25 μ M Cu^{2+} as $\text{Cu}(\text{NO}_3)_2$, with a change of buffer after day 1. Following this procedure, the Cu/protein ratio was typically in the range 1.5–2.1. The CO:Cu binding ratio of the fully reduced protein (see below) was found to be the best index of homogeneous

loading of the copper centers and the absence of adventitiously bound copper. A value for CO:Cu of 0.5 indicated homogeneous reconstitution.

2.2.6 Copper and Protein Concentration

Protein concentration was initially determined using the Bicinchoninic Acid Protein Assay Kit (Sigma). The extinction coefficient ($A_{0.1\%}$, 280 nm) was then calculated, and the average of five experiments was found to be 0.98. Thereafter, the OD_{280} was used to determine protein concentration. OD_{280} measurements were recorded on a Shimadzu UV-268 spectrophotometer at ambient temperature. Copper concentrations were determined by flame atomic absorption on a Varian-Techtron AA5 spectrometer against standard copper solutions spanning the range 5–20 μM ; all protein samples were diluted to be within this range. In most cases, protein and copper analyses were performed on the same 1 mL sample of enzyme, which eliminated dilution errors from the determination of copper-to-protein ratios.

2.2.7 Activity Measurements

Enzyme activity was determined from the rate of oxygen consumption using a Rank Brothers oxygen electrode at 37°C. The following reagents were added to a stirred cell and were allowed to equilibrate until a flat baseline was obtained. Mes, 1660 μL of 150 mM; Cu^{2+} , 100 μL of 100 mM; catalase, 200 μL of 130,000 units/mL stock solution; ascorbate, 10 μL of 220 mM; PHM, 10 μL of 0.3–1.5 mg/mL solution. The cell was fitted with a Lucite stopper with a minimal opening to prevent oxygen from the air entering the solution. The reaction was initiated with 20 μL of 25 mM peptide substrate N-Ac-tyr-val-gly (N-AcYVG) and was allowed to run until completion (around 3 min). The slope of the line was used to calculate activity, defined as micromoles of O_2 consumed per minute per milligram of enzyme, using a value of 178 μM for the concentration of oxygen in air-saturated buffer at 37°C (Handbook of Physical Chemistry). Activities of preparations used in this study varied between 15 and 20 units/mg.

2.2.8 Measurement of CO Binding Stoichiometry

A modification of the protocol described by Reedy and Blackburn [1994] was used to measure the stoichiometry of CO binding to the copper centers in PHMcc. Sixty microliters of a concentrated PHM sample (at least 800 μM in Cu) was transferred to an airtight conical vial. An equal volume of buffer was transferred to a second airtight conical vial. Both samples were made anaerobic by vacuum flushing with Ar, and a 5-fold excess of ascorbate was added to reduce the copper centers. Both vials were connected via a T-piece to a single gas line and equilibrated with the same partial pressure of CO (~ 1 atm). A 50 μL sample of the carbonylated enzyme was removed for infrared analysis.

A small volume (5.5 μL) of hemoglobin (~ 3.4 mM in Fe sites) was made anaerobic in a serum vial by repeated vacuum flushing with Ar. To this were added 3 μL of anaerobic buffer (50 mM potassium phosphate, pH 7.5) and 2 μL of ascorbate oxidase (1 unit/ μL in 50 mM potassium phosphate, pH 7.5). The mixture was gently vacuum flushed until it darkened slightly. Two microliters of anaerobic ascorbate (330 mM in 100 mM sodium acetate, pH 6.0) was added with continued Ar flushing. After 15 min, an additional 2 μL of ascorbate was added with vacuum flushing, and the mixture was left under Ar for 20 min. A 2 mm path-length quartz cuvette fitted with an airtight septum was vacuum flushed with Ar, and 700 μL of anaerobic acetate buffer (100 mM, pH 6.0) was added. This solution was used to zero the baseline of the UV-vis spectrophotometer. After the baseline was recorded, 5 μL of ascorbate (330 mM in acetate buffer, pH 6) and 5 μL of ascorbate oxidase (1 unit/mL in 50 mM potassium phosphate, pH 7.5) were added, and the cell was inverted 10 times. An aliquot (4 μL) of the hemoglobin solution was added to the cell, the cell was inverted to mix the reagents, and a visible spectrum was recorded from 400 to 460 nm. The spectrum was rerecorded every 20 min until the absorbances at 419 nm (Hb-O₂ and Hb-CO) and 430 nm (deoxyHb) remained constant. This procedure ensured complete deoxygenation of the hemoglobin solution.

CO-saturated buffer was titrated into the deoxyhemoglobin solution in aliquots of 0.6 μL , and the absorbance at 419 nm was recorded. The change in absorbance

($\Delta\epsilon_{419}$) was plotted against the total volume of CO-saturated buffer added. The $[\text{CO}]_{\text{buffer}}$ was calculated using the equation:

$$[\text{CO}]_{\text{buffer}} = (SV)/(\Delta\epsilon_{419}l)$$

where S is the slope of the plot of $\Delta\epsilon_{419}$ versus aliquots of CO added, V is the total volume in the cuvette at the end of the titration, $\Delta\epsilon_{419}$ is the difference between the extinction coefficients of carbonmonoxy- and deoxy-hemoglobin at 419 nm, and l is the path length of the cuvette. The titration was continued using 0.6 μL aliquots from the PHM-CO reaction mixture, and the $[\text{CO}]_{\text{PHM+buffer}}$ was calculated similarly. The difference between $[\text{CO}]_{\text{PHM+buffer}}$ and $[\text{CO}]_{\text{buffer}}$ gave the concentration of CO bound to the enzyme. An aliquot of the PHM-CO reaction mixture was then analyzed for copper content, allowing the $[\text{CO}]/[\text{Cu}]$ binding ratio to be determined.

2.2.9 CO Binding to PHM in the Presence of Substrate

A 2-fold excess of substrate (N-AcYVG or hippuric acid) was added to 40 μL of PHMcc in a conical vial. The solution was made anaerobic by repeated vacuum flushing with Ar and left under 1–1.5 atm of Ar for 15 min. A 5-fold excess of ascorbate was then added with additional flushing of Ar. The vial was vacuum flushed with CO three times and was left under a constant pressure of CO for at least 20 min. Samples for IR, XAS, and stoichiometry measurements were prepared from the product.

2.2.10 Isotope Shifts and Reversibility of CO Binding

A sample of PHMcc (800 μM) was made anaerobic in a 1 mL conical vial fitted with a septum and then reduced with a 5-fold excess of ascorbate. A 2.5 mL volume of ^{13}CO gas was injected via gastight syringe into the vial (to increase the p_{CO} to approximately 2–2.5 atm), and the PHM-CO reaction mixture was allowed to equilibrate on ice for 20 min, after which its IR spectrum was recorded. The sample was then flushed with ^{12}CO at ambient pressure, and the IR spectrum was again recorded. The experiment was repeated in the presence of a 2-fold excess of N-AcYVG or 10 mM hippuric acid.

2.2.11 Titration of PHM with N-AcYVG and Subsequent Carbonylation

A sample of oxidized PHM, with an initial concentration of 1.6 mM, was separated into 5 aliquots of 40 μ L each. Each portion of enzyme received an increasing number of mole equivalents N-AcYVG peptide substrate (0.0, 0.1, 0.5, 1.0, 5.0 equiv, respectively). Each mixture was then sealed with a septum in a separate vial and made anaerobic by vacuum flushing with Ar. After anaerobiosis was achieved, the enzyme was reduced with a 5-fold excess of anaerobic ascorbate, and the PHM-substrate adduct was exposed to pure CO by vacuum flushing. Each vial was left under a pressure of CO for at least 20 min. (This time was determined previously to be sufficient for full carbonylation of small volumes of concentrated enzyme.) For each sample, 35 μ L was transferred anaerobically to an infrared cell for IR analysis.

2.2.12 IR Spectroscopy

Solution IR spectra were recorded on a Perkin-Elmer System 2000 FTIR with a liquid nitrogen-cooled mercury cadmium telluride detector. Protein solutions were injected into a 0.050 cm path-length transmission IR cell fitted with CaF₂ windows and placed in a constant humidity sample compartment that was kept at 10°C. Samples were kept at 10°C to inhibit formation of bubbles from the outgassing of carbon monoxide during infrared irradiation of the sample. Two hundred scans were collected for each sample, and the compilation and analysis of spectra were performed using the Perkin-Elmer program Spectrum for Windows. An initial spectrum (200 scans) of the empty chamber was taken and used as the background which was subtracted automatically by the program from each subsequent spectrum. To remove the large water band at 2140 cm^{-1} , 200 scans of deionized water were averaged and then manually subtracted from the protein spectra. Water background subtraction was completed using the interactive polynomial baseline subtraction routine of the Spectrum program.

2.2.13 X-ray Absorption (XAS) Data Collection and Analysis

XAS data for the CO complex of PHM were collected at the Stanford Synchrotron Radiation Laboratory (SSRL) on beam line 7.3, operating at 3.0 GeV with beam currents between 100 and 50 mA. A Si220 monochromator with 1.2 mm slits was used to provide monochromatic radiation in the 8.8–10 keV energy range. The monochromator was detuned 50% to reject harmonics. The protein samples were measured as frozen glasses in 21% glycerol at 11–14 K in fluorescence mode using a 13-element Ge detector. To avoid detector saturation, the count rate of each detector channel was kept below 100 KHz by adjusting the hutch entrance slits or by moving the detector in or out from the cryostat windows. Under these conditions, no dead-time correction was necessary. The summed data for each detector was then inspected, and only those channels that gave high quality backgrounds free from glitches, drop outs, or scatter peaks were included in the final average. Twelve 35 min scans were collected for the PHM–CO complex.

Raw data were averaged, background subtracted, and normalized to the smoothly varying background atomic absorption using the EXAFS data reduction package EXAFSPAK [George, 1990]. Energy calibration was achieved by reference to the first inflection point of a copper foil (8980.3 eV) placed between the second and third ion chambers. In any series of scans, the measured energy of the first inflection of the copper foil spectrum varied by less than 1 eV. Averaged EXAFS data were referenced to the copper calibration of the first scan of a series, since the energy drift in any series of scans was too small to perturb the EXAFS oscillations.

Data analysis was carried out by the least-squares curve-fitting program EXCURV98 which utilizes full curved-wave calculations as described by Gurman and coworkers [Gurman et al., 1984, 1986; Binsted et al., 1988; Gurman, 1989]. The application to metalloprotein systems, particularly the treatment of imidazole rings from histidine residues, and of linearly coordinated carbonyl groups by multiple scattering analysis has been described in detail in previous papers from this laboratory [Strange et al., 1987; Blackburn et al., 1991; Pettingill et al., 1991; Sanyal et al., 1993]. The parameters refined in the fit were as follows: E_0 , the photoelectron energy threshold; R_i , the distance from Cu to atom i ; and $2\sigma_i^2$, the Debye-Waller

(DW) term for atom i . In general, coordination numbers were fixed at values consistent with the crystallographic description of PHMcc and the measurements of CO binding stoichiometry, but were allowed to float in some fits to test the consistency between spectroscopic, biochemical, and crystallographic results. In the latter case, the coordination numbers were constrained to produce DW factors within reasonable limits (first shell, $0 < 2\sigma^2 < 0.015$; second shell \geq first shell). The goodness of fit was judged by reference to a goodness of fit parameter, F , defined as:

$$F^2 = \frac{1}{N} \sum_{i=1}^n k^6 (\text{data}_i - \text{model}_i)^2$$

2.3 RESULTS

2.3.1 Stoichiometry of CO Binding to Wild-Type PHM

Purified wild-type (wt) PHMcc was found to contain ≤ 0.3 Cu/protein. Therefore, it was necessary to reconstitute the enzyme with copper as described in Section 2.2. For enzyme samples used in the present work, this protocol produced enzyme with 1.3–2.1 coppers bound/molecule of PHMcc. The stoichiometry of CO binding to reduced PHMcc was determined using these reconstituted protein samples. Results from four separate experiments showed that one molecule of CO binds per two active-site coppers, with a calculated average of 0.50 CO/Cu. Data from two representative experiments are shown in Table 2.1. These results are comparable to previous results for D β M and PAM, which were also found to bind 0.5 mole equivalents of CO per Cu(I) [Blackburn et al., 1990; Boswell et al., 1996]. It is thus clear that, like D β M and PAM, the two copper centers in PHMcc are inequivalent with respect to reactivity towards carbon monoxide.

2.3.2 Infrared Analysis of CO Binding to wtPHM

Fig. 2.2a shows the Fourier transform infrared (FTIR) spectrum of CO-bound wtPHMcc. A single, strong, infrared frequency is observed at $\nu(\text{CO}) = 2093 \text{ cm}^{-1}$ assignable to the PHMcc–carbonyl complex. This value is reported in Table 2.2

Table 2.1
Stoichiometry of Carbon Monoxide Binding to Reduced PHMcc

	[CO] _{sample} (mM)	[CO] _{buffer} (mM)	[CO] _{bound} (mM)	[Cu] (mM)	[CO]/[Cu]
WT PHM ^a					
3/97	1.40	1.08	0.31	0.57	0.54
4/97	1.42	0.84	0.58	1.24	0.46
DβM ^b	2.79	2.10	0.70	1.38	0.50
PAM ^c					0.52
H242A ^a					
1/98	1.08	1.18	0	1.00	0
6/98	0.83	0.71	0	0.83	0

^a This work.

^b From Pettingill et al., 1991.

^c From Boswell et al., 1996.

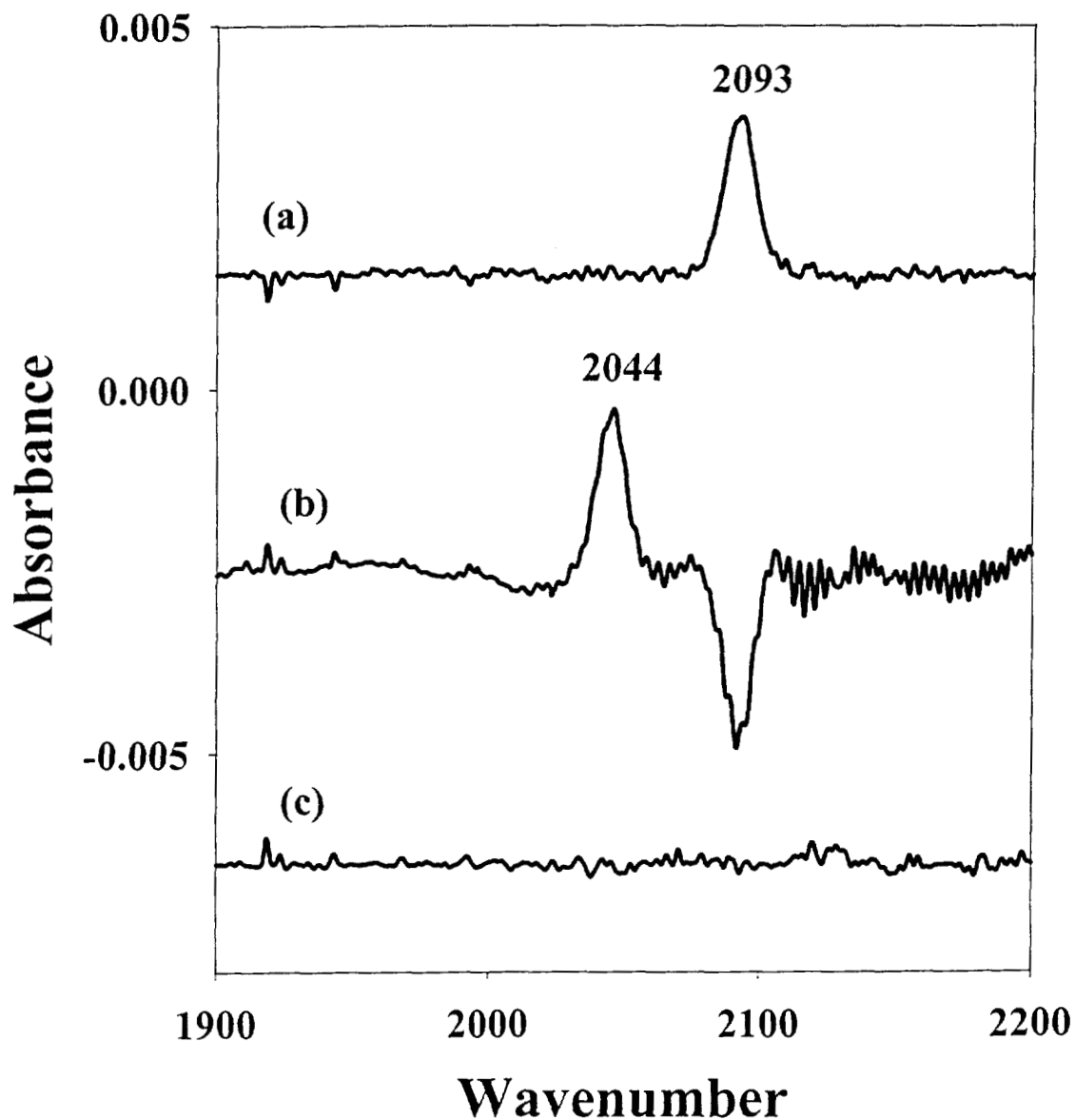


Fig. 2.2 Fourier transform infrared spectra of the complexes formed in the reaction of carbon monoxide with reduced PHMcc and a H242A site-directed mutant. (a) CO complex of wt reduced enzyme. (b) ^{13}CO minus ^{12}CO difference spectrum for the wtPHM-CO complex: the ^{12}CO spectrum was generated by vacuum flushing of the PHM- ^{13}CO complex with natural abundance CO gas. (c) FTIR spectrum of the reduced H242A mutant reacted with CO using identical conditions as in (a).

Table 2.2
Infrared Frequencies and Isotope Shifts
for Carbonyl Complexes of PHMcc and Other Copper Proteins

Protein	¹² CO	¹³ CO	$\Delta\nu(\text{CO})$	Reference
PHM^a	2093	2044	-49	This work
PHM + AcYVG ^a	2093	2044	-49	This work
	2062	2016	-46	
PHM + hippuric acid ^a	2093	2044	-49	This work
	2075	2028	-47	
DβM^b	2089			Pettingill et al., 1991
PAM^c	2093			Eipper et al., 1995
Hc^d				
Molluscan	2063	2017	-46	Fager and Alben, 1972
Limulus	2053	2007	-47	Fager and Alben, 1972
Arthropodal	2043			Fager and Alben, 1972
Cytochrome oxidase^e				
aa ₃	2062			Alben et al., 1981
bo ₃	2065			Puustinen et al., 1997

along with $\nu(\text{CO})$ values for other carbonyl complexes of copper proteins including bifunctional PAM, D β M, hemocyanin (Hc), and cytochrome *c* oxidase (CCO) for comparison. The infrared band for PHMcc is close to the published value of $\nu(\text{CO}) = 2089 \text{ cm}^{-1}$ for D β M-CO, which was assigned as the C-O stretching frequency for CO bound at the Cu_M (methionine ligated) center. The IR frequencies for molluscan Hc [Fager and Alben, 1972] and CCO [Alben et al., 1981; Dyer et al., 1989; Hosler et al., 1994; Puustinen et al., 1997] are 2063 and 2062 cm^{-1} , respectively, 20 cm^{-1} lower than the Cu-carbonyls of PHM or D β M.

2.3.3 ¹³CO Isotope Binding Data

The results of the binding of isotopically labeled ¹³CO to wtPHMcc are shown in Fig. 2.2b and Table 2.2. The FTIR spectrum of the ¹³CO-treated enzyme shows a single band at 2044 cm^{-1} , which represents an isotope shift of 49 cm^{-1} , close to the expected isotope shift of 47 cm^{-1} for a linearly coordinated CO molecule. This allows definitive assignment of the peak as a carbonyl. When the PHM-¹³CO sample was flushed with ¹²CO, the 2044 cm^{-1} peak was replaced by the 2093 cm^{-1} peak, as shown by the difference spectrum (¹³CO-¹²CO) in Fig. 2.2b. This is good evidence that CO binding to PHM is completely reversible. Similar isotope frequency shifts are found in other Cu(I)-carbonyl adducts (Table 2.2). For example, the $\nu(\text{CO})$ for Hc downshifts 46 cm^{-1} when CO is replaced with ¹³CO.

2.3.4 Copper Binding, CO Stoichiometry, and Infrared Spectroscopy of the H242A Mutant

Our data show that PHMcc binds CO at only one copper center, and comparison to previously published data on native D β M [Pettingill et al., 1991; Reedy and Blackburn, 1994] suggests that the binding occurs at the methionine-containing Cu_M center. Therefore, we examined the stoichiometry and IR spectroscopy of CO binding to a mutant which was expected to lack the Cu_M center. M314, H242, and H244 are the three endogenous ligands to Cu_M, and mutation of any one of these to a noncoordinating residue such as isoleucine or alanine would be expected to disrupt copper binding to the site. Unpublished work from our laboratory

has shown that the M314I mutant is probably unable to form the Cu_M center and that it has an unusual EXAFS spectrum indicative of a 2-coordinate, all histidine copper center (Cu_H) in its reduced form. However, this mutant still appeared to bind low levels of CO (≤ 0.2 CO/Cu) with a similar frequency to wtPHMcc, suggesting that the Cu_M center may still be able to form in the presence of CO. To overcome this ambiguity, we have investigated CO binding to the H242A mutant. The EXAFS spectrum of the reduced H242A derivative [unpublished data] is identical to that of the reduced M314I derivative with no contribution from the S(M314), which establishes unambiguously that the Cu_M center has been disrupted. Following identical protocols used for total copper reconstitution in wtPHM, the mutant H242A was found to bind only one copper per protein, confirming that one of the copper centers has been lost. The single copper in the H242A mutant was unable to bind carbon monoxide. Data from two separate CO binding experiments are presented in Table 2.1, and the FTIR spectrum (measured under identical experimental conditions to wtPHMcc) is shown in Fig. 2.2c. These data support the premise that the binding of CO takes place at the Cu_M site in PHM.

2.3.5 XAS of PHM-CO

EXAFS data for a sample of the PHM-CO complex (0.50 CO/Cu) are shown in Fig. 2.3. The Fourier transform shows a well-resolved splitting of the first shell due to the presence of short (~ 1.8 – 2.0 Å) Cu-C(CO) and Cu-N(imid) interactions and the longer (2.3 Å) Cu-S(methionine) interaction. Since the crystal structure has defined the ligand set at each of the copper centers and the stoichiometry measurement shows that CO binds to only one of the two copper centers (Cu_M), meaningful simulation of the EXAFS data can only be achieved by using a two-site model which treats each copper center separately. Our simulation method thus allowed the imidazole shells (single and multiple scattering) associated with each copper to refine independently, together with the contributions from 0.5 CO and 0.5 S(methionine) ligands. The best fit obtained is shown in Fig. 2.3 with metrical parameters listed in Table 2.3.

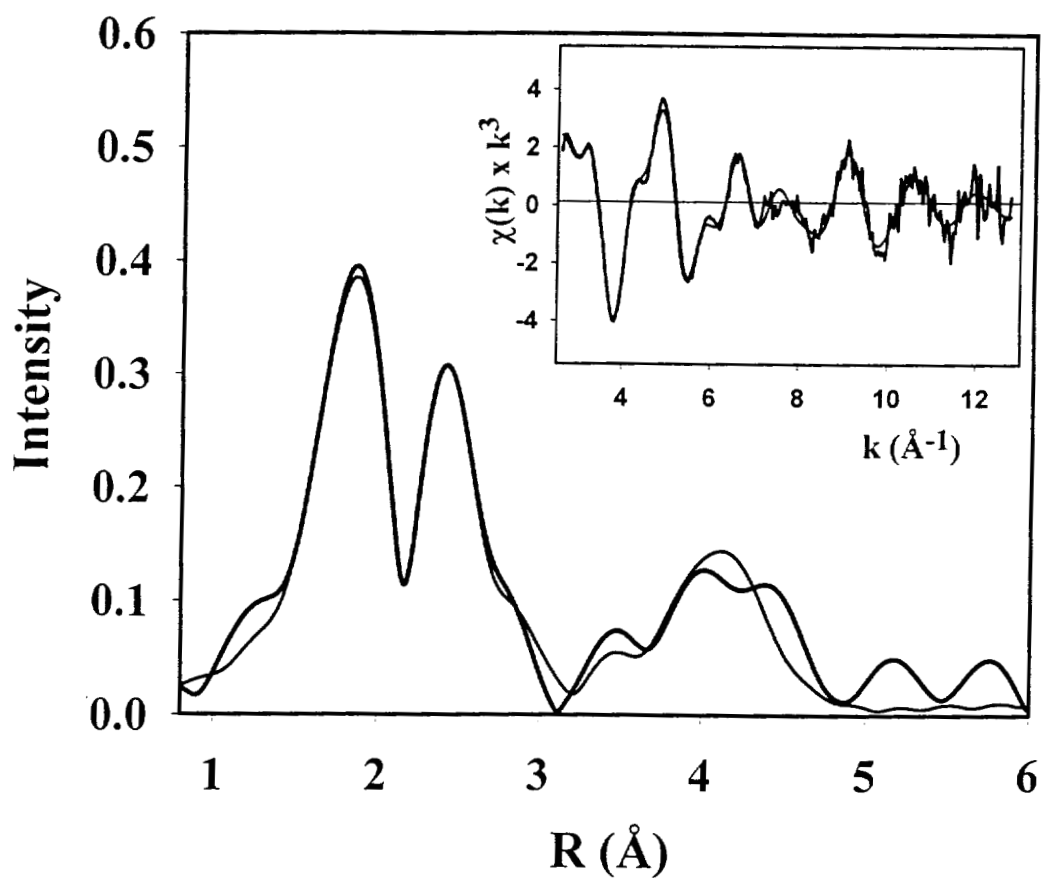


Fig. 2.3 Fourier transform and EXAFS (inset) of reduced wtPHMcc reacted with carbon monoxide. Solid thick lines represent the experimental data; solid thin lines represent the simulated data. Parameters used to generate the fit to the EXAFS data are listed in Table 2.3.

Table 2.3

**Parameters Used to Simulate the EXAFS and Fourier Transform
of Reduced Carbonylated PHMcc (PHM-CO)**

First Shell ^a			Outer Shells ^a			
Shell (X)	R (Å)	2σ ² (Å ²)	Shell (Y)	R (Å)	∠ Cu-X-Y (deg)	2σ ² (Å ²)
$F = 0.776, E_0 = -1.90 \text{ eV}$						
0.5 C (CO)	1.82	0.003	0.5 O (CO)	2.85	179	>0.050
1 N _α (imid A)	1.90	0.006	1 C _β (imid)	2.90	128	0.007
			1 C _β (imid)	2.82	235	0.007
			1 C _γ /N _γ (imid)	4.08	197	0.012
			1 C _γ /N _γ (imid)	4.15	162	0.012
1 N _α (imid B)	2.01	0.007	1 C _β (imid)	2.96	236	0.008
			1 C _β (imid)	3.02	128	0.008
			1 C _γ /N _γ (imid)	4.22	201	0.012
			1 C _γ /N _γ (imid)	4.29	164	0.012
0.5 S (M314)	2.34	0.009				

^a Estimated errors in distances are $\pm 0.01 \text{ Å}$ for the first shell and $\pm 0.03 \text{ Å}$ for outer shells except for the Cu-C(CO) distance where the error is $\pm 0.03 \text{ Å}$. Estimated errors in coordination numbers are $\pm 25\%$. $\angle \text{Cu-X-Y}$ (deg) represents the angle between the first shell scatterer (X) and the outer shell scatterer (Y). Estimated errors in angles are $\pm 5^\circ$ except for the $\angle \text{Cu-C-O}$ where the high Debye-Waller term for the carbonyl O atom precludes precise determination.

The EXAFS simulations give Cu-C(CO) and Cu-S(met) distances of 1.82 ± 0.03 and 2.33 ± 0.01 Å, respectively, and show the presence of two distinct populations of Cu-imidazole interactions at 1.90 ± 0.01 and 2.01 ± 0.01 Å, respectively. Although this splitting is at the limit of the resolution of the data ($\Delta R = \pi/2\Delta k = 0.11$ Å), it is consistent with one 2- or 3-coordinate center (Cu_H) with histidine-only coordination [Cu-N(imid) 1.90 Å] and one 4-coordinate copper center (Cu_M) with two histidines (2.01 Å), methionine-S (2.33 Å), and CO (1.82 Å). The Cu-S(met) distance is 0.10 ± 0.02 Å longer than found in uncarbonylated reduced enzyme, which is consistent with replacement of a weakly bound coordinated solvent with the stronger-field carbonyl ligand and provides strong evidence that the CO is bound at the methionine site. The Cu-CO distance of 1.82 Å is in the range expected for a Cu(I)-carbonyl [Sorrell and Malachowski, 1983; Pasquali and Floriani, 1984; Sorrell and Borovik, 1987; Villacorta and Lippard, 1987; Patch et al., 1990]. Interestingly, no multiple scattering is detected from the supposedly linear Cu-C-O triatom unit, perhaps suggesting a statically disordered orientation for the CO group.

2.3.6 CO Binding to PHMcc in the Presence of Substrate

The stoichiometry of CO binding to PHMcc in the presence of the peptide substrate N-AcYVG was determined, and the results are shown in Table 2.4. These data show that the CO binding stoichiometry for peptide-bound wtPHM increases from 0.5:1 to close to 1:1. Comparison with the data in Table 2.1 shows that the increase of CO bound per copper appears as an increase in the concentration of CO complexed in the aqueous PHM-CO sample, rather than a decrease in the copper concentration. Four individual experiments were run on four distinct preparations of PHM, and the average ratio for the stoichiometry was found to be 0.85. This strongly suggests that binding of peptide to reduced PHM activates a second site for CO binding which may be at the second copper center (Cu_H).

Table 2.4

**Stoichiometry of Carbon Monoxide Binding to wtPHMcc
in the Presence of the Peptide Substrate N-AcYVG**

Preparation	$[\text{CO}]_{\text{PHM}+\text{buffer}}$ (mM)	$[\text{CO}]_{\text{buffer}}$ (mM)	$[\text{CO}]_{\text{PHM}}$ (mM)	$[\text{Cu}]_{\text{PHM}}$ (mM)	$[\text{CO}]/[\text{Cu}]$
A	1.68	0.93	0.75	0.92	0.80
B	1.29	0.96	0.33	0.55	0.59
C	1.62	0.47	1.15	1.29	0.89
D	2.23	0.76	1.47	1.31	1.13
Average					0.85

2.3.7 Infrared Spectra and Isotope Shifts for CO Binding to PHMcc in the Presence of Substrate

The infrared spectrum of N-AcYVG-bound PHM + CO is shown in Fig.

2.4a. A second IR band at a frequency of 2062 cm^{-1} is reproducibly observed along with the original carbonyl stretching frequency at $\nu(\text{CO}) = 2093\text{ cm}^{-1}$. ^{13}CO isotope labeling studies show a shift in each band of -46 and -49 cm^{-1} , respectively, which revert back to the original frequencies upon flushing with naturally abundant CO (Fig. 2.4b). When the alternative substrate hippuric acid (benzoylglycine) was used instead of N-AcYVG, the second band shifted to 2075 cm^{-1} with an isotope shift of -47 cm^{-1} (Fig. 2.4c and d). The isotope shifts conclusively assign the substrate-induced frequencies as copper-carbonyls and show that the binding is completely reversible.

Two possibilities exist to explain the origin of the second CO band. Substrate binding could perturb the copper coordination at Cu_M such that the CO frequency was itself perturbed. In this case, we would expect that, at the high substrate concentrations used here (2 orders of magnitude above the K_m), the 2093 cm^{-1} band would be completely converted into the 2062 cm^{-1} band, as the resting state was completely converted into the substrate activated form. On the other hand, if the second CO band arises from CO binding at a second site, then we would expect the 2093 and 2062 cm^{-1} bands to coexist even at high substrate concentrations. The CO binding stoichiometry argues in favor of the latter. However, as a more stringent test, we undertook an IR titration of the enzyme under a CO atmosphere with up to a 5-fold excess of substrate. The results are shown in Fig. 2.5. The 2062 cm^{-1} band grows in and maximizes with no loss in intensity of the 2093 cm^{-1} band, indicating that the 2062 cm^{-1} band must arise from binding of CO at a second site.

2.4 DISCUSSION

The activation of dioxygen by copper monooxygenases has been studied for over three decades. Crystallographic studies on hemocyanin [Volbeda and Hol, 1989; Hazes et al., 1993; Cuff et al., 1998] and catechol oxidase [Klabunde et al., 1998] have provided a clear picture of the way that dioxygen binds and is activated in

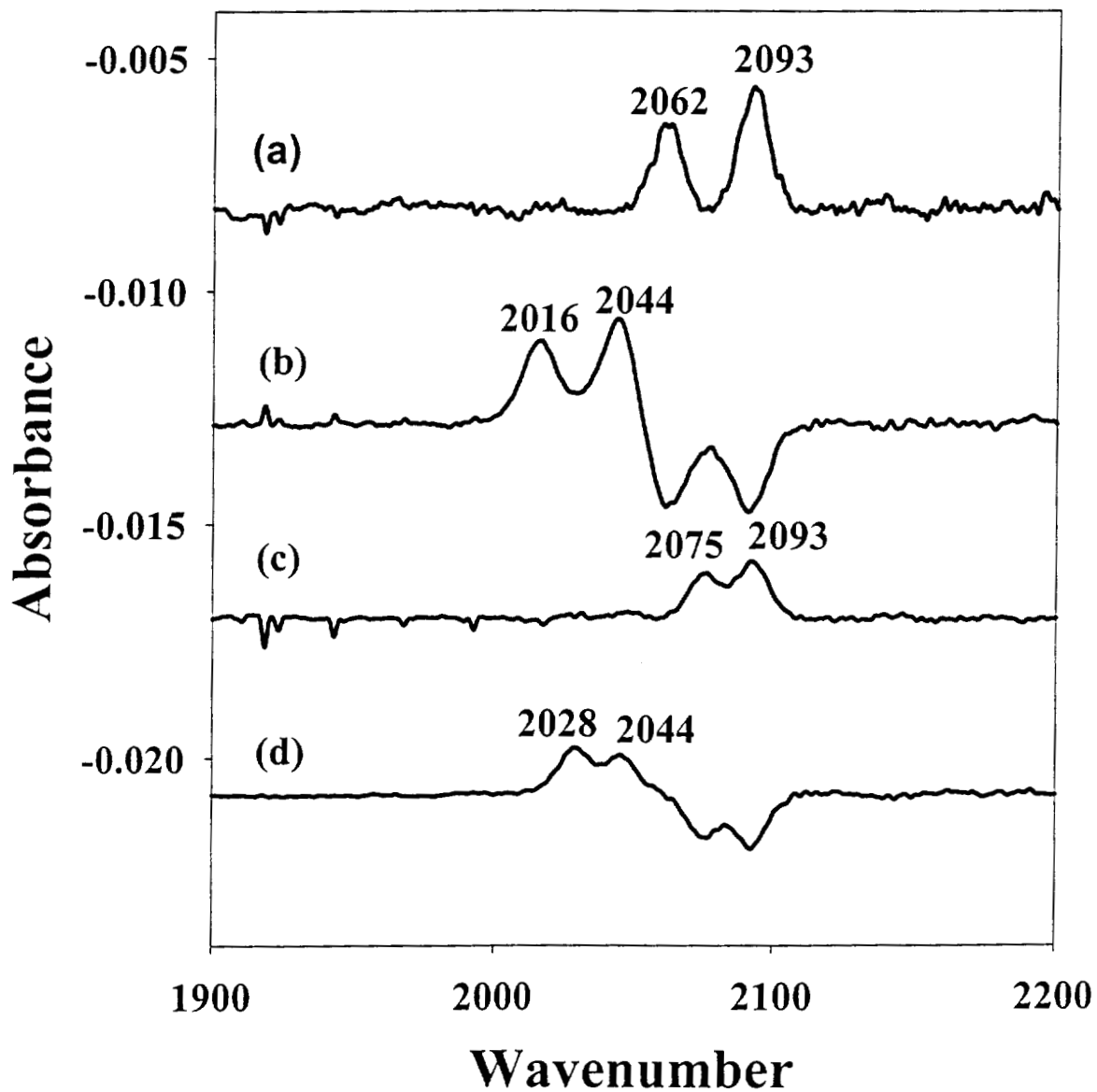


Fig. 2.4 Fourier transform infrared spectra of the complexes formed in the reaction of carbon monoxide with reduced PHMcc in the presence of substrates. (a) CO complex of wt reduced enzyme + 2 molar equivalents N-AcYVG. (b) ^{13}CO minus ^{12}CO difference spectrum for the wtPHM-CO complex + N-AcYVG; the ^{12}CO spectrum was generated by vacuum flushing of the PHM- ^{13}CO complex with natural abundance CO gas. (c) CO complex of wt reduced enzyme + 10 mM hippuric acid. (d) ^{13}CO minus ^{12}CO difference spectrum for the wtPHM-CO complex + 10 mM hippuric acid; the ^{12}CO spectrum was generated by vacuum flushing of the PHM- ^{13}CO complex with natural abundance CO gas.

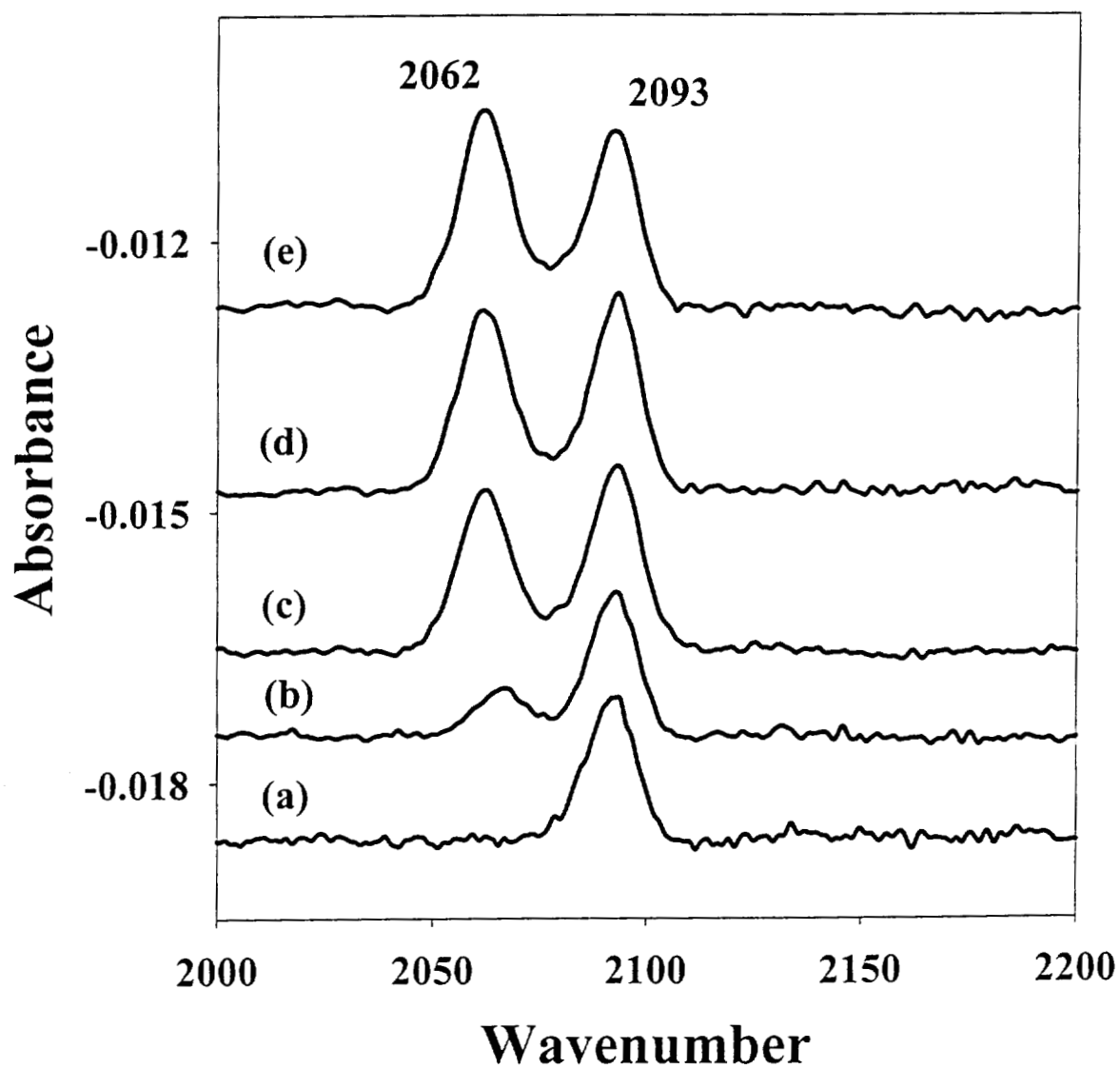


Fig. 2.5 Titration of the PHM-CO complex with increasing amounts of N-AcYVG substrate. (a) 0 equiv substrate; (b) 0.1 equiv; (c) 0.5 equiv; (d) 1.0 equiv; (e) 5.0 equiv.

dinuclear active sites. For example, in hemocyanins, the two copper atoms are each ligated by three histidine residues and are separated by 3.5–4 Å. This configuration allows the O₂ molecule to bridge in a η_2 - η_2 (side-on) fashion and to accept one electron from each copper to form coordinated peroxide. In contrast to these dinuclear systems, PHM and D β M contain mononuclear, chemically inequivalent copper centers separated by 11 Å. Comparison of the X-ray crystal structure (oxidized enzyme) with EXAFS results (oxidized and reduced forms) has revealed the catalytic copper centers in considerable detail [Boswell et al., 1996; Prigge et al., 1997]. The Cu_H center is coordinated by three histidines (H107, H108, and H172) via their N δ nitrogens in what appears to be T-shaped geometry. More recent EXAFS analysis of the reduced enzyme [unpublished data] supports a model in which the H107 and H108 residues are approximately trans to each other with short (1.88 Å) Cu–N bonds and no detectable interaction with His172. Cu_M is ligated by two histidines (H242 and H244) and a methionine (M314) with some evidence for a fourth solvent ligand. Since these centers differ by the substitution of one histidine at Cu_M for a methionine, for clarity we will refer to the Cu_H center as the histidine site and the Cu_M center as the methionine site. A crystal structure of the oxidized enzyme soaked with diiodotyrosylglycine shows that this substrate binds with its carboxylate group salt-bridged to the guanidinium group of R240 and with a further H-bond to the hydroxyl of Y318, such that the peptide is oriented towards the methionine site. In this conformation, the C $_{\alpha}$ of the substrate is nicely aligned to interact with a peroxide located at the solvent-accessible coordination position on Cu_M.

A crucial mechanistic question is how such an intermediate could be formed. The 11 Å intermetal distance precludes any kind of dioxygen bridge which might facilitate direct electron transfer from each Cu(I) to O₂. One alternative is for O₂ to bind at one of the Cu(I) centers forming a Cu(II)–superoxo complex and for the second electron necessary to complete the formation of peroxide to arrive via long-range electron transfer. Previous studies from this laboratory used CO binding to probe potential binding sites for O₂ in the related PAM and D β M enzymes and concluded that the methionine (Cu_M) locus was the site of CO/O₂ binding, based on the following evidence [Blackburn et al., 1990; Pettingill et al., 1991; Reedy and

Blackburn, 1994; Boswell et al., 1996]. First, both enzymes bound only 0.5 CO/copper, indicating that CO bound at only one of the two coppers. Second, a single intraligand CO stretching frequency was observed in the FTIR spectra at 2093 and 2089 cm^{-1} for PAM and D β M, respectively, a frequency which was more consistent with the His-His-Met ligand set at Cu_M than the (His)₃ ligand set at Cu_H. Third, we were able to prepare a Cu_H-depleted derivative of D β M, which was shown to retain both the S scattering contribution from the methionine in the EXAFS and the CO binding activity (1 CO/Cu).

On the basis of their crystal structure, Prigge and coworkers [1997] also proposed that dioxygen binds to the methionine site and is converted to peroxide via a long-range ET event. However, since the copper centers are located in different domains and the structure reveals no through-bond ET pathway shorter than ~ 50 Å, they were forced to propose that electron transfer occurs through the intervening solvent. Amzel and coworkers have recently published an X-ray crystal structure of the reduced enzyme. From comparisons with the structure of the substrate-bound oxidized form, they have proposed a novel mechanism in which electron transfer between the two coppers is mediated by the bound substrate [Prigge et al., 1999]. As discussed by Gray and Winkler [1996], long-range ET rates are strongly dependent on the medium, being greatest for β -structure and significantly less for α -helices. The efficiency of ET through H-bonded networks of *ordered* water molecules appears to be roughly equivalent to the lower limit for α -helices, predicting maximum k_{ET} values of $< 10^6$ s^{-1} for a donor-acceptor distance of 11 Å [H. B. Gray, personal communication]. The fastest step in the PHM mechanism (with hippuric acid as substrate) has been estimated by Klinman and coworkers to be the decomposition of ESO₂ with a first-order rate constant of 810 ± 120 s^{-1} [Francisco et al., 1998]. Thus, solvent-mediated ET could be consistent with the observed reaction rates, provided that the solvent provided an ordered network of H-bonds connecting the two copper centers.

Two other factors are likely to dramatically reduce the ET rates in the PHM system. First, the different coordination geometries preferred by Cu(II) and Cu(I) often impose severe Frank Condon restrictions on ET rates; second, the

reorganizational energies inherent in ET between solvated metal ions embedded in bulk solvent are also likely to lead to slower reactions. Although no data are available on electron-transfer rates in systems comparable to PHM, some insights can be obtained from comparisons of self-exchange rates of Cu(II/I) redox couples.

Cu(II/I) self-exchange rates span a wide range of values [Xie et al., 1999 and references therein]. Among the fastest are the k_{11} values for cupredoxins which lie between 10^5 and $10^3 \text{ M}^{-1} \text{ s}^{-1}$ with associated k_{ET} values around 10^6 s^{-1} [Winkler and Gray, 1992; Xie et al., 1999]. These rapid rates are generally attributed to low reorganizational energies resulting from an "entatic" state, i.e., a strained geometry around the copper center which lies midway between the preferred coordination geometries of cupric (tetragonal or square) and cuprous (tetrahedral or trigonal) sites [Holm et al., 1996]. Inorganic complexes containing macrocyclic ligands which constrain the amount of structural change possible during redox also lead to fairly rapid self-exchange rates in the range 10^3 – $10^5 \text{ M}^{-1} \text{ s}^{-1}$ [Dunn et al., 1995, 1997a,b]. Stanbury and coworkers [Xie et al., 1999] have undertaken a quantitative analysis of the internal structural reorganizational energy and the solvent reorganizational energy that accompanies redox and have correctly predicted differences between self-exchange rates. For example, although k_{11} values for the couples [Cu(II/I)(bib)₂] [bib=2,2'-bis(2-imidazolyl)biphenyl] and [Cu(II/I)(bimdpk)₂] [bimdpk=bis(1-methyl-4,5-diphenylimidazol-2-yl)ketone] are 0.16 and $1.9 \times 10^4 \text{ M}^{-1} \text{ s}^{-1}$, respectively, differing by 5 orders of magnitude, molecular dynamics calculations show convincingly that this difference can be traced to the much greater angular distortions that accompany redox reactivity of the [Cu(II/I)(bib)₂] system. For systems involving large changes in both structure and coordination number, dramatically slower self-exchange rates are observed, for example [Cu(II/I)(aq)], $5 \times 10^{-7} \text{ M}^{-1} \text{ s}^{-1}$, and [Cu(II/I)(Im)_n], $1 \times 10^{-7} \text{ M}^{-1} \text{ s}^{-1}$ [Sisley and Jordan, 1992]. These studies provide a quantitative basis for the premise that ET rates in copper complexes depend critically on the extent of structural and solvent reorganization, which accompanies the redox process and will be slow in cases involving large angular distortions or changes in coordination number.

As discussed above, our XAS data have provided evidence for significant structural change at both copper centers in PHM during redox. The Cu_H center changes from 4- or 5-coordinate tetragonal to highly distorted (T-shaped) trigonal with an estimated 0.3–0.5 Å movement of a histidine ligand (His172). The Cu_M center changes from 4- or 5-coordinate tetragonal to trigonal or tetrahedral coordination, with an estimated 0.5 Å movement of the M314 ligand. In addition, whereas the model complexes discussed above are presumed to form an outer-sphere donor–acceptor complex in which the coordination spheres of each complex touch in the transition state (with center-to-center distances of < 8 Å [Holm et al., 1996], the coordination spheres of each copper center in PHM are constrained to remain separated by 11 Å during the ET event. These structural elements all point to the conclusion that solvent-mediated ET between the copper centers of PHM is likely to be extremely slow, and other mechanisms for the formation of the Cu_M-OOH reactive intermediate should be considered.

The present work has used CO to probe the chemistry of dioxygen interaction with the copper centers of PHMcc. The results indicate a stoichiometry of 0.5 CO/Cu and a single band in the FTIR spectrum [$\nu(\text{CO}) = 2093 \text{ cm}^{-1}$]. Thus, they parallel the earlier work on PAM and D β M and establish that PHMcc also binds a single CO at the methionine site. Isotope substitution with ¹³CO confirms that the 2093 cm⁻¹ band is a Cu-carbonyl, while the facile exchange of ¹³CO with ¹²CO indicates that binding is reversible. Two other pieces of evidence provide confirmation of the assignment. First, a His242 to Ala site-directed mutant (which lacks the ability to bind copper at the methionine site) is unable to bind CO and has no IR band in the 1950–2300 cm⁻¹ region. Second, binding of CO to wtPHMcc causes a 0.10 ± 0.02 Å increase in the Cu–S(met) bond length, which is consistent with replacement of a weakly coordinating solvent by a strong field ligand such as CO at the Cu_M center. These results provide unambiguous evidence that, in the absence of substrate, a single CO binds to the methionine site.

How can this result be reconciled with the unfavorable nature of ET through solvent? The answer may lie in the additional CO binding site observed in the presence of peptide substrates. When 1 equiv of N-AcYVG is added to the CO

binding assay, the CO:Cu ratio increases towards 1 (average of 0.85), and a second FTIR band appears at 2062 cm^{-1} . The 2062 cm^{-1} band titrates with the added substrate without loss in intensity of the 2093 cm^{-1} band. ^{13}CO substitution induces a 49 cm^{-1} downshift, indicative of a coordinated carbonyl, while facile exchange with ^{12}CO establishes reversibility. This new band thus has all the properties of a Cu-carbonyl. The fact that its formation affects neither the frequency nor the intensity of the Cu_M -CO adduct proves that it must bind at a site other than Cu_M . Hence, we propose that the 2062 cm^{-1} band arises from substrate-induced binding of CO at the Cu_H (histidine) site. Of particular interest is the observation that $\nu(\text{CO})$ is dependent on the nature of the bound substrate, since with hippuric acid (benzoylglycine) the band is found at 2075 cm^{-1} , 13 cm^{-1} above that of N-AcYVG.

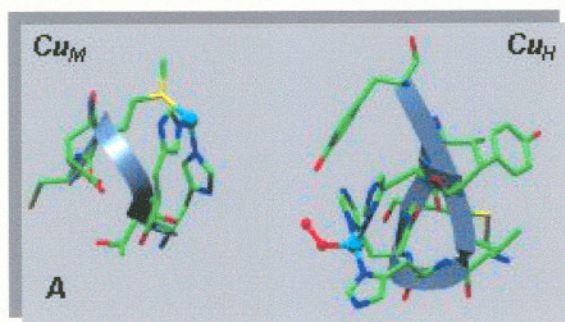
The observed frequency of the second Cu-CO is 20–30 cm^{-1} lower than that for the Cu_M -carbonyl. The lower frequency is entirely consistent with the proposed $\text{Cu}(\text{His})_3\text{CO}$ coordination. Histidine is a stronger donor than methionine, and the additional electron donation allows more back-bonding from Cu(I) to CO, thus lowering the frequency. The extensive literature of structurally characterized Cu(I) carbonyls makes it possible to further quantify this correlation between IR frequency and ligand donor set/coordination number [Pasquali and Floriani, 1984; Villacorta and Lippard, 1987; Blackburn et al., 1990]. Four-coordinate complexes with N_3CO donor atom sets typically absorb in the range 2065–2085 cm^{-1} , while three coordinate N_2CO complexes absorb above 2090 cm^{-1} . Thus, the 2093 cm^{-1} Cu_M -CO adduct obeys the correlation if we assume that the thioether S atom is essentially neutral with respect to its electron-donating power, while the 2062 cm^{-1} band is at the lower end of the range expected for a N_3CO donor atom set. It should be noted that the Cu(I)-CO complexes of other proteins with $\text{Cu}(\text{His})_3$ active sites, such as molluscan hemocyanin and cytochrome *c* oxidase, absorb at the same frequency (2062 cm^{-1}) as the Ac-YVG-induced PHM-CO complex [Fager and Alben, 1972; Alben et al., 1981; Dyer et al., 1989; Hosler et al., 1994; Puustinen et al., 1997].

The discovery that substrate binding turns on CO- and (by inference) O_2 -binding activity at the Cu_H center in PHM has allowed us to suggest a completely new mechanism for oxygen activation and formation of the reactive peroxo intermediate as

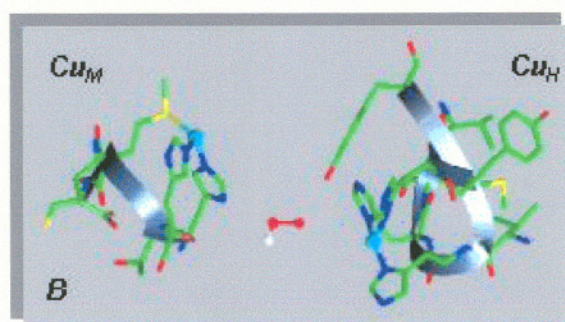
shown in Fig. 2.6. We propose that in the resting enzyme, the Cu_H site is unreactive to either CO or O_2 . Substrate binding induces a structural or electronic perturbation at Cu_H , which turns on its O_2 reactivity and results in the initial formation of a $\text{Cu}_H(\text{II})\text{-O}_2^\bullet$ intermediate. Such a step would be entirely consistent with a recent finding that the mechanism is equilibrium ordered with substrate binding first [Francisco et al., 1998]. The superoxide next dissociates from the Cu_H , either as a solvated anionic species or it picks up a proton and dissociates as the neutral HO_2^\bullet . It then diffuses across the 11 Å solvent channel where it reacts with the reduced $\text{Cu}(\text{I})_M$ center, forming the proposed Cu_M -hydroperoxo intermediate. In this mechanism, the extra electron and possibly also the proton required to form the hydroperoxo intermediate would be carried by the oxygen substrate itself rather than via a protein-based ET pathway.

A problem that remains is how the enzyme prevents diffusion of superoxide out of the channel, with the resulting uncoupling of dioxygen reduction and substrate hydroxylation. At present this remains an open question, but a number of possible scenarios exist that could circumvent superoxide leakage. One possibility is that Y79, located 4 Å from Cu_H (Fig. 2.6), could H-bond to the superoxide anion, providing an assisted channeling pathway. A second option is that dioxygen might bind at both copper centers, generating a $\text{Cu}(\text{II})$ -superoxo species at each. The superoxide formed at Cu_H might then channel, assisted by H-bonding to Y79, and undergo a dismutation reaction with the superoxide bound at Cu_M , forming the $\text{Cu}(\text{II})_M\text{-OOH}$ intermediate and regenerating a molecule of O_2 . This alternative would require superoxide to channel over a much shorter distance via the Y79-assisted pathway and provides a mechanistic role for dioxygen bound at Cu_M , thereby rationalizing our finding that CO binds strongly to the Cu_M center.

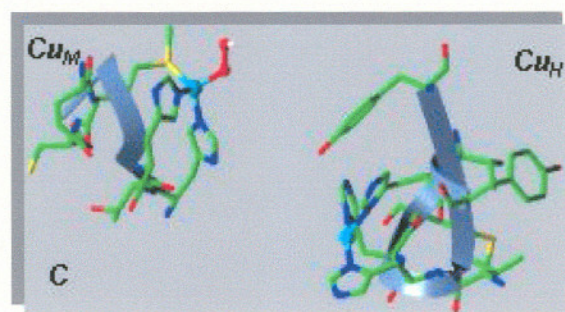
The mechanism by which substrate binding induces the proposed switch in O_2 reactivity at Cu_H remains obscure. A substrate-mediated change in the charge within the active-site pocket might induce changes in reactivity of the Cu_H center. This latter speculation is attractive since binding of substrate will neutralize the positive charge on R240, which is equidistant (7 Å) from each copper. Alternatively, it is noteworthy that the evidence for substrate binding near Cu_M comes from crystallographic studies



O₂ binds first at Cu_A forming superoxide



Superoxide channels between the Cus, which are separated by 11 Å



HO₂⁻ binds at Cu_B accepting a 2nd e and forming the hydroperoxy intermediate

Fig. 2.6 A proposed mechanism for superoxide channeling between the two copper centers of PHMcc.

on the oxidized protein, and it is possible that in the reduced form substrate might bind in a different location, closer to Cu_H . In support of this idea, we note that the infrared frequency of the CO ligand bound at Cu_M (2093 cm^{-1}) is unaffected by substrate binding, whereas $\nu(\text{CO})$ for the substrate-induced Cu_H -CO complex is extremely sensitive to the nature of the substrate (hippuric acid, 2075 cm^{-1} ; N-AcYVG, 2062 cm^{-1}). This suggests that in the reduced enzyme the substrate does not bind at the crystallographically defined position close to Cu_M , since the $\sim 4\text{ \AA}$ approach of the pro-S hydrogen atom to the CO ligand would be expected to perturb the frequency. Rather, a structural and/or electronic interaction of the substrate with the Cu_H -carbonyl seems necessary to produce the observed sensitivity of $\nu(\text{CO})$ to substrate structure. Further studies are underway to clarify these and other intriguing features of the PHM mechanism.

CHAPTER 3
CHARACTERIZATION OF A HALF-APO DERIVATIVE OF
PEPTIDYLGLYCINE MONOOXYGENASE.
INSIGHT INTO THE REACTIVITY OF EACH ACTIVE SITE COPPER*

3.1 INTRODUCTION

Copper monooxygenases use the reducing potential of copper to reversibly bind and activate oxygen for insertion into the C-H bond. They include the dicopper enzymes catechol oxidase, tyrosinase, dopamine β -monooxygenase ($D\beta M$), peptidylglycine α -hydroxylating monooxygenase (PHM), and the more complex membrane-bound methane monooxygenase (pMMO). The first two enzymes are similar to the oxygen binding protein hemocyanin, and possess binuclear copper active sites with short (2.9–4.6 Å) Cu–Cu distances and similar trishistidine ligation environments [Volbeda and Hol, 1989; Hazes et al., 1993; Cuff et al., 1998; van Gastel et al., 2000]. The short metal distances allow the formation of bridging Cu–O₂–Cu species for reduction and utilization of dioxygen [Magnus et al., 1994; Cuff et al., 1998]. $D\beta M$ and PHM fall into a different subclass due to their longer Cu–Cu distance (11 Å) and inequivalent mononuclear copper sites [Klinman, 1996; Prigge et al., 2000]. Both enzymes have similar active site structures and possess a Cu_M site, with two histidine ligands and one methionine ligand, and a Cu_H site, with three histidine ligands [Blackburn et al., 1991, 2000; Prigge et al., 1997, 1999]. PHM and $D\beta M$ also appear to reduce oxygen in a similar manner, although the exact

* Originally published in this or similar form in *Biochemistry* and used with permission of the American Chemical Society.

Jaron, S., and Blackburn, N. J. (2001) Characterization of a half-apo derivative of peptidylglycine monooxygenase. Insight into the reactivity of each active site copper. *Biochemistry* **40**, 6867–6875.

mechanism is still under investigation [Francisco et al., 1998]. A particularly intriguing question is how each copper is able to donate an electron to reduce dioxygen without forming a Cu-O₂-Cu bridging species.

PHM catalyzes the hydroxylation of glycine-extended peptide hormones, the first step in the carboxy-terminal amidation of these messenger molecules [Bradbury and Smyth, 1987; Perkins et al., 1990; Merkler and Young, 1991]. The overall mechanism is shown in Fig. 3.1. Hydroxylation of substrates by PHM is dependant on ascorbate, molecular oxygen, and copper [Tajima et al., 1990]. The two active site copper atoms redox cycle through Cu(I) and Cu(II) forms, beginning in the resting state as Cu(II) [Freeman et al., 1993]. Ascorbate binds to the enzyme reducing the coppers, followed by the ordered binding of peptide substrate and then oxygen [Francisco et al., 1998]. Electrons are donated by each copper, reducing dioxygen to peroxide which is believed to be bound at the Cu_M site. The O-O bond is homolytically cleaved, and one atom of oxygen recombines at the glycine α-C atom of the peptide substrate forming the hydroxylated product and glyoxalate [Young and Tamburini, 1989; Zabriskie et al., 1991; Merkler et al., 1992; Noguchi et al., 1992]. Recent research has attempted to elucidate the method of electron donation by each copper. Crystal structures of PHM clearly show that the coppers are too far apart to form any type of bridging complex with dioxygen, and substrate turnover by the crystal has excluded the possibility of the coppers moving close together during turnover [Prigge et al., 1997, 1999].

Two separate mechanisms have been proposed to explain how electron transfer might occur. The first mechanism is based on changes seen in the crystal structures of a variety of PHM adducts. Binding of substrate in these crystals creates a peptide bridge that significantly shortens the through-bond distance that the electron has to travel [Prigge et al., 1999]. Each copper plays a unique role in this mechanism, where Cu_M is the oxygen binding site, as historically assigned [Reedy and Blackburn, 1994; Boswell et al., 1996], and Cu_H is the electron donor. Although appealing, this mechanism has the major drawback that this type of outer-sphere reaction demands there be very little reorganization of the copper ligands under redox conditions. However, we recently reported that major structural changes occur at both copper

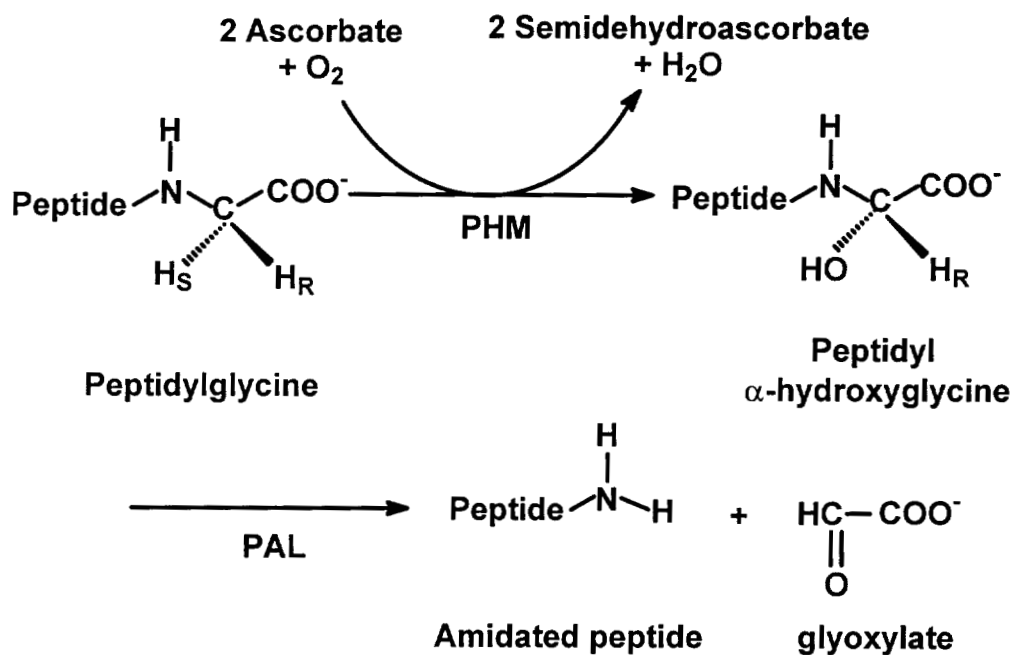


Fig. 3.1 Overall reaction scheme of the bifunctional enzyme peptidylglycine α -amidase (PAM) broken down into its two constituent activities: peptidylglycine monooxygenase (PHM) and peptidyl α -hydroxyglycine (PAL).

sites during reduction and oxidation [Blackburn et al., 2000]. Large structural changes of this sort have a significant reorganizational energy barrier, which is likely to impede the electron transfer reaction. The second mechanism proposes that electron transfer takes place through the channeling of a superoxide molecule from one copper to the other [Jaron and Blackburn, 1999]. Reorganization of the copper ligands is not so problematic in this type of inner-sphere reaction, since ligand rearrangement during the oxidation of the copper centers might initiate the transfer of superoxide. While this mechanism is an interesting possibility, it too has major drawbacks; for example, superoxide may be more likely to diffuse away from the solvent accessible active site than to travel to the second copper.

The superoxide channeling mechanism was based on studies which suggested that both coppers might interact with dioxygen or oxygen intermediates during turnover. Infrared (IR) experiments revealed that there were two sites available for CO binding in the reduced enzyme: one that was activated by the reduction of copper with ascorbate and a second that was activated by the subsequent addition of peptide substrate. The IR frequencies associated with the two sites were 2092 cm^{-1} and 2062 cm^{-1} , respectively, and were in the Cu-carbonyl stretching region [Pasquali and Floriani, 1984; Nakamoto, 1986]. Earlier work on a half-apo derivative of the enzyme $D\beta M$ definitively established the existence of a $\text{Cu}_M\text{-CO}$ with a similar IR frequency of 2089 cm^{-1} [Blackburn et al., 1990; Pettingill et al., 1991; Reedy and Blackburn, 1994]. Assignment in PHM of 2092 cm^{-1} as a $\text{Cu}_M\text{-CO}$ stretch was in part based on the findings from $D\beta M$, along with extended X-ray absorption fine structure (EXAFS) data of PHM-CO showing a lengthening of the $\text{Cu}_M\text{-S(Met)}$ bond upon coordination of CO. Appearance of the second CO stretch at 2062 cm^{-1} was not accompanied by any change in the 2092 cm^{-1} stretch, ruling out the possibility of a second CO associated with Cu_M . Therefore, we proposed that CO binding at the Cu_H site caused the substrate-inducible IR frequency.

To establish the role of each copper in the reaction mechanism of PHM, it is necessary to individually characterize the chemistry at Cu_M and Cu_H . To this end, we have used previously developed methodologies to create a half-apo derivative of the native PHM [Reedy and Blackburn, 1994]. Here we present our results on the

selective removal of Cu_H from the active site of PHM and the subsequent characterization of Cu_M chemistry. The half-apo derivative confirms our original assignment of the Cu_M -CO infrared stretching frequency at 2092 cm^{-1} and provides evidence supporting the assignment of the 2062 cm^{-1} stretch as due to Cu_H -CO. Interestingly, binding of peptide substrate continues to activate the second CO infrared stretch at 2062 cm^{-1} , originally attributed to Cu_H -CO. We suggest that binding of substrate might actively participate in metal transfer between the copper sites, allowing CO binding at the Cu_H site. If this is the case, it may imply that there is a second peptide binding site close to the Cu_H site.

3.2 EXPERIMENTAL PROCEDURES

3.2.1 Purification of Native PHM

Native enzyme (PHMcc, catalytic core residues 42–356) was purified from a Chinese hamster ovary cell line overexpressing PHM. Complete details of the preparation of the cell line, cell growth, and enzyme isolation were previously published [Kolhekar et al., 1997a; Jaron and Blackburn, 1999].

3.2.2 Determination of Copper and Protein Concentration

Protein concentration was calculated using the OD_{280} ($1\% \text{ w/w} = 0.98$). Measurements were recorded on a Shimadzu UV-268 spectrophotometer at ambient temperature. Flame atomic absorption was used to determine copper concentrations in samples. Measurements were made on a Varian-Techtron AA5 spectrometer.

3.2.3 Synthesis of the Half-Apo PHM Derivative

Samples of native PHM were selected that were known to have a copper-to-protein ratio of 2:1, activities in the normal range, and which showed normal spectroscopy. An aliquot ($500\ \mu\text{L}$) of the enzyme was dialyzed in 800 mL of buffer (50 mM potassium phosphate, pH 7.5) on ice with stirring. Carbon monoxide was then bubbled through the buffer for at least 8 h. Once the buffer and the sample were equilibrated with CO, an excess (at least 5 equiv per Cu) of anaerobic ascorbate

(stock, 330 mM in MES, pH 5) was added directly to the dialysis bag in an anaerobic environment. The dialysis bag was returned to the buffer, and bubbling with CO was continued for at least another 8 h. This procedure left the enzyme in the dialysis bag reduced and carbonylated, while excess ascorbate was dialyzed away. An aqueous stock solution of 0.1 M NaCN/0.2 M NaCl was bubbled with argon until anaerobic. Enough of this solution was transferred anaerobically to the dialysis buffer to produce a 10 μ M final cyanide concentration. Again, CO was bubbled through the buffer for at least 8 h to allow cyanide equilibrium across the dialysis membrane while maintaining the [CO] at saturating levels. Cyanide is able to bind to Cu(I) centers with vacant coordination sites and eventually will strip the metal out of the protein. Theoretically, carbon monoxide should protect the Cu(I) center from cyanide attack by effectively competing with CN⁻ for the vacant coordination position. Following cyanide equilibration, the dialysis tubing containing the treated enzyme sample was transferred under anaerobic conditions to fresh, CO-saturated, anaerobic potassium phosphate buffer (50 mM, pH 7.5), free of cyanide. This again was allowed to equilibrate for at least 8 h with CO bubbling, and the previous step was repeated to allow complete removal of copper-cyanide complexes and any free cyanide. The sample was then transferred to a conical vial under anaerobic conditions and left under an atmosphere of CO. Samples were removed for copper analysis, CO stoichiometry, infrared spectroscopy, high pressure liquid chromatography (HPLC) analysis, and X-ray absorption spectroscopy (XAS).

3.2.4 Measurement of CO Stoichiometry

The half-apo sample, created by the previous method, produces a carbonylated enzyme. A sample of the half-apo enzyme (10 μ L) and a sample of the CO saturated dialysis buffer were each transferred to separate conical vials. The dialysis buffer was used to determine the background CO concentration. An equal pressure (\sim 1 atm) of CO was introduced to both samples in tandem. The concentration of carbon monoxide in each sample was measured as previously described [Jaron and Blackburn, 1999].

3.2.5 Infrared Spectroscopy of Protein Samples

IR spectroscopy was carried out on a Perkin-Elmer System 2000 FTIR with a liquid nitrogen-cooled mercury cadmium telluride detector. Samples of enzyme solutions (50 μL) were injected into a 0.050 cm path-length sample cell with CaF_2 windows. The cell was placed in a constant humidity chamber and kept at 10°C to control the outgassing of carbon monoxide in the solution. Two hundred scans of each sample were collected and averaged using Spectrum for Windows (Perkin-Elmer). Interference from the large water absorption at 2140 cm^{-1} was eliminated by subtraction of a water spectrum. Simulation of the IR data to determine the peak frequency and area was performed on Grams/386 version 3.04 (Galactic Industries Corp.).

3.2.6 XAS Data Collection and Analysis

XAS data were collected at the Stanford Synchrotron Radiation Laboratory (SSRL) on beam lines 7.3 (BL 7.3) and 9.3 (BL 9.3) operating at 3.0 GeV with beam currents between 100 and 50 mA. An Si220 monochromator with 1.2 mm slits was used to provide monochromatic radiation in the 8.8–10 keV energy range. Harmonic rejection was achieved either by detuning the monochromator 50% at the end of the scan (9731 eV, BL 7.3) or by means of a rhodium-coated mirror with a cutoff of 13 keV placed upstream of the monochromator (BL 9.3). The protein samples were measured as frozen glasses in 20–30% ethylene glycol at 11–14 K in fluorescence mode using either a 13-element (BL 7.3) or 30-element (BL 9.3) Ge detector. To avoid detector saturation, the count rate of each detector channel was kept below 110 kHz, while the rise in fluorescent counts through the edge was kept below 20 kHz per channel. Under these conditions, no dead-time correction was necessary. A Soller slit assembly fitted with a 6μ Ni filter was used in conjunction with the 30-element detector of BL 9.3 to decrease the elastic scatter peak and further reduce detector saturation. The summed data for each detector channel were then inspected, and only those channels that gave high-quality backgrounds free from glitches, drop outs, or scatter peaks were included in the final average. Data analysis was performed as previously described [Blackburn et al., 2000; Eisses et al., 2000]. The parameters

refined in the fit were as follows: E_0 , the photoelectron energy threshold; R_i , the distance from Cu to atom i ; and $2\sigma_i^2$, the Debye-Waller (DW) term for atom i . Multiple scattering contributions were included for CO and imidazole ligands. Imidazole rings were simulated as rigid groups with fixed internal ring geometry, such that the imidazole outer shell distances were defined by the Cu-N(imid) distance and the orientation of the ring to the Cu-N bond axis. The orientation was initially chosen to be symmetrical, with the ring plane coincident with the Cu-N axis, but Cu-C β and Cu-C γ /N γ distances were later allowed to vary by up to 5% of their idealized values during refinement. The coordination numbers were also allowed to vary but were constrained to produce DW factors within reasonable limits (first shell, $0 < 2\sigma^2 < 0.015$; $\sigma^2_{\text{second shell}} \geq \sigma^2_{\text{first shell}}$). The goodness of fit was judged by reference to a goodness of fit parameter, F , defined as

$$F_2 = \frac{1}{N} \sum_{i=1}^n k^6 (\text{data}_i - \text{model}_i)^2$$

3.2.7 Activity Measurements and Substrate Turnover

HPLC was used to measure production of the hydroxylated product by the half-apo derivative. Oxygen consumption by a particular enzyme sample was first measured on a Strathkelvin Instruments 1302 oxygen electrode connected to a model 781 oxygen meter. Samples were kept at 37°C by water circulation in a RC300 respiration cell, and a magnetic spinbar was placed in the chamber for continuous stirring. Various reaction mixtures were created, and the volume was equilibrated to 2000 μL by addition of MES (100 mM, pH 5.5). All reactions were steady state and were left open to air. Final concentrations in the mixture were 0.1 μM PHM, 250 μM *N*-acetyl-Tyr-Val-Gly (YVG) or dansyl-Tyr-Val-Gly (d-YVG), 1.5 mM ascorbate, 0.01 mg/mL catalase, and 5 mM Cu^{2+} . Reaction mixtures analyzed were (1) half-apo, d-YVG, (2) half-apo, d-YVG, ascorbate, (3) half-apo, d-YVG, Cu, and (4) half-apo, d-YVG, Cu, ascorbate. All reaction mixtures were allowed to equilibrate without d-YVG, and activity was initiated by the addition of peptide substrate. Oxygen consumption was measured for 2 min, and after 10 min of reaction time, each

mixture was quenched with 200 μL of TFA (0.1% in water). The samples were then passed through a 10,000 molecular weight cutoff membrane to remove large protein. The filtrate was injected onto a Waters Delta PAK column (5 μm C18 100A, 3.9 \times 150 mm), controlled by a Waters 501 HPLC pump, in solvent A (0.1% TFA in water), and the following solvent profile was used to separate peptides: 5 min with solvent A, 5 min gradient to a mixture of 50% solvent A and 50% solvent B (0.1% TFA in 80% acetonitrile), 5 min at this mixture, 5 min gradient to 100% solvent B, 5 min at 100% solvent B, 5 min gradient to 100% solvent A, and 10 min in 100% solvent A. Effluent was measured on a Waters 474 fluorescence detector set to an excitation $\lambda = 340$ nm and an emission $\lambda = 557$ nm. Retention times for d-YVG and its hydroxylated product (d-YVG-OH) were around 16 and 15.5 min, respectively.

3.3 RESULTS

3.3.1 Stoichiometry of Copper Binding to Half-Apo PHM

A fresh preparation of the fully metalated PHM (2 coppers) was carbonylated in the normal way. This strategy was previously shown to produce an enzyme with one CO per two coppers [Jaron and Blackburn, 1999]. Dialysis of the preparation with cyanide is expected to strip any copper from the enzyme that is not protected by the binding of CO. Following removal of excess cyanide, $\text{Cu}(\text{CN})_x^{(x-1)-}$ complexes, and any free copper by repeated dialysis with fresh buffer, the copper-to-protein ratio of PHM dropped to 0.97 (Table 3.1, average of eight independent determinations). At the chosen $[\text{CN}^-]$, the final Cu-to-PHM ratio was independent of the length of dialysis.

3.3.2 Oxygen Activity and Turnover by Half-Apo PHM

Oxygen consumption by the half-apo derivative was measured on an oxygen electrode. The specific activity of half-apo PHM without additional copper (d-YVG substrate) was 2.5 $\mu\text{mole of O}_2 \cdot \text{mg}^{-1} \cdot \text{min}^{-1}$. The addition of excess copper to the enzyme increased the specific activity to 3.4 $\mu\text{mole} \cdot \text{mg}^{-1} \cdot \text{min}^{-1}$. The activity of a

Table 3.1

**Copper-to-Protein Stoichiometry of Eight Individual Preparations
of Half-Apo PHM and Their Average**

Prep	XAS #	[Cu]	[protein]	Cu:protein
1		0.454	0.557	0.815
2	S200	1.000	0.875	1.143
3		0.540	0.627	0.861
4	9300	0.465	0.420	1.107
5	9500	0.371	0.428	0.867
6		3.735	3.700	1.009
7	S1199	0.582	0.504	1.155
8		0.224	0.283	0.792
average				0.969

fully metalated native control was $5.9 \mu\text{mole} \cdot \text{mg}^{-1} \cdot \text{min}^{-1}$. The specific activity is diminished in the half-apo derivative, even upon the addition of exogenous copper, and indicates that some PHM functionality is probably lost by the derivatization by cyanide dialysis. The ability of half-apo PHM to hydroxylate its peptide substrate was measured via HPLC (Fig. 3.2, peaks have been normalized). Loss of one copper site in half-apo PHM might be expected to abolish turnover of the enzyme. Addition of excess copper to the enzyme without ascorbate results in zero oxygen consumption and no product formation (Fig. 3.2a). However, when ascorbate is added, in either the presence or absence of copper, the enzyme begins to react with oxygen and product is formed. Without added copper, oxygen consumption is slow, and there is only 50% turnover of substrate within 5 min (Fig. 3.2b). When excess copper is added to the reaction, the oxygen activity increases, and within 5 min 80% of substrate has been converted to product. Clearly, loss of the second copper site affects the overall ability of half-apo enzyme to turn over substrate, although the enzyme is still partially active. Because the copper in oxidized PHM is labile, intermolecular copper transfer is possible, and this process can be accelerated by redox cycling. Thus, under steady-state conditions, roughly one-fourth of the molecules present might be fully metalated at any given time. Fully metalated molecules of PHM are likely to retain catalytic activity, thus explaining how a sample of half-apo might retain some activity. Alternatively, some reconstitution may occur from trace concentrations of cupric ions adsorbed to surfaces or present in reagents. Previous studies with apo D β M showed that it is almost impossible to prevent low levels of reconstitution of the enzyme from these trace sources of copper [Blackburn et al., 1980].

3.3.3 EXAFS Spectroscopy of Half-Apo PHM and Half-Apo PHM in the Presence of Bound YVG Substrate

The structural environment of the coppers in half-apo PHM was probed using EXAFS. All samples were previously determined to bind a single equivalent of copper. To produce a sample of half-apo PHM without bound CO, the carbonylated half-apo derivative was exposed to three cycles of vacuum flushing with argon. The

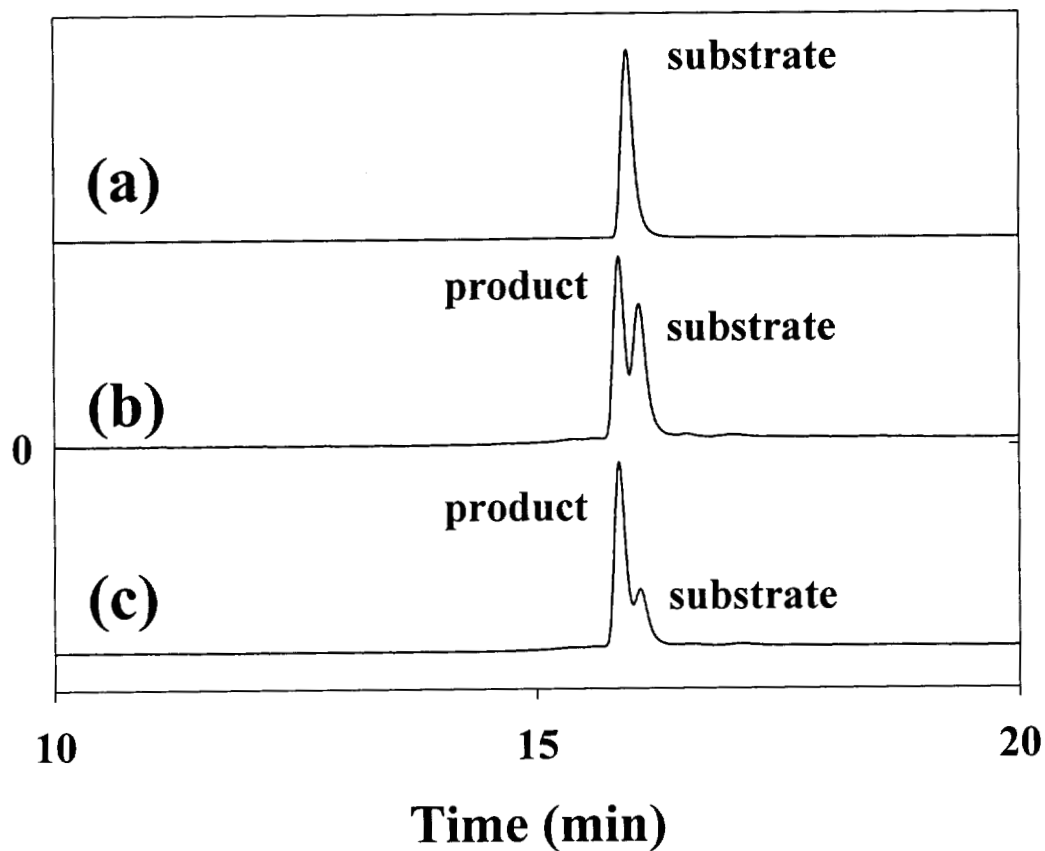


Fig. 3.2 HPLC separation of the dansylated substrate d-YVG from product d-YVG-OH following PHM turnover: (a) half-apo + catalase + Cu + d-YVG; (b) half-apo + catalase + ascorbate + d-YVG; (c) half-apo + catalase + Cu + ascorbate + d-YVG.

EXAFS and Fourier transform (FT, $\Delta k = k_{\min}$ to k_{\max}) of a typical half-apo sample (S1199, Tables 3.1 and 3.2) are shown in Fig. 3.3a (S1199 fit A, Table 3.2). The two resolved first shell peaks were fit [distance R (Å), DW (Å²)] with 2 N(His) at 1.96 (0.006) Å and 1 S(Met) at 2.31 (0.018) Å. Although the first shell distances are similar in half-apo and reduced native PHM, the splitting of the first shell Cu–N and Cu–S is more pronounced. To test the relationship to the native structure, the DW of the sulfur atom in the half-apo EXAFS was set to the value found in native PHM [Blackburn et al., 2000], and the coordination number and distance for this atom were refined. If, as anticipated, the enzyme contains only the Cu_M site, an increase in intensity of the sulfur shell in the EXAFS is expected, due to an increase in the average sulfur component from 0.5 S in native PHM to 1 S in the half-apo enzyme. With the DW fixed at 0.013 Å² (the value found previously for native reduced enzyme) the S coordination number rises from 0.5 to 0.9. This is fully consistent with the formulation of the half-apo derivative as having a single Cu_M center and no Cu_H. Fig. 3.3b shows the best fit obtained when the S(Met) contribution is eliminated. The high R shoulder on the first shell in the FT is not fit, the EXAFS fit becomes much poorer, and F more than doubles to 1.22. The results of curve fitting the EXAFS of four separate preparations of the half-apo enzyme are given in Table 3.2. The average Cu–N(His) and Cu–S(Met) distances and their DWs derived from these fits are 1.97 (0.007) Å and 2.28 (0.019) Å, respectively.

Fig. 3.4 shows the experimental and simulated EXAFS of the half-apo enzyme treated with the peptide substrate YVG. Binding of YVG substrate appears to have a significant effect on the XAS, which is most apparent in the FT. Simulation of the data indicated that fits employing a single shell of Cu(I)–imidazole interactions (2 imid at 1.93 Å, 1 S(Met) at 2.27 Å, $F = 0.78$) did not reproduce well the FT shells at 2.3 and 2.8 Å (S200 fit A, Table 3.2). On the other hand, fits which entertained the possibility of partial (~50%) copper migration to the H site were significantly better. Thus, splitting the imidazole shell into two (0.9 Cu–imid at 1.98 Å and 1.1 Cu–imid at 1.87 Å), together with a decreased intensity S(Met) interaction (0.5 S at 2.26 Å), provided a much improved fit, since the outer shell contributions from the shorter imidazole shell now fit well to the 2.8 Å transform feature. The split

Table 3.2
First Shell EXAFS Fitting Parameters for a Number of Different Preparations
of Half-Apo PHM and Their Derivatives with Bound Substrate and CO

Sample	N(His)			S(Met)			C(CO)			<i>F</i>
	<i>N</i>	Distance	DW	<i>N</i>	Distance	DW	<i>N</i>	Distance	DW	
Half-apo										
S1199 fit A	2	1.96	0.004	1	2.31	0.018				0.570
S1199 fit B	2	1.97	0.006	0						1.220
S200	2	1.94	0.007	1	2.27	0.019				1.006
9300	2	1.96	0.007	1	2.30	0.016				0.855
9500	2	2.00	0.010	1	2.25	0.022				1.025
Half-apo-YVG										
S200 fit A	2	1.92	0.010	1	2.27	0.019				0.784
S200 fit B	0.9 1.1	1.98 1.87	0.007 0.003	0.5	2.26	0.008				0.430
Half-apo-CO										
9300	2	1.97	0.005	1	2.28	0.019	1	1.82	0.001	0.699
9500	2	1.96	0.009	1	2.25	0.016	1	1.79	0.008	0.492

Distances are quoted in Å and DW factors in Å². Errors in coordination numbers are approximately 25% while errors in distances are ± 0.02–0.03 Å. *F* refers to the goodness of fit parameter defined in the text. Sample identity is defined in Table 3.1.

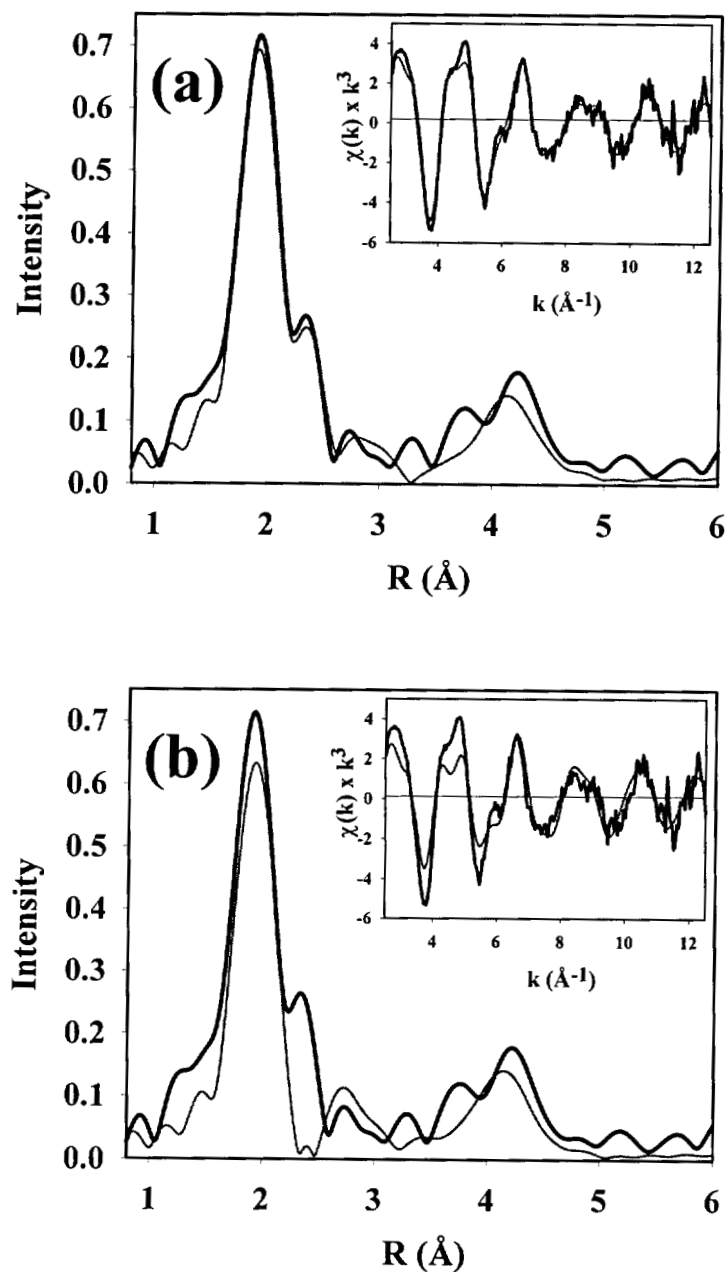


Fig. 3.3 Experimental and simulated FT and EXAFS (inset) for the sample S1199 of half-apo PHM: (a) simulated with a contribution from 1 S(Met) scatterer; (b) simulated without any contribution from the S(Met) scatterer. Raw data are shown with thick lines and simulated data with thin lines. Parameters used to fit the data are shown in Table 3.2.

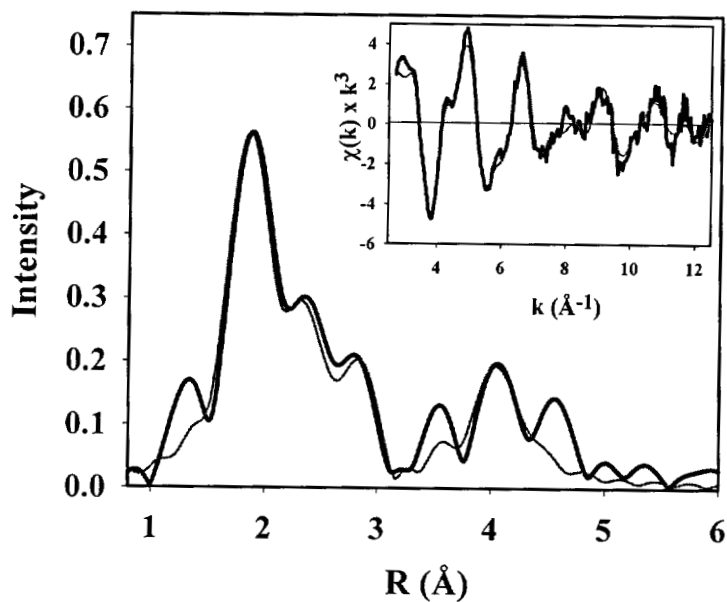


Fig. 3.4 Experimental and simulated FT and EXAFS (inset) for the sample S200 of half-apo PHM treated with 2 equiv per Cu of peptide substrate YVG. Raw data are shown with thick lines and simulated data with thin lines. Parameters used to fit the data are shown in Table 3.2.

imidazole shell fit produced an 81% decrease in the F value to 0.43 (S200 fit B, Table 3.2) and were reminiscent of fits obtained for the fully metalated reduced enzyme, where the Cu_M and Cu_H centers were found to have significantly different Cu-N(imid) bond lengths of 1.98 and 1.88 Å, respectively. An additional feature of the fit (Table 3.2) was the need to include an additional shell of low Z scatterers (0.5 N/O at 2.55 Å), without which the breadth of the transform in the 2.2–2.8 Å range could not be reproduced. The extra O/N shell may be derived either from an ordered water molecule or from the third histidine ligand at the H site (H172), which is only weakly coordinated to the copper [Blackburn et al., 2000]. Consistent with the 50% decrease in Cu-S(Met) occupation number, the data therefore suggest that binding of substrate to the half-apo enzyme induces migration of copper from Cu_M to Cu_H .

3.3.4 Stoichiometry of CO Binding to Copper in Half-Apo PHM

Following the construction of half-apo PHM, the enzyme was left under 1 atm of carbon monoxide gas. The concentration of half-apo-bound CO was determined by a titration of PHM into hemoglobin [previously described in Jaron and Blackburn (1999)]. Five different preparations and their average are shown in Table 3.3. An average ratio of 1.1 CO per copper was determined, which indicated that all of the copper atoms bound to the half-apo protein also bind CO.

3.3.5 Infrared Spectroscopy of Half-Apo PHM-CO

Following the assessment of copper and carbon monoxide content, samples of the half-apo enzyme were taken for infrared analysis. All samples analyzed were known to bind a single atom of copper and a single molecule of carbon monoxide. The infrared spectrum of the Cu-C \equiv O stretching region of a typical half-apo-CO sample is depicted in Fig. 3.5a and shows a single, strong absorption peak at 2092 cm^{-1} . Confirmation of this band as a Cu-CO and not inorganic $\text{Cu}(\text{CN})_3^{2-}$, the IR frequency of which is found at 2094 cm^{-1} [Nakamoto, 1986], comes from substitution with isotopically labeled ^{13}CO , which shows a shift of the CO stretch to 2044 cm^{-1} (Fig. 3.5b). Additionally, vacuum flushing of the carbonylated sample with argon leads to a loss of the 2092 cm^{-1} intraligand-stretching band, indicating that this stretch

Table 3.3

**Stoichiometry of CO Binding to Five Individual Preparations
of Half-Apo PHM and Their Average**

Prep	[CO]	[Cu]	CO/Cu
1	0.521	0.454	1.148
2	0.751	0.599	1.254
3	0.611	1.095	0.558
4	0.702	0.469	1.497
5	0.370	0.340	1.088
average			1.109

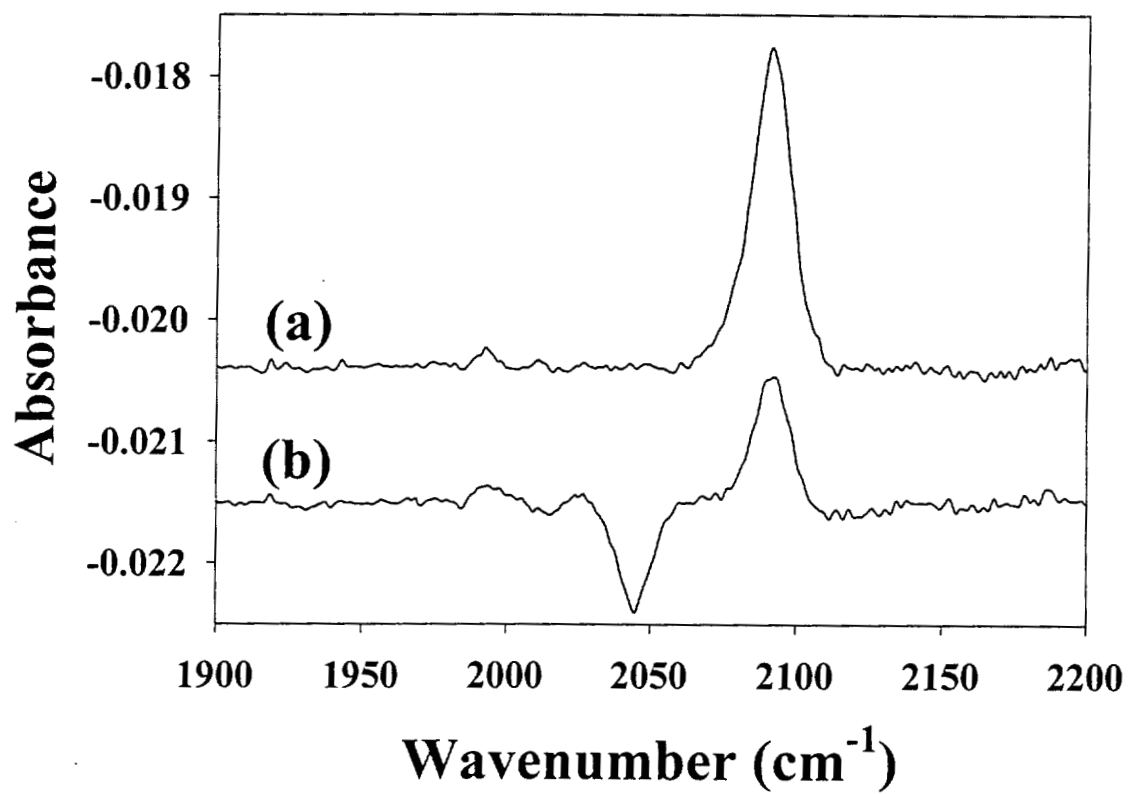


Fig. 3.5 Infrared spectra of the carbonylated half-apo enzyme: (a) half-apo PHM + ¹²CO; (b) ¹²CO minus ¹³CO data.

derives from a dissociable gaseous molecule, namely, CO. Because there is only one CO bound per Cu, all of the copper remaining bound in half-apo PHM binds carbon monoxide with a stretching frequency of 2092 cm^{-1} and therefore must have the same ligand environment. An identical $\text{C}\equiv\text{O}$ stretching frequency was identified in native PHM [Boswell et al., 1996; Jaron and Blackburn, 1999].

3.3.6 Infrared Spectroscopy of PHM-YVG-CO

Addition of YVG substrate to half-apo PHM, before or after the addition of CO, causes the appearance of a second CO stretching frequency at 2062 cm^{-1} (Fig. 3.6), similar to what was seen in native PHM. The integrated intensity of both the 2092 and 2062 cm^{-1} peaks remains approximately equal to that of the 2092 cm^{-1} single peak in the absence of substrate. However, the relative intensities of 2092 and 2062 cm^{-1} bands depend on the order of substrate addition. When CO is bound first (Fig. 3.6a), the 2062 cm^{-1} peak dominates the spectrum; when YVG is bound first (Fig. 3.6b), the 2092 cm^{-1} peak dominates. Additionally, a third peak is detected by Gaussian fitting at 2077 cm^{-1} in both cases, which is unique to the half-apo species. In an experiment using ^{13}CO gas, the 2092 and 2062 cm^{-1} bands were observed to red shift by 46–50 cm^{-1} , proving their identity as Cu-CO species; but in this case, no third band could be detected (data of low signal-to-noise not shown). In native PHM, binding of YVG was observed to activate CO binding at a second site (2062 cm^{-1}) regardless of order of substrate/CO addition and without a loss of intensity at 2092 cm^{-1} . The substrate-activated CO binding site in that enzyme was hypothesized to be at Cu_H because of an increase in the CO-to-Cu ratio from 0.5 to 1.0 that did not cause a shift in the 2092 cm^{-1} Cu_M -CO.

3.3.7 EXAFS Spectroscopy of Half-Apo PHM-CO

EXAFS and FT data for a sample of the half-apo-CO complex (sample 9500, Tables 3.1 and 3.2) are shown in Fig. 3.7. Simulations included the O atom of the C-O group (at the appropriate distance for a linear Cu-carbonyl) with its associated multiple scattering. The three different first shell ligands are clearly defined in the FT, 2 N(His) at 1.96 Å, 1 S(Met) at 2.25 Å, and a short Cu-C(CO) at 1.79 Å. One

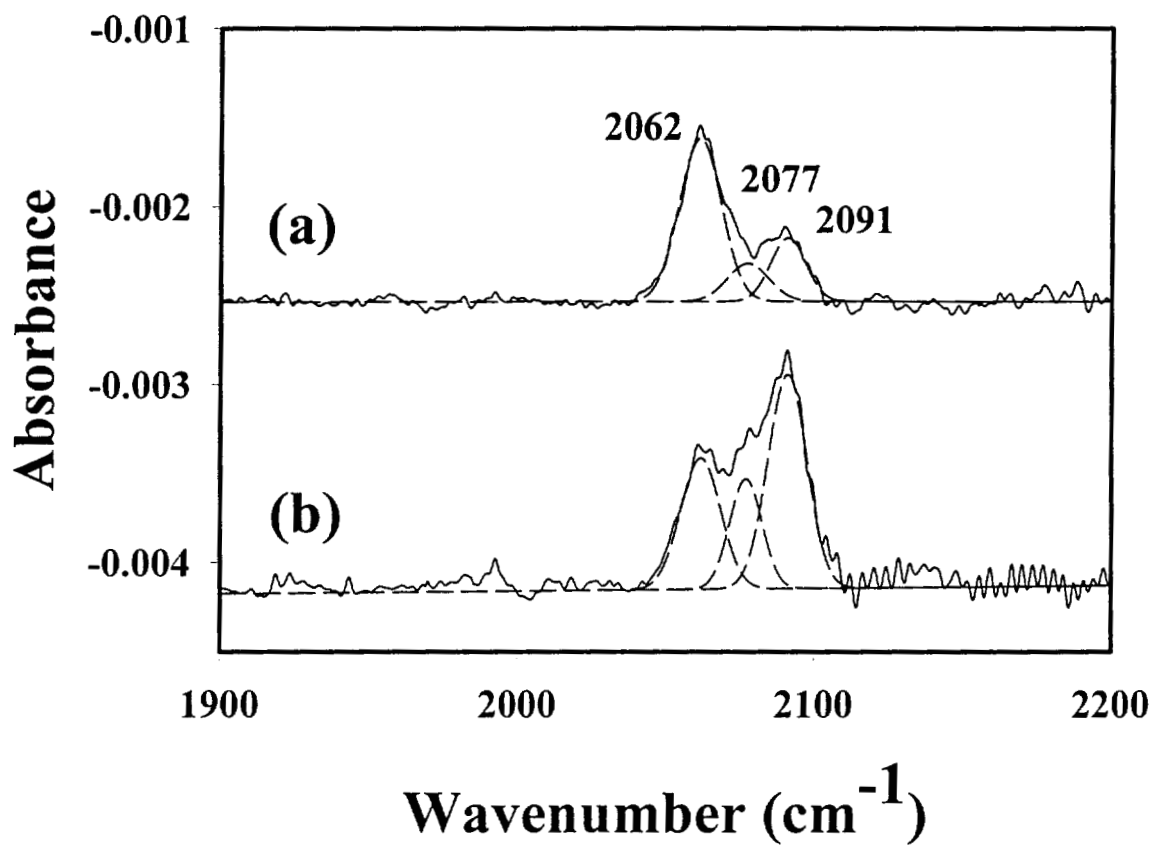


Fig. 3.6 Infrared spectrum of the carbonylated half-apo enzyme with bound YVG: (a) half-apo PHM exposed to CO and then treated with 2 equiv of YVG; (b) half-apo PHM treated with 2 equiv of YVG and then exposed to CO. Gaussian curve fitting of the IR peaks is included as dotted lines below the curves.

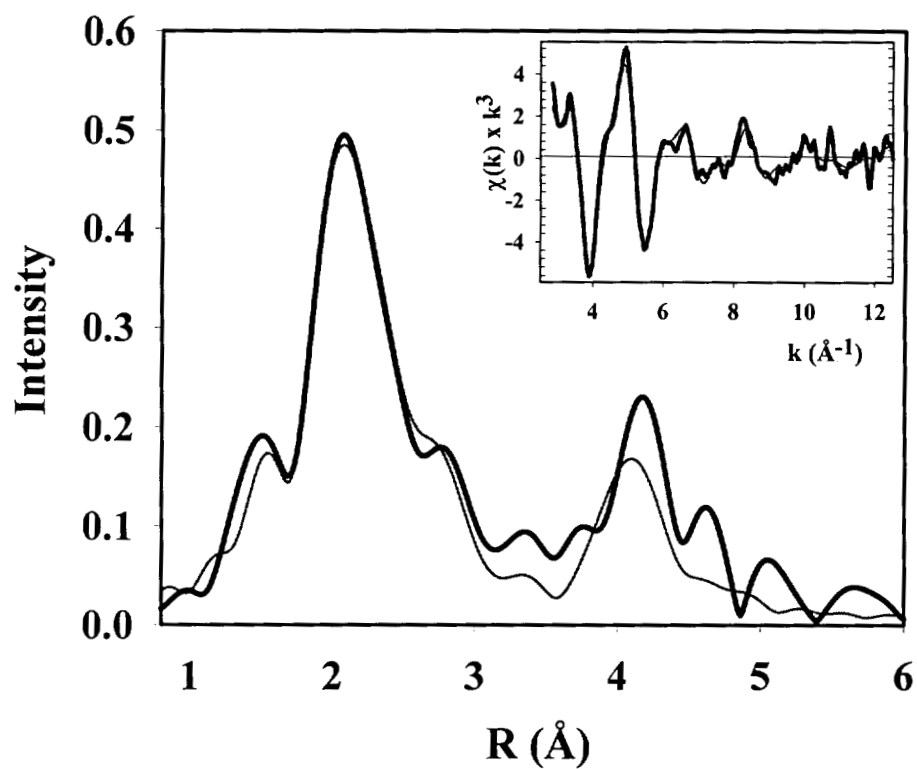


Fig. 3.7 Experimental and simulated FT and EXAFS (inset) for the sample 9500 of half-apo PHM-CO. Raw data are shown with thick lines and simulated data with thin lines. Parameters used to fit the data are shown in Table 3.2.

noticeable difference in the half-apo-CO structure is that the Cu-S distance remains unchanged from half-apo within experimental error. In native reduced PHM, there was a 0.08–0.10 Å lengthening of the Cu-S distance upon carbonylation of the enzyme [Jaron and Blackburn, 1999]. Regardless of the differences in $\Delta R_{\text{Cu-S}}$, these data indicate that in half-apo PHM the copper and the CO are both bound at the Cu_M site. Fits for two independent samples of half-apo PHM-CO are given in Table 3.2.

3.4 DISCUSSION

3.4.1 Characterization of the Half-Apo Cu_M -Carbonyl Complex

Determining the reactivity of each copper is crucial to understanding the mechanism of electron transfer in PHM, and information of this sort may aid in distinguishing between the conflicting mechanisms. One way to investigate each copper individually is to create PHM derivatives where a single copper is present. Here, we describe the successful preparation of a half-apo derivative containing only the Cu_M site and its subsequent characterization.

Cyanide is known to compete with oxygen for the Cu(I) binding sites in proteins such as D β M [Blackburn et al., 1984; Obata et al., 1987; Reedy and Blackburn, 1994] and hemocyanin [Beltramini et al., 1984; Zolla et al., 1984] due to its propensity to both coordinate and remove copper from the proteins. Results from the cyanide dialysis of native PHM show that demetalated derivatives can likewise be formed in this enzyme. Previous studies suggested that binding of CO initially takes place at only one copper center [Blackburn et al., 1990; Pettingill et al., 1991; Boswell et al., 1996; Jaron and Blackburn, 1999]. By occupying one coordination site with CO, the copper is protected from binding of additional ligands while the other copper is susceptible to stripping from the protein by cyanide in solution. Indeed, cyanide dialysis is able to remove the nonprotected copper center in PHM, leaving a half-apo derivative (copper-to-protein stoichiometry of 1:1). Furthermore, this manipulation does not adversely affect the enzyme's ability to hydroxylate substrate, because the addition of excess copper restores a significant fraction of native activity.

Carbonylation of the half-apo derivative produces a Cu-CO with a single IR stretching frequency of 2092 cm^{-1} and a 1:1 CO-to-Cu ratio. Previous investigations of the native PHM assigned the 2092 cm^{-1} IR frequency as a Cu_M -carbonyl. Since the structure of the copper center in half-apo PHM shows a strong Cu-S interaction derived from Met 314 in both the reduced and carbonylated forms, the half-apo enzyme must contain only the Cu_M center, providing unambiguous assignment of the 2092 cm^{-1} band as a Cu_M -monocarbonyl.

The 2.28 \AA Cu-S(Met) bond is 0.04 \AA longer than the distance in the reduced native enzyme (2.24 \AA), suggesting that removal of Cu_H causes a small perturbation at the Cu_M site. Carbonylation of native PHM caused a 0.1 \AA lengthening of this bond to 2.34 \AA due to the coordination of a fourth ligand at the Cu_M site. EXAFS data indicate that while binding of peptide substrate to the half-apo protein produces little change in the XAS-derived metrical parameters for the Cu_M center, it does appear to induce migration of copper from the M site to the H site. Consistent with this finding, IR evidence establishes that peptide binding activates an additional CO binding site (probably at Cu_H) in a fashion similar to what is observed in native reduced PHM [Blackburn et al., 2000]. On the basis of this, we would reason that binding of peptide appears to increase the affinity of the H site for Cu(I). However, crystallographic results of substrate binding oxidized PHM show substrate binding close to the Cu_M , requiring the active site residues Asn 316, Tyr 318, and Arg 240 to form hydrogen bonds to the peptide backbone of the substrate [Prigge et al., 1999]. Two of these residues, Asn 316 and Tyr 318, are located on the same β -strand as Met 314, and perturbation by the binding of substrate would be expected to affect the position of Met 314 in relation to Cu_M . Indeed, the K_m for YVG was significantly increased in the M314I mutant [Eipper et al., 1995]. Since there are no major changes in the Cu_M ligand environment in either the half-apo enzyme or native PHM when substrate is bound, we suggest that there might be a second stable substrate binding site as yet undetected by crystallography. We have observed that the substrate-activated $\text{C}\equiv\text{O}$ stretching frequency (2062 cm^{-1} for YVG) is dependent upon the specific substrate bound (benzoylglycine, 2075 cm^{-1} [Jaron and Blackburn, 1999]; DL-benzoylalanine, 2070 cm^{-1} [unpublished]), while the 2092 cm^{-1} Cu_M -CO frequency

is not. This would lead us to conclude that substrate binding is taking place close to a second site of CO binding that is somewhat distant from Cu_M . It is possible that during catalysis, peptide substrate is mobile, but when one or more components needed for turnover are limiting, an intermediate can be trapped. The observed intermediate might be unique, depending on the experimental method (i.e., pH and temperature), explaining why crystallography and EXAFS show conflicting results for substrate binding. If more than one substrate binding site is important in the mechanism of PHM, it is possible that during catalysis substrate switches between the two sites, perhaps initiated by the oxidation of one copper and facilitating electron transfer.

In the related enzyme $D\beta M$, a chemically derived half-apo $D\beta M$ was created which also selectively removed the Cu_A (Cu_H in PHM) site [Reedy and Blackburn, 1994]. An infrared frequency of 2089 cm^{-1} from the carbon monoxide adduct of half-apo $D\beta M$ was assigned to CO binding at the Cu_M center, which is similar to that described here for half-apo PHM. Nonetheless, the EXAFS of the half-apo $D\beta M$ EXAFS differs significantly from that of half-apo PHM. For both enzymes an increase in the average sulfur component from 0.5 S per Cu in fully metalated protein to 1.0 S per Cu in half-apo protein is expected to increase the intensity and/or decrease the DW term of the sulfur shell in the FT. Half-apo $D\beta M$ indeed follows this rule, with a significant decrease in the DW from 0.015 \AA^2 in the reduced enzyme to 0.006 \AA^2 in the half-apo enzyme [Blackburn et al., 1991; Reedy and Blackburn, 1994]. In the PHM case, although the intensity of the S shell doubles in half-apo as expected, the DW is large (0.017 \AA^2) for a single Cu-S(Met) interaction. Large DW terms generally indicate either a spread in metal-ligand distance or partial site occupancy. We have already determined that the copper in half-apo PHM all resides in the same chemical environment; therefore, it is likely that the large DW term for the Cu-S bond in half-apo PHM is due to a spread in the Cu-S distances. Reduced native PHM was also found to have a Cu-S DW (0.013 \AA^2) that was unusually large for a unique Cu-S bond, whereas in the native CO adduct the DW decreased and the Cu-S interaction became much better defined. This decrease in DW in half-apo-CO is not observed. These anomalous DW terms imply that a variety of configurations

exist with differing Cu-S interactions, suggesting the existence of “methionine-on” and “methionine-off” conformers. The movement of the Met ligated to Cu_M thus appears to be coupled in some way to the occupancy (and/or oxidation state [Blackburn et al., 2000]) of the Cu_H center and may indicate a significant role for this ligand in the mechanism of oxygen activation and/or electron transfer. How these ligand dynamics are involved and what trigger initiates the changes are still unclear.

3.4.2 Changes in the Active Site Caused by Substrate Binding

Cu_M has been unambiguously identified as the sole copper site in the active site of half-apo PHM, and this has helped confirm the assignment of the Cu_M-CO infrared frequency as 2092 cm⁻¹. In our earlier work, we identified a second CO binding site in native PHM that was activated by peptide substrate binding and showed an IR frequency of 2062 cm⁻¹ [Jaron and Blackburn, 1999]. We proposed that this CO vibration was a copper-carbonyl caused by CO binding at the Cu_H site. In half-apo, binding of substrate was therefore not expected to induce binding of CO at any additional sites or significantly perturb the Cu_M-CO already bound. Surprisingly, when substrate was bound to half-apo PHM, there was a significant decrease in the Cu_M-CO IR intensity (2092 cm⁻¹) along with the appearance of two new peaks at 2077 and 2062 cm⁻¹.

The 2077 cm⁻¹ stretch is most likely caused by small quantities of the copper-cyanide complex [Cu(CN)₄]³⁻ remaining in solution, which becomes detectable due to the low intensity of the 2092 and 2062 cm⁻¹ Cu-CO stretches. However, the presence of the second CO binding site with a 2062 cm⁻¹ frequency is unanticipated in an enzyme thought to lack all but a single copper site. There appear to be two possible explanations for this IR frequency that fit with our previous data. First, substrate binding in the vicinity of Cu_M in half-apo PHM might “super” activate the copper to ligate two or more molecules of carbon monoxide, or, second, substrate binding in half-apo might cause transfer of copper to the Cu_H site where it is activated to bind copper. Indeed, the EXAFS simulations described above have provided evidence that the latter may indeed occur.

The first hypothesis, suggesting that Cu_M binds additional molecules of CO, is appealing because half-apo PHM contains only a Cu_M site, which is thought to be a site of oxygen activity in the native enzyme. However, the copper-carbonyl stretching frequency should shift to higher frequency with ligation of additional CO groups. Studies on the coordination of CO to osmium compounds [$\text{OsHCl}(\text{CO})(\text{PPh}_3)_2$ and $\text{OsH}_2(\text{CO})_2(\text{PPh}_3)_2$] emphasize this point. The monocarbonyl-Os complex exhibits one IR detectable frequency: the asymmetric stretch at 1912 cm^{-1} . Coordination of a second molecule of CO to form the bis complex induces a second IR frequency, a bending mode, at 2014 cm^{-1} and causes a shift to higher frequency (1990 cm^{-1}) of the asymmetric stretching mode [Nakamoto, 1986]. The fact that there is no upward shift in the Cu_M 2092 cm^{-1} frequency suggests that the Cu_M site is not involved in the substrate-activated CO binding site. A further argument against the biscarbonyl assignment for the 2092 cm^{-1} band can be made on the basis of the expected decrease in π -back-bonding. As the number of bound CO molecules increases, the extent of back-bonding to each CO should diminish with an associated increase in $\nu(\text{CO})$ rather than the decrease in frequency to 2062 cm^{-1} , which is observed experimentally. Thus, it appears very unlikely that the 2062 cm^{-1} IR frequency seen in half-apo PHM is due to CO binding as $\text{Cu}_M(\text{CO})_2$.

The second explanation for the appearance of a stretch at 2062 cm^{-1} is that binding of substrate induces movement of the copper from the Cu_M site into the Cu_H site. We have argued in a previous paper that the peptide-induced CO stretch in native PHM falls into the range of trishistidine-ligated coppers and is therefore consistent with CO binding at the three histidine-ligated Cu_H site [Jaron and Blackburn 1999]. Model compounds of trisimidazole-Cu complexes with bound CO are reported to have a $\nu(\text{CO})$ at 2080 cm^{-1} [Sorrell and Borovick, 1987] at the high end, while CO complexes in hemocyanins are found between 2043 and 2063 cm^{-1} [Fager and Alben, 1972]. Substrate binding in half-apo PHM appears to induce CO binding at a site similar to the trishistidine models. The empty Cu_H center in half-apo clearly fits this description, and the IR spectra of native PHM-CO with bound substrate which showed the same $\text{C}\equiv\text{O}$ stretch at 2062 cm^{-1} was assigned as CO binding to the Cu_H site. If this is also true in half-apo PHM, then the Cu must be lost from the M-

site and rebound at the H-site. Consistent with this idea, integration of both 2093 and 2062 cm^{-1} peaks in the presence of YVG provides a total area equal to that without bound YVG, suggesting that the total concentration of CO has remained constant. This also indicates that copper is not lost from half-apo but is redistributed between the two sites.

The question then arises: how does the substrate modulate the thermodynamic or kinetic stability of the copper centers? A partial explanation may lie in the observed magnitudes of the DW terms in the EXAFS simulations. Because the DW term for the Cu-S interactions is larger in half-apo than native enzyme, it is likely that the Cu-S bond is weaker, providing a mechanism for lowering of the K_m for copper binding in the Cu_M -carbonyl. Alternatively, it is possible that the peptide substrate may actively assist in the transfer of copper from Cu_M to Cu_H , perhaps via itself becoming a ligand to Cu_H in the substrate-activated carbonyl complex. This suggestion would explain the sensitivity of the 2062 cm^{-1} band to the structure of the peptide substrates.

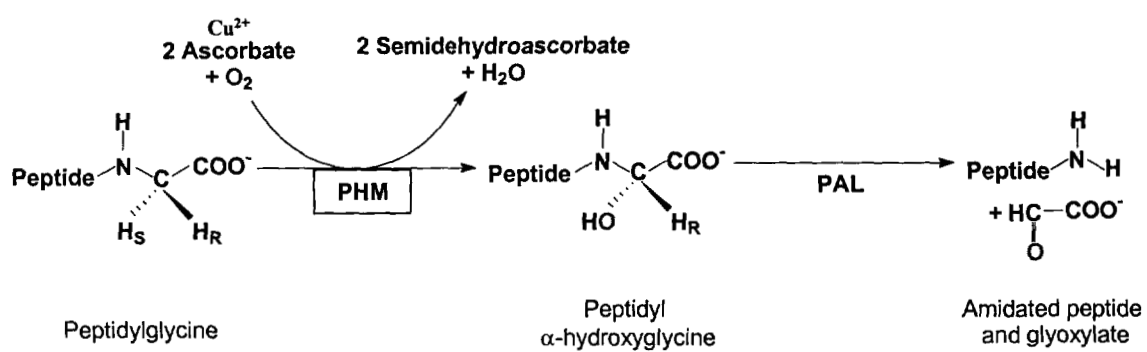
In conclusion, half-apo PHM has unambiguously established binding of CO at the Cu_M center and has provided evidence that the chemistry at the active site of the native PHM is more complex than first thought. The possibility of an alternative peptide binding site perhaps involving ligation of peptide substrate to Cu_H is intriguing. Full characterization of the Cu_H site in the absence of Cu_M will be necessary to further substantiate these findings, and these experiments are underway.

CHAPTER 4
INFRARED AND EXAFS CHARACTERIZATION OF THE H172A MUTANT
OF PEPTIDYLGLYCINE α -HYDROXYLATING MONOOXYGENASE

4.1 INTRODUCTION

Many biologically relevant neuropeptides have an amidated C-terminus. These hormones, which control such functions as digestion, labor, excretion, and regulation of blood pressure, are inactive without such a modification [Merkler, 1994]. The bifunctional enzyme peptidylglycine α -amidating monooxygenase (PAM, EC 1.14.17.3) carries out this post-translational modification in a two-step reaction [Young and Tamburini, 1989; Merkler and Young, 1991]. A different enzyme activity is responsible for each step of the reaction; they can be found together as the bifunctional enzyme PAM or as separate enzymes within close proximity [Kato et al., 1990; Perkins et al., 1990]. The first of these enzymes, termed peptidylglycine α -hydroxylating monooxygenase (PHM, EC 1.4.17.3), is responsible for the hydroxylation of the peptide substrate at the α -C carbon of a C-terminal glycine (Scheme 4.1) in a copper-, ascorbate-, and molecular oxygen-dependant manner [Freeman et al., 1993]. The product of this reaction is then converted to the amidated peptide and glyoxylate by the zinc-dependent enzyme peptidyl α -glycine lyase (PAL, EC 4.3.2.5) [Eipper et al., 1991].

Recombinant cell lines have made it possible to produce a truncated form of the PHM enzyme termed PHMcc [Kolhekar et al., 1997a]. This 35-kDa protein consists solely of the residues necessary for enzymatic activity, and crystal structures of the oxidized, reduced, and substrate-bound forms of PHMcc have recently been published [Prigge et al., 1997, 1999]. The overall structures of the three forms were similar, with a root mean square deviation of C_{α} coordinates of 0.3–0.2 Å, and



Scheme 4.1 The amidating reaction of peptidyl α -amidating monooxygenase (PAM). PHM, peptidyl α -hydroxylating monooxygenase; PAL, peptidyl α -amidating lyase.

showed that the two copper centers reside in different subdomains. Domain 1 coordinates Cu_M , which is held in a tetrahedral geometry by three backbone residue ligands (His242, His244, and Met314). Domain 2 coordinates the second copper (Cu_H), 11 Å away, in a planar T-shaped geometry by three histidine ligands (His107, His108, His172). The only major changes found between oxidized, substrate-bound, and reduced forms were the positions of two PHM residues, Gln170 and His108 (a Cu_H ligand); in reduced PHMcc, Gln170, and His108 residues are hydrogen bonded, whereas in oxidized PHMcc, a water molecule bridges the two residues. Additionally, Gln170 is connected to the peptide substrate through a water molecule in the substrate-bound form, and there is a direct connection between Q170 and H108. These crystal structures suggest a possible through-bond connectivity between Cu_H and Cu_M , mediated by the binding of peptide substrate. Recent work published by Eipper and coworkers proposed that this connectivity provides a viable electron transfer pathway from Cu_H to Cu_M through residues 108, 170, and the peptide substrate [Prigge et al., 1999].

EXAFS analyses disagreed with the crystallographic results and showed that major changes in the coordination spheres surrounding each copper occurred upon reduction of the enzyme [Blackburn et al., 2000]. The Cu_H environment changed from a 4- or 5-coordinate tetragonal to a 2- or 3-coordinate conformation, where one of the ligands became undetectable by EXAFS, implying that it had lengthened by more than 0.3 Å. The Cu_M changed from 4- or 5-coordinate tetragonal to trigonal or tetrahedral coordination with the Met-S ligand moving by 0.3–0.5 Å. Large conformational changes at a metal site are most often seen where inner-sphere molecular reactions occur, for example methane monooxygenase (MMO) [Rosenzweig et al., 1995] and galactose oxidase (GO) [Clark et al., 1990, 1994].

In wild-type PHMcc (wtPHMcc), CO binding experiments revealed that two copper sites are active toward small molecules and, by inference, O_2 binding. This suggested the possibility that Cu_H might be a site of oxygen activation. Binding of peptide substrates activated the second site for CO binding and produced a CO stretching frequency in the range of a Cu–CO, which was hypothesized to be located at Cu_H . Neither crystallography nor EXAFS have found significant changes in the

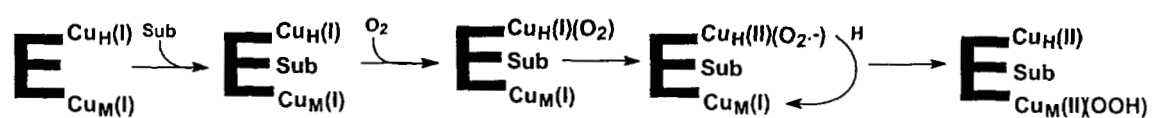
active site structure upon binding of substrate to either the oxidized or reduced forms of wtPHMcc. How substrate binding activates this site for CO/O₂ binding without causing detectable changes in the structure is unclear. Based upon the assumption that binding of CO indicates a potential O₂ binding site, a mechanism for electron transfer was proposed. This mechanism differed substantially from the substrate-mediated electron-transfer model and asserted that electron transfer is mediated by a superoxide molecule, which shuttles from Cu_H to Cu_M (Scheme 4.2) [Jaron and Blackburn, 1999]. Both mechanisms have interesting and compelling arguments in their favor, and neither can be ruled out at this time.

The detailed structural characterization of the H172A mutant of PHM is described here and was undertaken to determine the importance of this Cu_H ligand in the catalytic activity of PHM. Mutation of this histidine caused a 97% loss of the activity of the enzyme, although the structure of the oxidized enzyme is unchanged. However, reduction of the mutant caused structural changes related to a change in the ligand geometry at the Cu_H site. Further, the CO chemistry provided evidence to support our initial assignment of the peptide-induced CO binding site being located at or near the Cu_H.

4.2 EXPERIMENTAL PROCEDURES

4.2.1 Purification of the Mutant Enzyme

The Chinese hamster ovary cell line expressing the mutant PHMcc protein, H172A, was kindly provided to us by Drs. Richard E. Mains and Betty A. Eipper (Department of Neuroscience, The Johns Hopkins School of Medicine). Full details of its preparation are described by Eipper and coworkers [Kolhekar et al., 1997a]. Cells were grown in a Cellmax 100 1.1 m² hollow-fibre bioreactor (Spectrum) on CSFM as previously described except that the complete serum-free medium was supplemented with 0.5% Fetal Clone II (Hyclone). Medium containing the expressed enzyme was collected daily, and seven days' worth were combined for each purification. Proteins were purified by column chromatography, which was controlled by a Pharmacia LCC-500 fast protein liquid chromatography (FPLC)



Scheme 4.2 Proposed reaction mechanism for channeling of superoxide between the two coppers in PHM.

instrument. The protocol for protein purification incorporated a two-column process, which resulted in 99% pure enzyme. Complete details for the medium for cell culture, cell growth, and enzyme isolation were reported previously by our lab [Jaron and Blackburn, 1999].

4.2.2 Calculation of Copper and Protein Concentrations

As isolated, H172A contained only ~ 0.3 Cu/protein. Following purification, the protein was dialyzed for 2 days in 0.05 M potassium phosphate containing $25 \mu\text{M}$ Cu^{2+} as $\text{Cu}(\text{NO}_3)_2$, with a change of buffer after the first day. Following this procedure, the Cu:protein ratio was typically in the range of 1.1:1 to 1.9:1. Protein concentrations were determined using the OD_{280} , with a previously determined extinction coefficient of 0.98 [Jaron and Blackburn, 1999]. Copper concentrations were determined by flame atomic absorption on a Varian-Techtron AA5 spectrometer against standard copper solutions spanning the range 5–20 μM ; all protein samples were diluted to be within this range. In most cases, protein and copper analyses were performed on the same 1 mL sample of enzyme, which eliminated dilution errors from the determination of copper-to-protein ratios.

4.2.3 Specific Activity Measurements

Enzyme activity was determined from the rate of oxygen consumption using a Strathkelvin Instruments (SI) 1301 oxygen electrode interfaced with an SI oxygen meter, model 781. The assay mixture consisted of 0.25 μM H172A PHMCC, 150 mM MES buffer, 13,000 U/mL of catalase, 5 mM Cu^{2+} , 1.65 mM ascorbate, 0.25 mM peptide substrate, and, in some cases, 10.5 mM imidazole. All reagents except peptide substrate were equilibrated to 37°C in the cell fitted with the oxygen electrode until a flat baseline was achieved. The reaction was initiated with one of two peptide substrates, either acetyl-TyrValGly (YVG) or dansyl-TyrValGly (dYVG), and allowed to go to completion. Specific activity, defined as micromoles of O_2 consumed/min/mg of enzyme, was calculated from the initial rate of oxygen consumption. The concentration of oxygen dissolved in air-saturated buffer at 37°C was taken to be 178 μM calculated from tabulated data in the Handbook of Physical

Chemistry. wtPHMcc was used as a control for activity measurements in this study and had activities ranging between 15 and 20 U/mg. For confirmation of the results from the oxygen electrode, 200 μ L samples of the mixtures reacted with dYVG were quenched with 200 μ L of a solution of 0.1% TFA v/v (in water). These samples were then separated by HPLC.

4.2.4 HPLC Analysis

HPLC samples of enzymatic reactions were prepared by the addition of an equal volume of HPLC solvent A (0.1% TFA in water) to the sample. The acidified solution was then ultra-filtered through a 10 kDa molecular weight cutoff Microcon[®] (Millipore) centrifuge filter to remove large proteins. Samples were injected onto a Waters Delta PAK column (5 μ C18 100A, 3.9 \times 150 mm), controlled by a Waters 501 HPLC pump, in solvent A (0.1% TFA in H₂O) and the following solvent profile was used to separate peptides: 5 min with solvent A, 5 min gradient to a mixture of 50% A and 50% B (0.1% TFA in 80% acetonitrile), 5 min at this mixture, 5 min gradient to 100% B, 5 min at 100% B, 5 min gradient to 100% A, 10 min in 10% A. Effluent was measured on a Waters 474 fluorescence detector set to an excitation λ = 340 nm and an emission λ = 557 nm. Generally, the retention times for dYVG and the hydroxylated product (d-YV-OH) were \sim 16 and 15.5 min, respectively.

4.2.5 CO Binding

Binding of the CO to H172A PHMcc was carried out in the following manner. Between 50 and 150 μ L of purified H172A (\sim 1 mM in PHM) was added to a conical vial fitted with a rubber and silicone septum and kept on ice. In some experiments, YVG and/or imidazole was then added (aerobically) to achieve final concentrations equal to 3 mM. The vial was made anaerobic by gently vacuum flushing with argon no less than 8 times with 3 successive repeats over a period of 40 min. The mutant protein was reduced with a two-fold excess of ascorbate per copper. Anaerobic conditions ensured the absence of any monooxygenase activity. Carbon monoxide was introduced by vacuum flushing, and the H172A mutant sample was allowed to sit under a CO atmosphere for 20 min. At this time, it was assumed that

binding of CO was complete and samples could be removed for infrared and EXAFS analysis.

4.2.6 FTIR Analysis

Solution IR spectra were recorded on a Perkin-Elmer System 2000 FTIR with a liquid nitrogen-cooled mercury cadmium telluride detector. Protein solutions were injected into a 0.050-cm path-length transmission IR cell fitted with CaF₂ windows and placed into a constant humidity sample compartment kept at 10°C. Low temperature was needed to inhibit the formation of bubbles in the IR sample due to the out-gassing of carbon monoxide during irradiation. Each sample spectra consisted of 200 scans, compiled and background subtracted using Spectrum for Windows (Perkin-Elmer). Subtraction of a water spectrum from the protein spectrum eliminated the large water absorption at 2140 cm⁻¹. This procedure was completed using the interactive polynomial baseline subtraction routine of the Spectrum program.

4.2.7 X-ray Absorption (XAS) Data Collection and Analysis

XAS data were collected and simulated as previously described [Jaron and Blackburn, 1999]. For complete details of the beamline parameters, see Section 3.2.6.

4.3 RESULTS

4.3.1 Copper Binding Stoichiometry

Table 4.1 lists the copper binding stoichiometry for a number of individual preparations of H172A. The average copper-to-protein ratio was 1.4:1, indicating that, while both copper sites are present in the mutant enzyme, one or both copper sites has a weaker binding affinity than in wtPHMcc. wtPHMcc typically binds 1.5–2.1 Cu/protein under identical conditions [Jaron and Blackburn, 1999]. The crystal structure of wtPHMcc implicates His172 as an important Cu_H ligand, and removal of this ligand would be expected to disrupt the copper binding at this site. Interestingly, there appears to be partial or complete binding of copper to Cu_H. One

Table 4.1

**Copper-to-Protein Stoichiometry
for Five Independent Preparations of H172A PHMcc**

Preparation Number	[Cu] (mM)	[Protein] (mM)	Cu:Protein
1	3.300	1.700	1.9
2	1.500	0.971	1.5
3	0.403	0.300	1.3
4	0.175	0.179	1.0
5	1.365	1.000	1.4
Average			1.4

explanation for this disparity is that His172 may be a weak copper ligand in the reduced wtPHMcc and thus only has a limited contribution to the stability of Cu_H binding. Another possibility for the retention of copper binding at the Cu_H site is that some other molecule or residue is recruited to substitute for His172 and stabilize copper binding at this site.

4.3.2 Steady-State Activity of H172A and Lack of Rescue by Imidazole

wtPHMcc consumes 10–20 $\mu\text{M O}_2/\text{min}/\text{mg}$ [Jaron and Blackburn, 1999], while the H172A mutant measured in the same way had a specific activity of 0.065 $\mu\text{M O}_2/\text{min}/\text{mg}$. This weak activity was confirmed by an HPLC separation of substrate and product, shown in Fig. 4.1a. Only a 3% conversion of dYVG to its hydroxylated product was detected, which shows up as a small peak eluting at an earlier time than substrate compared with 90% conversion by wild type in the same time period. Mutation of His172 causes almost complete loss of PHM activity without significant loss of copper binding at Cu_H, establishing an essential role for His172 in the catalytic mechanism. An attempt to rescue turnover by the addition of 5 equiv of imidazole per protein was unsuccessful (Fig. 4.1b). Theoretically, if the reactivity of the Cu_H toward oxygen is solely reliant upon the coordination of a third histidine ligand, addition of exogenous imidazole may restore some wild-type activity. However, addition of imidazole has no effect on the oxygen consumption or turnover reaction of H172A.

4.3.3 FTIR Spectroscopy of CO Binding to H172A With and Without Bound YVG

Binding of the oxygen analog, CO, was studied using infrared spectroscopy. Infrared spectra of CO-bound H172A, in the presence and absence of peptide substrate, YVG, are shown in Fig. 4.2. In the absence of YVG, H172A binds CO with a stretching frequency of 2093 cm^{-1} (Fig. 4.2a). An identical C \equiv O stretching frequency at 2093 cm^{-1} was found in the wtPHMcc-CO and half-apo PHMcc-CO enzymes, which was assigned to a copper-carbonyl occurring at the methionine-ligated copper, Cu_M [Jaron and Blackburn, 1999, 2001]. Assuming that the Cu_M center

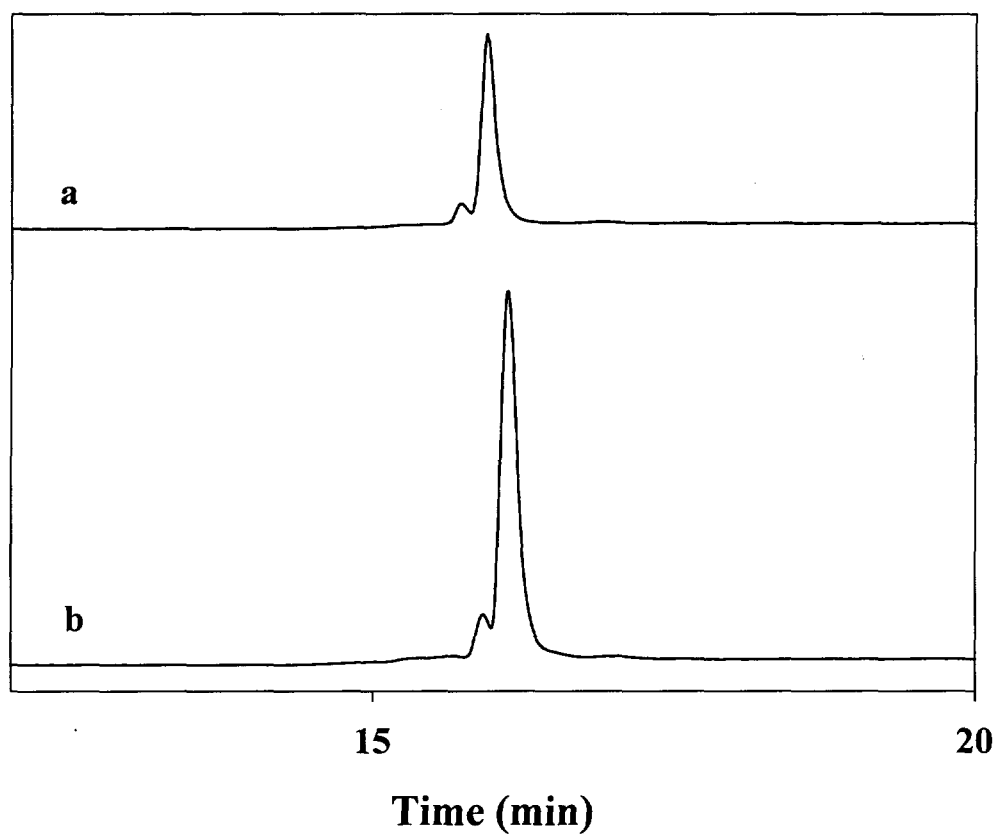


Fig. 4.1 HPLC separation of the dansylated substrate from product. Roughly 3% of the substrate is converted to product in both (a) H172A + ascorbate + copper + catalase + dYVG and (b) the previous reaction with added imidazole.

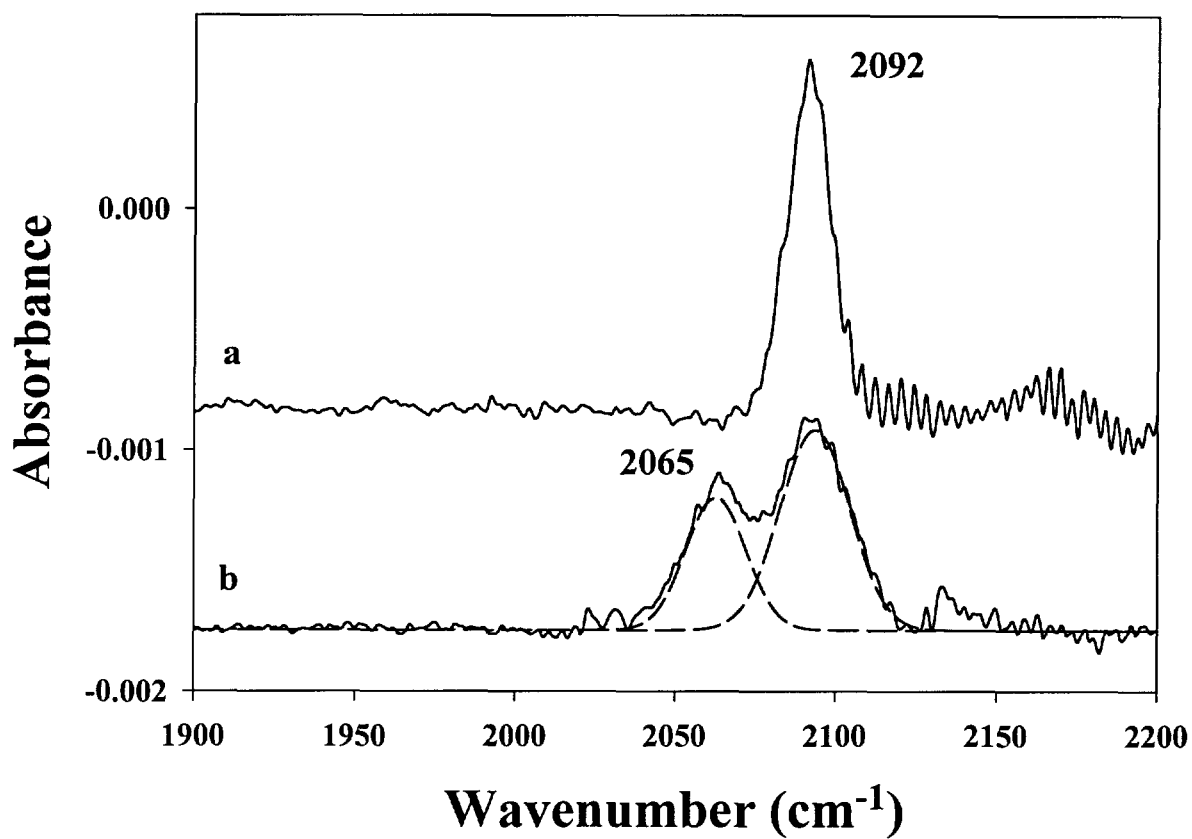


Fig. 4.2 Infrared spectra of the carbonyl stretching region for copper-carbonyls. In the absence of substrate, (a), H172A-CO has a single IR stretch at 2093 cm⁻¹. However, the presence of substrate, (b), causes an additional stretch to appear at 2065 cm⁻¹ for (H172A + YVG)-CO, which is 3 cm⁻¹ shifted from wild-type CO (2062 cm⁻¹).

remains intact in the H172A mutant, the 2093 cm^{-1} $\text{C}\equiv\text{O}$ stretch can also be assigned as a Cu_M -carbonyl.

Addition of the peptide substrate, YVG, activates a second CO binding site in H172A with an IR stretching frequency of 2065 cm^{-1} while maintaining binding of CO at Cu_M (Fig. 4.2b). A similar result was observed for wtPHMcc where binding of substrate activated a CO binding site with an IR frequency of 2062 cm^{-1} [Jaron and Blackburn, 1999]. Mutation of His172 gives rise to a 3 cm^{-1} shift to higher frequency of the substrate-activated CO stretch, suggesting that the histidine residue is involved in this site of CO binding or at least influences its frequency. There is a significant decrease in the relative intensity of the 2065 cm^{-1} stretch from wtPHMcc-CO (from 45% of the total intensity in wild type to 28% in H172A), which cannot be increased by the addition of excess peptide. The Cu:protein stoichiometry in H172A is less than 2 (see above) and, taken in conjunction with the IR intensities, can be explained by partial site occupancy of copper at the substrate-induced CO binding site.

4.3.4 X-ray Absorption Spectroscopy

4.3.4.1 Oxidized H172A. The background subtracted EXAFS spectrum of the oxidized H172A mutant and its Fourier transform are shown in Fig. 4.3 (parameters are shown in Table 4.2). The spectrum was fit with an average of 4 O/N first shell scatterers at a distance of 1.97 \AA . The intense peak in the Fourier transform at 1.97 \AA , with minor peaks at ~ 3.5 and 4.0 \AA , is typical of the histidine coordination seen in oxidized wtPHMcc [Blackburn et al., 2000]. The minor peaks represent imidazole outer shell scattering. Simulations including a first shell S (Met314) were excluded because they gave no improvement in the fit index, indicating that the Cu-S bond must be weak and/or long. The EXAFS spectra provide an averaged structure for all coppers in the protein and therefore suggest either (a) there is a single copper site, Cu_M , in the mutant enzyme or (b) there are two copper sites, a Cu_M site and a 4-coordinate Cu_H site. H172A has a Cu/protein > 1.2 , which implies that there is more than one copper site and strongly favors interpretation b. Therefore, we conclude that, like the wtPHMcc structure, oxidized H172A consists of two 4-coordinate copper sites ligated only by histidines and water.

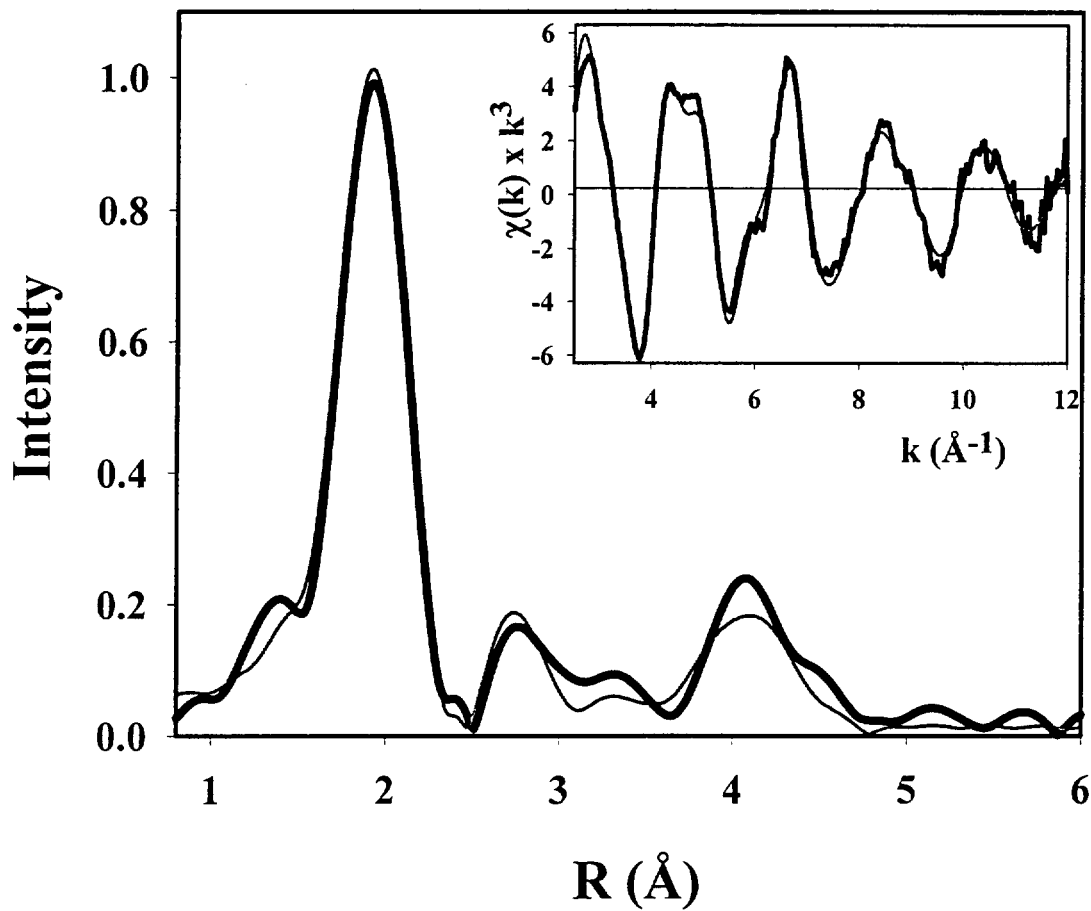


Fig. 4.3 EXAFS spectrum (inset) and Fourier transform of oxidized H172A. Raw data are shown with thick lines and the fits are shown with thin lines. Parameters used to fit the data are shown in Table 4.2.

Table 4.2

XAS Refinement Results for Oxidized H172A Using EXCURVE 98

First shell			Outer shells			
Shell	R (Å)	$2\sigma^2$	Shell	R (Å)	Cu- N_α -X (deg)	$2\sigma^2$
Fit index = 0.22 $E_0 = -4.82$						
2.0 N_α (imid)	1.96	0.010	2.0 C_β (imid)	2.92	125	0.012
2.0 O_α	1.96	0.010	2.0 C_β (imid)	2.92	239	0.012
			2.0 N_γ (imid)	4.12	164	0.014
			2.0 C_γ (imid)	4.12	203	0.014

The structure of the mutant enzyme appears to be identical to wtPHMcc, and therefore His172 may be replaced by a water molecule in the active site of oxidized/resting H172A.

4.3.4.2 Reduced H172A. The EXAFS spectra and Fourier transform of reduced H172A are shown in Fig. 4.4a with parameters shown in Table 4.3. The simplest analysis treats the spectrum as an average of the copper coordination (2 N and 0.5 S), and the first shell data are fit with 2 N(His) at 1.89 Å and 0.5 S(Met) at 2.24 Å. In comparison with reduced wtPHMcc, which has a Cu-N at 1.96 Å (Fig. 4.5), the His shell in H172A is shortened by 0.07 Å, indicating either one or both copper sites are affected by the mutation. Because the coppers are separated by 11 Å, it seems unlikely that mutation at the Cu_H site should have a great effect on the Cu_M site. Simulating the reduced EXAFS data with a split histidine shell, which allowed the contribution from each copper to be fit separately, tested this theory. Both coppers were modeled as in the wild type, where Cu_H was a 2-coordinate site and Cu_M was a 3- or 4-coordinate site. Fig. 4.4b and Table 4.3 show the results of these simulations. The two site model fit Cu_H with two imidazoles at 1.83 Å and Cu_M with two imidazoles at 1.96 Å and one S(Met) at 2.26 Å; the fit was of comparable quality to that without the split histidine shell (the goodness of fit parameter was within 10% of that with a single shell). Copper ligand distances at the Cu_M site are essentially unchanged from those found in the wild type. However, the Cu-N(His) distances at Cu_H are significantly shorter (1.83 Å versus 1.88 Å in wild type) and are at or below values found in 2-coordinate complexes [Sanyal et al., 1993].

As in the wild type, reduction of the mutant enzyme with ascorbate appears to shorten the Cu-S(Met) bond, indicated by a distinct sulfur EXAFS contribution at 2.24 Å in both simulations. However, the Debye-Waller (DW) value for the Cu-S bond is high, 0.015, for a copper site with a single Cu-S bond distance. Large DW terms for this shell have also been observed in reduced wtPHMcc and half-apo PHMcc [Jaron and Blackburn, 1999, 2001]. In the latter, we interpreted the large DW in terms of either a spread in the Cu-S distance at a single copper site, or an averaging of different “methionine-on” and “methionine-off” conformations. The fifth His residue that is undetectable in reduced wtPHMcc EXAFS is also absent in

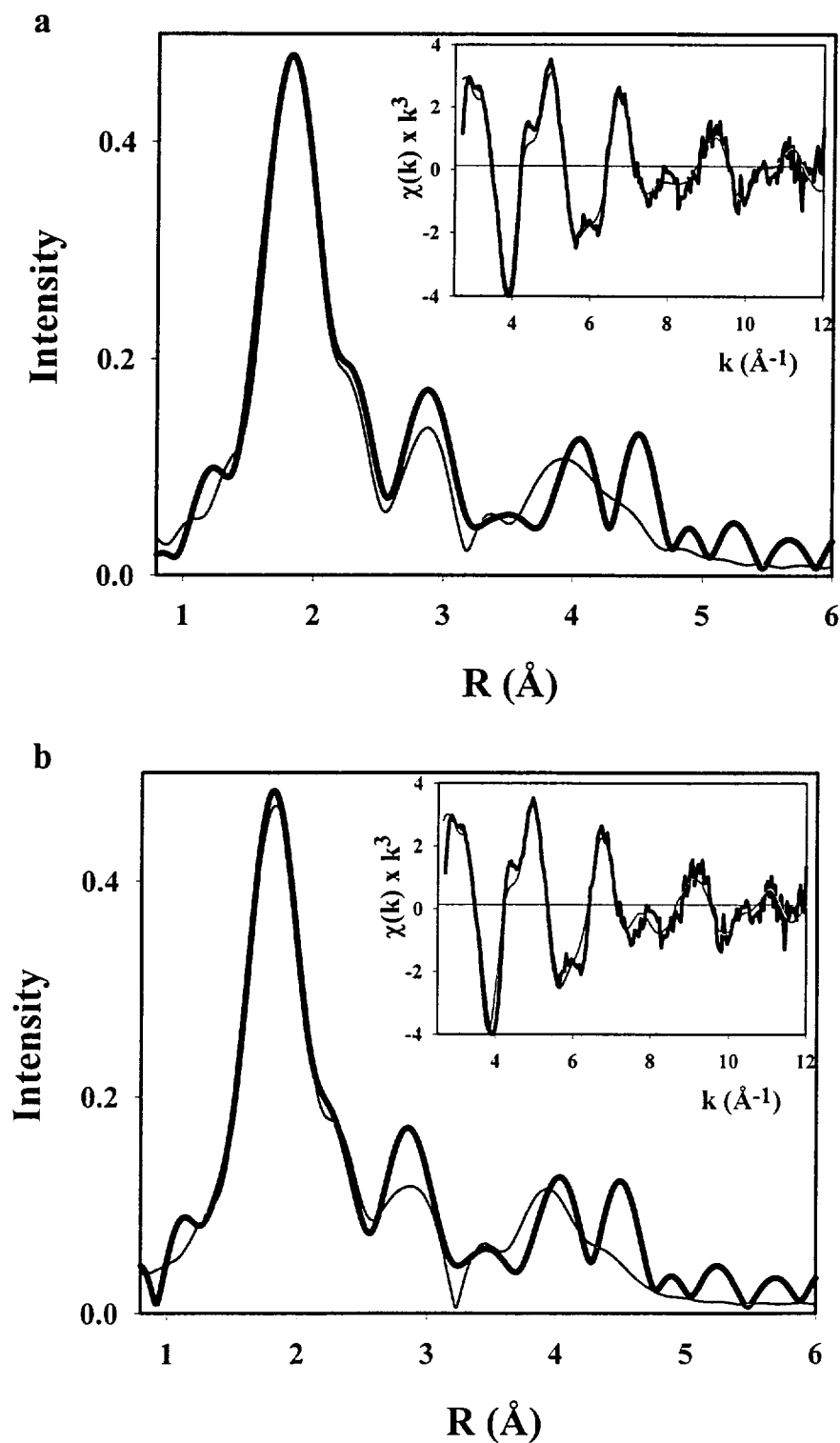


Fig. 4.4 EXAFS spectrum (inset) and Fourier transform of reduced H172A. Raw data are shown with thick lines and the fits are shown with thin lines. (a) Fit using 1 shell of histidines; (b) fit using 2 shells of histidines in order to distinguish between Cu_M and Cu_H . Parameters used to fit the data are shown in Table 4.3.

Table 4.3

**Parameters Used to Simulate the EXAFS
and Fourier Transform of Reduced H172A**

First shell			Outer shells			
Shell	R (Å)	2σ ²	Shell	R (Å)	Cu-N _α -X (deg)	2σ ²
EXAFSPAK 1 shell fit, 2 histidines, 0.5 sulfur. Fit index = 0.602 E ₀ = 0.20						
2.0 N _α (imid)	1.89	0.014	2.0 C _β (imid)	2.87	237	0.014
			2.0 C _β (imid)	2.95	135	0.014
0.5 S _α (Met)	2.24	0.015	2.0 N _γ (imid)	4.19	202	0.014
			2.0 N _γ (imid)	4.05	164	0.014
EXAFSPAK 2 shell fit, 2 histidines, 0.5 sulfur. Fit index = 0.668 E ₀ = -0.80						
1.0 N _α (imid A)	1.83	0.004	1.0 C _β (imid A)	2.87	235	0.004
			1.0 C _β (imid A)	2.87	135	0.004
			1.0 N _β (imid A)	4.05	202	0.015
			1.0 C _β (imid A)	4.05	164	0.015
1.0 N _α (imid B)	1.96	0.003	1.0 C _β (imid B)	3.01	135	0.003
			1.0 C _β (imid B)	3.01	230	0.003
			1.0 N _β (imid B)	4.23	167	0.028
			1.0 C _β (imid B)	4.23	205	0.028
0.5 S _α (Met)	2.26	0.013				

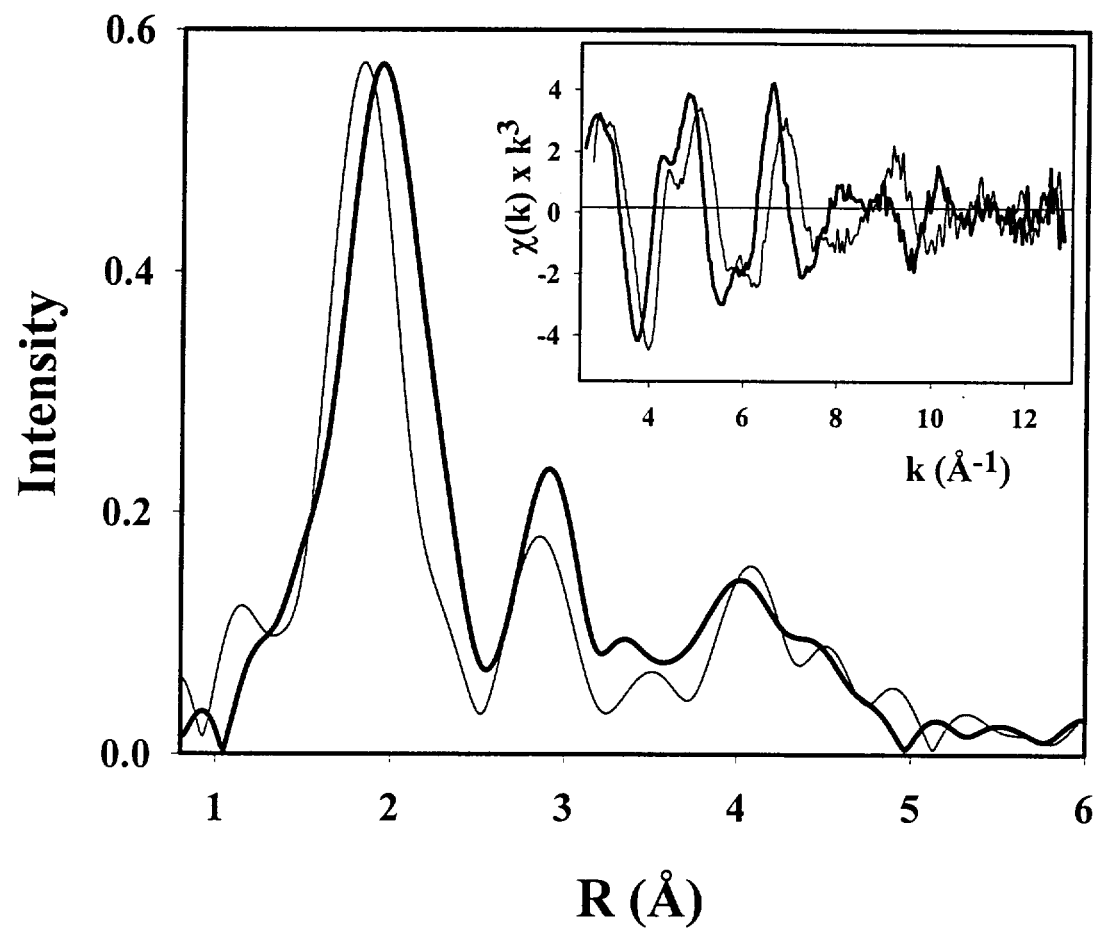


Fig. 4.5 EXAFS spectrum (inset) and Fourier transforms of reduced wild-type PHM (thick lines) versus reduced H172A (thin lines).

the reduced H172A EXAFS, suggesting that His172 may be the weakly bound ligand in reduced wtPHMcc.

It is possible to distinguish 2- and 3-coordinate Cu(I) sites by the position and intensity of the edge feature in the X-ray absorption near edge structure (XANES) region of the XAS spectrum. Model compounds of Cu(I) complexes have been used to assign the intense feature at 8983 eV to a $1s \rightarrow 4p$ transition and to show that variation in this peak can be correlated with the copper ligand geometry and coordination number [Kau et al., 1987; Blackburn et al., 1989]. The amplitude of this peak was found to be directly dependant on the geometry, with linear 2-coordinate complexes having the highest intensity of the pre-edge peak. Fig. 4.6 shows the absorption edge data for reduced H172A and reduced wtPHMcc. The edge feature of H172A is most similar to M314I, which was previously assigned to a 2-coordinate linear copper geometry arising from the loss of the methionine ligand at Cu_M. This strongly suggests the copper environment in H172A is also 2-coordinate linear [Blackburn et al., 2000].

It is clear from the significantly shortened Cu-N bond lengths, and the change to a more linear 2-coordinate structure in reduced H172A, that the presence of His172 is important to maintain the correct Cu environment.

3.4 DISCUSSION

In previous work, we have argued that the Cu_H site may indeed be the site of initial O₂ interaction with the enzyme. This proposal was the basis of our superoxide channeling mechanism in which O₂^{•-}, generated by O₂ reactivity at Cu_H, channels to Cu_M where it is further reduced to a Cu_M(peroxo) intermediate. Within this framework, His172 may be a key element of the O₂ reactivity of Cu_H. Characterization of the H172A PHMcc mutant was carried out to determine the importance of the Cu_H histidine ligand in the catalytic mechanism of the monooxygenase. This, in turn, requires knowledge of the influence of each ligand on the redox chemistry of Cu_H. Mutation of His172 perturbs the copper binding at one (or both) sites and most likely lowers the binding affinity for copper at the Cu_H site.

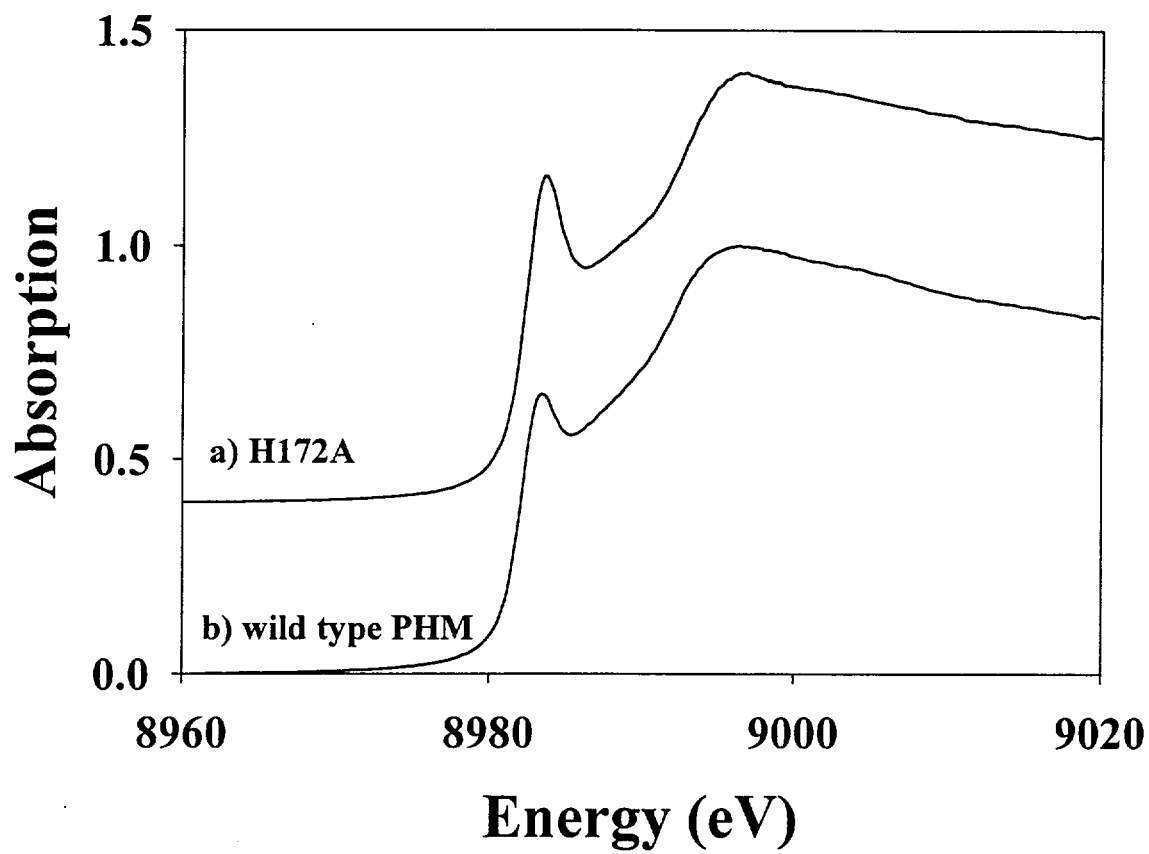


Fig. 4.6 XANES pre-edge data for (a) H172A and (b) wild-type PHM.

The H172A mutation also reduces the catalytic activity to less than 3% of wild type. However, H172A does produce some hydroxylated product, suggesting that electron flow from Cu_H to Cu_M has not been shut off, only slowed down. Investigation of the active site structure of the mutant and its CO binding chemistry provides clues to the role of His172 in the Cu_H environment and redox activity.

Factors that affect the reactivity of copper(I) complexes with oxygen include the availability of an open coordination sphere on the copper, the redox potential of the Cu(I,II) couple, and the ligand environment of the copper. The availability of an open coordination sphere is partially dependent on the solvent interaction with both copper and oxygen (i.e., steric bulk, hydrogen bonding, and dipole interaction). However, in the case of the mutant enzyme, we expect solvent to have little effect, because H172A and PHMcc should both have an available O_2 binding site. A change in redox potential of Cu_H , however, will likely play an important role in catalysis by the mutant. Reduction potentials for known copper complexes cover a wide range of values (-1.5 to +1.3 V versus NHE [Karlin et al., 1993]), although the one electron reduction of dioxygen becomes unfavorable at positive potentials since the E^0 is -0.33 V for $\text{O}_2 + e^- \rightarrow \text{O}_2^-$. The redox potential of a metal site and the stability of a dioxygen adduct are directly related to the ligand environment of the copper complex. wtPHMcc has a 3-coordinate Cu_H site that we have speculated to be important in oxygen binding by the enzyme. The loss of one of these imidazole ligands in the H172A enzyme creates a 2-coordinate Cu_H site. 2-Coordinate copper sites are generally unable to bind CO/O_2 . Model compounds have been created to test the dioxygen (and CO) reactivity of $\text{Cu}-(\text{imidazole})_n$ complexes, and they reveal that linear 2-coordinate Cu(I) complexes are unreactive toward O_2 and CO [Sanyal et al., 1993; Tyeklár and Karlin, 1993]. Reaction of these complexes with a single molar addition of the imidazole ligand creates a 3-coordinate complex that is oxidized by O_2 , suggesting that a distorted trigonal Cu(I) environment may be necessary for O_2 binding and redox activity. Therefore, the loss of activity in H172A may be due to an increased redox potential at Cu_H caused by a change in the ligand environment at this copper.

With this in mind, we attempted to rescue wtPHM activity by the addition of exogenous imidazole to H172A. Addition of a third ligand at the Cu_H site might cause the geometry at this site to revert to a more wild-type-like site. In addition to the copper-imidazole models, the activity of many mutant Fe-heme proteins, lacking the axial histidine, has been successfully recovered by the addition of imidazole [Decatur et al., 1996]. An azurin mutant, lacking one copper-His ligand, has also been successfully reconstituted by the addition of imidazole [van Gestel et al., 1999]. This reconstitution restored the copper coordination environment and spectroscopy associated with wild-type azurin. In the case of PHMcc, if His172 functioned as a dissociable ligand to Cu_H , imidazole might be expected to act as an adequate substitute. However, addition of imidazole was unable to recover full wtPHM activity. Therefore, either imidazole does not bind at the copper site or coordination of a fourth ligand to $\text{Cu}_H(\text{I})$ is not the only initiator needed for oxidation of this metal.

4.4.1 Oxidized Enzyme

An examination of the copper environment in the oxidized enzyme sheds little light on the method of inactivation of the enzyme. In fact, there appear to be only minute differences in the raw EXAFS data and the simulated structures of oxidized wtPHMcc and oxidized H172A. It is evident from the crystallographic data that the Cu_H of oxidized wtPHMcc is ligated by His172, and therefore the two oxidized enzymes must possess different copper ligation environments. However, both sets of raw data are equally well fit with four first shell ligands in some variation of N (His) and O (H_2O), and we must conclude that His172 in the mutant enzyme has been replaced by water. Simulations of first shell EXAFS data are known to be incapable of distinguishing between O- (H_2O) and N- (His) ligands and generally rely on outer shell multiple scattering to predict if a water or histidine molecule is present. However, the fourth ligand in H172A is indistinguishable from that in wild type and suggests that the technique may also be unable to discriminate between copper sites with small outer shell differences in this particular enzyme.

4.4.2 Reduced Enzyme

In the reduced form of H172A the effects of removing the histidine ligand at the Cu_H site are manifested as a change in the coordination environment at this copper. X-ray pre-edge data for reduced H172A have provided convincing evidence that removal of His172 causes the Cu_H site to assume a more linear 2-coordinate structure than seen in wtPHMcc. In fact, the pre-edge of H172A is very similar to the pre-edge of compound I-8 (Cu(pze)BF₄), a model compound which is close to linear 2-coordinate with Cu–N bond lengths of 1.87 Å (Kau et al., 1987). Additionally, EXAFS data clearly show a shortening of all Cu–N(His) bonds, indicating that the absence of His172 has perturbed the geometry at the Cu_H site and possibly the Cu_M site as well. This would not be unexpected, as crystallography has shown His172 to be important in both the oxidized and reduced forms of PHMcc. Previous EXAFS analysis of the reduced wtPHMcc enzyme suggested that, upon reduction, the Cu_H site becomes either 2-coordinate or T-shaped with a weakly bound His172 that is undetectable by EXAFS [Blackburn et al., 2000]. In reduced H172A, removal of the weakly coordinating His172 residue forces the Cu_H center to become more rigorously 2-coordinate. This structural change would be expected to decrease the redox potential via the enhanced stability of the 2-coordinate Cu(I) center. It is well known that 2-coordinate Cu(I) complexes are extremely stable towards oxidation by molecular oxygen [Sanyal et al., 1993]. In the PHMcc case, the absence of a potential third histidine ligand might further reduce the reactivity with respect to dioxygen since Cu(I)-dioxygen chemistry seems to be favored by the presence of three N-donors. Based on the comparison of data for H172A and wild type, we conclude that in reduced wtPHMcc the Cu_H structure is more T-shaped with His172 holding the other Cu_H ligands at the correct distance, possibly to encourage redox or O₂ reactivity.

4.4.3 Ligand Binding to H172A

To further investigate the hypothesis that His172 might be an important regulator of O₂ reactivity, the ligand binding activity of H172A was probed using the O₂ analog, CO. CO has been used in many systems, including wtPHMcc, as a model

for oxygen binding [Hirota et al., 1999; Jaron and Blackburn, 1999]. Both exogenous ligands, CO and O₂, have empty π -antibonding orbitals that are available for interactions with filled metal d-orbitals. Stretching frequencies of protein-bound copper-carbonyls are generally found in the range of 1950–2150 cm⁻¹ and are dependent on the structure of the copper site and its ligand environment. wtPHMcc was found to have two distinct CO/O₂ binding sites, with infrared frequencies of 2062 and 2093 cm⁻¹, assigned as terminally bound copper-carbonyls at Cu_H and Cu_M, respectively. Assignment of the 2062 cm⁻¹ peak came from comparison with known copper-carbonyls in other oxidases shown in Table 4.4, although absolute proof of the site of CO binding has been elusive. Mutation of the histidine ligand at Cu_H should therefore have an effect on the 2062 cm⁻¹ IR frequency if its assignment as a Cu_H-carbonyl is correct.

Mutation of His172 does not appear to hinder in any way the ability for Cu_M to bind CO. However, there is a small yet reproducible effect on CO binding at the peptide substrate-induced site as detected by the shift in $\nu(\text{CO})$ from 2062 to 2065 cm⁻¹. Although CO is apparently able to bind at the substrate-induced site, the shift in IR frequency indicates that His172 is somehow involved in CO binding at this site. While removing His172 may have some long-range electronic effect at a distant CO binding site, it is more likely that the affected CO binding site is in close proximity to this residue. This is because removal of His172 clearly has no long-range influence on the frequency of the Cu_M-CO species. Hence, it is likely that the 3 cm⁻¹ upshift reflects a perturbation of a Cu_H-CO complex as previously suggested. Because the carbonyl is known to be a copper ligand, and there appear to be only two coppers bound to H172A, the only copper intimately affected by the removal of His172 is the Cu_H. These data, therefore, provide strong evidence that the substrate-induced CO binding site is located at Cu_H, as previously suggested. On the other hand, the inability to eliminate the substrate-induced CO binding at Cu_H may suggest that His172 does not function to activate the site towards O₂. Alternatively, the O₂ and CO reactivity could differ.

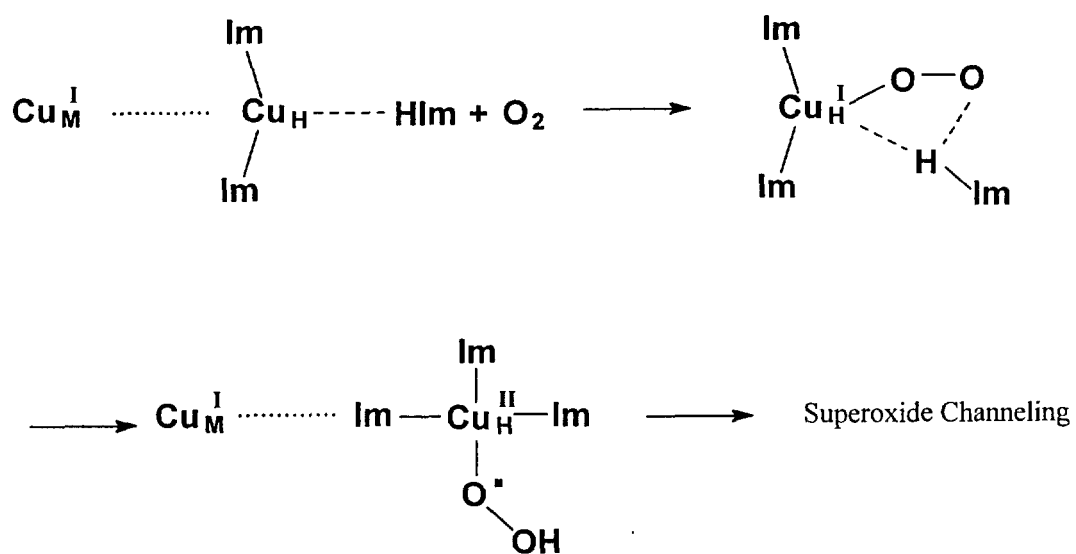
The characterization of the H172A mutant has suggested that this His ligand has a significant role in enzyme turnover without being critical for copper

Table 4.4

**Copper-Carbonyl Infrared Stretching Frequencies
for Proteins That Have Tris-Histidine Ligation**

Protein	$\nu(\text{CO})$	Reference
molluscan	2063	Fager and Alben, 1972
limulus	2053	Fager and Alben, 1972
arthropodal	2043	Fager and Alben, 1972
cytochrome oxidase		
aa ₃	2062	Alben et al., 1981
bo ₃	2065	Puustinen et al., 1997
PHM	2062	Jaron and Blackburn, 1999

coordination or CO chemistry. This may suggest an alternative role involving proton donation. The pH dependence of PHMcc is in the acidic range (maximal catalytic activity is achieved at pH 5.5 [unpublished data]), which implies that during catalysis His172 is protonated. We described earlier that this residue appears to be weakly coordinated in the reduced wild-type enzyme, suggesting it is only ligating in the oxidized enzyme. This movement is likely important during the oxidation and reduction of this copper site. Reduction of dioxygen at the Cu_H center requires the donation of a proton from a nearby residue; His172 is ideally located for this function. Depicted in Scheme 4.3 is a proposal for the role of His172 in the redox activity at the Cu_H site. This model clearly supports superoxide channeling as the mode of electron transfer from Cu_H to Cu_M , although other electron transfer pathways cannot be ruled out.



Scheme 4.3 Proposed proton donation by H172 to bound superoxide, following oxidation of Cu_H .

CHAPTER 5
pH-DEPENDANT STRUCTURAL CHANGES OF THE ACTIVE SITE
IN PEPTIDYLGLYCINE α -HYDROXYLATING MONOOXYGENASE (PHM)

5.1 INTRODUCTION

Peptidylglycine α -hydroxylating monooxygenase (PHM) is the enzyme responsible for the first step in the C-terminal amidation of a wide variety of mammalian peptide hormones [Bradbury et al., 1982; Young and Tamburini, 1989]. It catalyzes the incorporation of a single atom of oxygen into the α -carbon of a terminal peptidylglycine residue in a copper-, dioxygen-, and ascorbate-dependant manner, which forms the hydroxylated peptide and glyoxylate [Eipper and Mains, 1991; Merkler et al., 1992]. Activity of PHM depends on the presence of two copper atoms, Cu_M and Cu_H , with a $Cu_H(His)_3O...Cu_M(His)_2O_2$ ligation environment located at the enzyme's active site. Both coppers cycle through Cu(I) and Cu(II) oxidation states, each donating a single electron to reduce molecular oxygen. The structure of the active site has been studied extensively by X-ray crystallography and X-ray absorption spectroscopy, resulting in conflicting structures [Jaron and Blackburn, 1999; Prigge et al., 1999; Blackburn et al., 2000].

Early structural investigations using extended X-ray absorption fine structure (EXAFS) spectroscopy suggested that, in the oxidized enzyme, copper is coordinated only by N(His) and O(solvent). No copper-copper interaction was observed, suggesting the two metal sites were separated by more than 5 Å. Upon reduction of PHMcc, one additional Cu-S interaction at 2.27 Å was observed [Eipper et al., 1995; Boswell et al., 1996]. Through mutational studies, the sulfur was determined to stem from Met314 [Blackburn et al., 1994]. Further studies indicated that only the Met ligated copper site (Cu_M) interacted with dioxygen, while the other site (Cu_H)

functioned to transfer electrons [Boswell et al., 1996; Jaron and Blackburn, 1999]. These results suggested that methione is only ligated in the reduced form and is replaced by solvent in the oxidized. We recently published a detailed EXAFS study of PHMcc and a mutant (M314I), which supported the idea of structural changes in conjunction with redox cycling of the copper centers [Blackburn et al., 2000]. In the oxidized state, Cu_M exhibited a 4- or 5-fold coordination with 2 His at 1.97 Å and 2–3 water molecules at 1.97 Å, whereas Cu_H was coordinated by 3 His at 1.97 Å and 1 H_2O at 1.97 Å. The assignment of the ligands to Cu_H and Cu_M was derived from X-ray crystallographic studies [Prigge et al., 1997]. Upon reduction, the coordination at both the Cu_M and Cu_H sites changed significantly. Met314 moves closer into the coordination sphere of Cu_M to 2.24 Å while the water molecules become undetectable. Additionally, Cu_H becomes more 2-coordinate with 2 His at 1.88 Å and the third His ligand becoming undetectable by EXAFS.

The X-ray crystal structure of oxidized PHMcc, published by Amzel and coworkers, showed that the coppers at the active site have unique ligand environments. They are located on different protein sub-domains and are separated by 11 Å, in agreement with what was observed in the EXAFS study [Prigge et al., 1999, 2000]. The domains are held in contact by a hydrophobic region, which is distant from the active site coppers. The closest through-bond pathway between the coppers, including hydrogen bonds, is more than 50 Å. This is longer than any known electron transfer pathway [Prigge et al., 1997]. The $\text{Cu}_M(\text{II})$ site exhibits a pseudo-tetrahedral coordination. It is ligated by two N_ϵ of H242 and H244 at 1.91 Å and 2.09 Å, respectively, one S from Met314, which is long at 2.42 Å, and one O from H_2O . The second site, $\text{Cu}_H(\text{II})$, has square pyramidal geometry and is ligated by three histidine N_δ (H107, H108, H172) at 1.92, 1.92, and 2.29 Å, respectively, and two solvent molecules. The substrate binding site was revealed close to the Cu_M center involving two backbone residues (Y318, N316) which are located on the same β -sheet as M314. The structures of the copper sites in the PHMcc–substrate complex were unaffected by binding of substrate. More recently, the structure of the reduced enzyme was published, which established that the copper sites in both the oxidized and reduced oxidation states are identical [Prigge et al., 1999].

While EXAFS data suggest large structural changes at the copper centers during redox cycling, X-ray crystallography does not detect any changes. This leads to two distinct electron transfer mechanisms: (1) superoxide channeling derived from EXAFS and (2) substrate mediated electron transfer supported by the crystal structure. Both of the mechanisms are described in detail in Chapter 2. It is unclear why the two methods generate such dramatically different results, although Prigge and coworkers suggested it could be due to the difference in experimental conditions. One major difference may be the pH: pH 5.5 for crystallography and pH 7.5 for EXAFS [Eipper et al., 1995; Boswell et al., 1996; Prigge et al., 1997, 1999; Blackburn et al., 2000]. The pH was shown to have a significant effect on the coordination at copper sites in studies on plastocyanin [Guss et al., 1986]. Here, differences in the ligand environment of the reduced copper, at pH 5.1 and 7.0, were as large as the differences between reduced and oxidized copper at the same pH (6.0). The active site of PHM is composed of protonatable residues: Tyr79, Tyr318, His107, His108, His172, His242 and His244. Changing the pH may affect these residues, thus changing the coordination environment at one or both coppers.

This chapter describes a detailed analysis of the oxidized and reduced PHMcc enzyme at pH 5.5 and 9.0 to determine if the differences between X-ray crystallography and EXAFS are due in the main to the experimental pH.

5.2 EXPERIMENTAL PROCEDURES

5.2.1 Enzyme Isolation

Peptidylglycine α -amidating monooxygenase catalytic core (PHMcc) was expressed in Chinese hamster ovary cells as previously described [Jaron and Blackburn, 1999]. Drs. Richard Mains and Betty Eipper (Department of Neuroscience, Johns Hopkins School of Medicine) kindly provided the recombinant cell line. Purified PHMcc was reconstituted with Cu(II) nitrate, either at pH 7.5 for use in the specific activity measurements or in the following way for EXAFS analysis. Samples used for EXAFS were dialyzed overnight in either 150 mM MES/25 μ M Cu²⁺ at pH 5.5 or in 50 mM Borate/25 μ M Cu²⁺ at pH 9.0. Final copper-to-protein

ratios were in the range of 1.5:1 to 2:1, and the protein integrity was checked by activity measurements, SDS PAGE electrophoresis, and EPR spectroscopy. Reduced samples were made by the addition of a 5-fold excess of buffered ascorbate and substrate-bound samples included a 2-fold excess of N-Ac-TyrValGly (YVG).

5.2.2 X-ray Absorption Spectroscopy

X-ray absorption spectroscopic data were collected at the Stanford Synchrotron Radiation Laboratory (SSRL), Menlo Park, CA, using beamlines 7.3 and 9.3. Full details of the beamline parameters are described in Section 3.2.6.

5.3 RESULTS

5.3.1 Oxidized PHMcc, pH 9.0

The background-subtracted and k^3 -weighted EXAFS and Fourier transform (FT) of the oxidized PHMcc sample at pH 9.0 are shown in Fig. 5.1a. The data were fit using the parameter file determined for oxidized enzyme at pH 7.5 [Blackburn et al., 2000] (Table 5.1). The best fit was attained with little refinement of these parameters and resulted in 2.5 Cu-N(imid) at 1.96 Å and 1.5 Cu-O(solvent) at 1.96 Å, which is virtually indistinguishable from the oxidized enzyme at pH 7.5. Raising the pH from 7.5 to 9.0, therefore, had no obvious structural effect.

5.3.2 Reduced PHMcc, pH 9.0

Simulation of reduced wild-type PHMcc EXAFS data at pH 9.0 employed a protocol similar to that described above. The parameter set for reduced wild-type PHM at pH 7.5 was obtained and refined until a best fit was obtained (Table 5.1). EXAFS and FT are shown in Fig. 5.1b. A single histidine-shell fit was attempted, although splitting the first shell histidines improved the fit by 30%. The data were simulated with 1 N(His) at 1.98 Å, 1 N(His) at 1.86 Å, and 0.5 S(Met) at 2.26 Å, which is identical to the structure determined at pH 7.5. Clearly, no change in the reduced structure has occurred upon raising the pH.

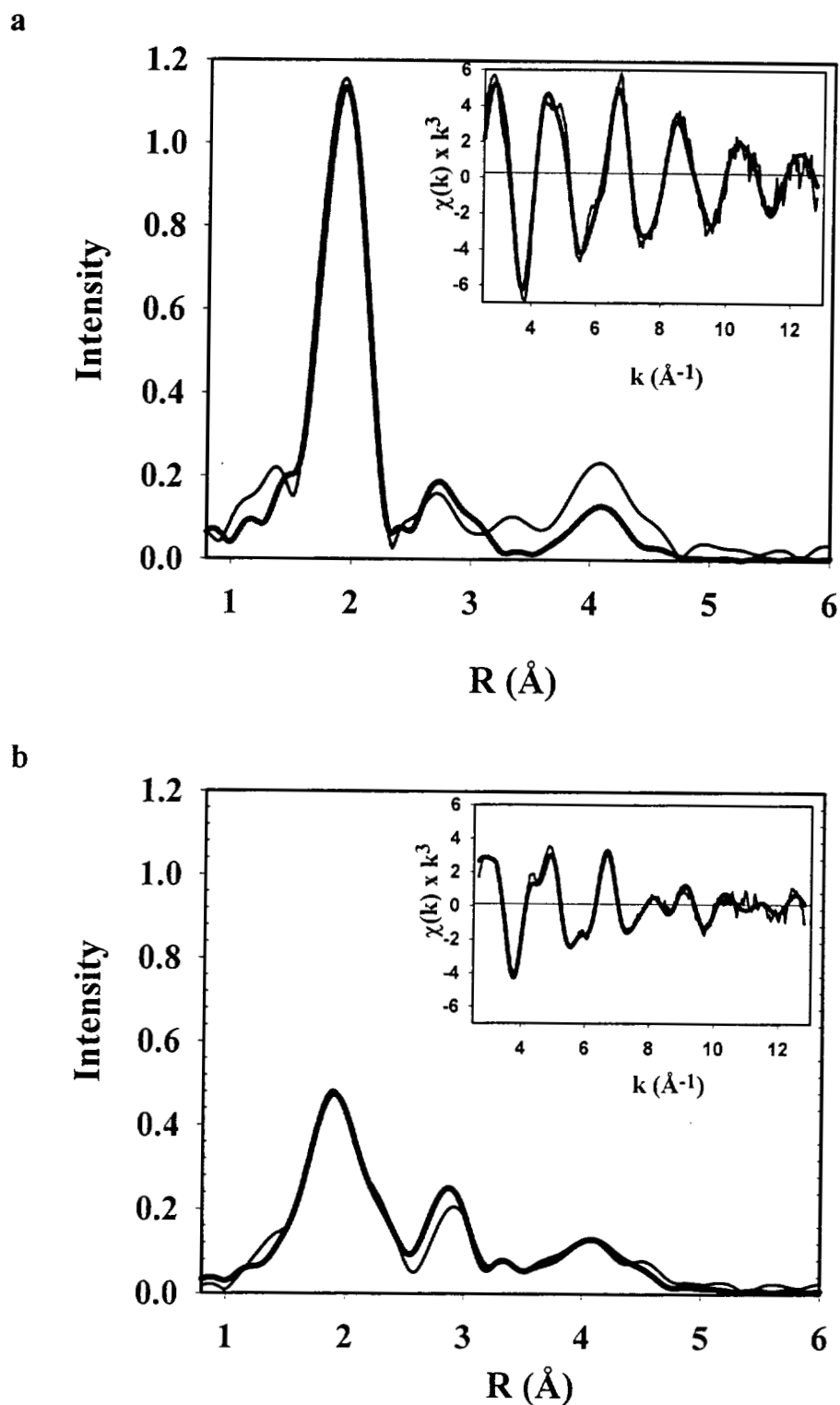


Fig. 5.1 X-ray absorption spectra of PHMcc at pH 9.0 collected on BL7.3. Thin lines are experimental data; thick lines represent the fit. (a) Oxidized, Cu(II), spectrum; (b) reduced, Cu(I), spectrum.

Table 5.1

EXAFS Parameters for Oxidized and Reduced PHMcc at pH 9.0

First shell			Outer shells			
Shell	R (Å)	$2\sigma^2$	Shell	R (Å)	Cu- N_α -X (deg)	$2\sigma^2$
Oxidized PHMcc, pH 9.0, EXAFSPAK fit. Fit index = 0.19 $E_0 = -4.73$ eV						
2.5 N_α (imid)	1.96	0.009	2.5 C_β (imid)	2.83	121	0.012
			2.5 C_β (imid)	2.99	240	0.012
1.5 O_α (Solvent)	1.96	0.009	2.5 N_γ (imid)	4.11	167	0.015
			2.5 N_γ (imid)	3.92	220	0.015
Reduced PHMcc, pH 9.0, EXAFSPAK fit. Fit index = 0.27 $E_0 = -0.81$ eV						
1.0 N_α (imid)	1.98	0.002	1.0 C_β (imid)	2.95	236	0.007
			1.0 C_β (imid)	2.95	131	0.007
			1.0 N_γ (imid)	4.23	203	0.010
			1.0 N_γ (imid)	4.23	157	0.010
1.0 N_α (imid)	1.86	0.006	1.0 C_β (imid)	2.88	126	0.007
			1.0 C_β (imid)	2.88	231	0.007
			1.0 N_γ (imid)	4.10	158	0.008
			1.0 N_γ (imid)	4.10	205	0.008
0.5 S_α (Met)	2.26	0.011				

5.3.3 Oxidized Enzyme With and Without Bound Substrate, pH 5.5

The background-subtracted and k^3 -weighted EXAFS and FT spectra of oxidized PHMcc at pH 5.5 are shown in Fig. 5.2. The copper spectra are similar to those in oxidized PHMcc at higher pH and show typical copper-histidine ligation. The Fourier filtered first shell data [not shown] were fit with an average of 4 O/N at 1.97 Å. The unfiltered data at pH 5.5 were refined using the parameter set published for oxidized PHMcc at pH 7.5, with consideration of both single and multiple scattering pathways [Blackburn et al., 2000]. A Cu-S(Met) bond length of 2.419 Å was reported in the crystal structure [Prigge et al., 1997], although a structure derived from EXAFS data at pH 7.5 found no contribution from this atom. The best fit was achieved using 2.5 N(His) at 1.97 Å with no contribution from the S(Met) ligand. This supported the EXAFS results at higher pH, suggesting that the S(Met) was a weak ligand and therefore undetectable by EXAFS (parameters for pH 5.5 without S(Met) shown in Table 5.2). However, the inclusion of 0.5 S at 2.52 Å, caused a 25% decrease in the fit index. The observed Debye-Waller (DW) term for Cu-S, indicative of the mean deviation in bond length, is large for a first shell interaction (0.031), providing further evidence that the Cu-S(Met) is only weakly coordinated. Detection of a Cu-S(Met) interaction in the oxidized enzyme suggests that lowering the pH has induced a movement of either the Met residue or the copper atom or both. A similar result was observed in the structure of reduced plastocyanin (Cu(I)) [Guss et al., 1986]. Lowering the pH of plastocyanin caused a shortening of the Cu(I)-S(Met92) bond length by 0.4 Å. This was attributed to a movement of the Cu atom by 0.4 Å towards the plane of N(His37), S(Cys84), and S(Met92).

EXAFS data for substrate-bound oxidized PHMcc were also collected and are shown in Fig. 5.3. At pH 7.5, the EXAFS data were identical to oxidized PHMcc without bound substrate and were fit with only His and solvent ligands. The parameter set determined for oxidized enzyme without bound substrate at pH 5.5 (no S(Met)) was refined with the substrate-bound data, until the fit was minimized (parameters shown in Table 5.3). A good fit was obtained with 2.5 N(His) ligands at 1.96 Å; however, visually, the fit appeared to lack a component at ~ 2.4 Å (Fig. 5.3a). A sulfur shell at 2.4 Å was added to the fit and allowed to minimize to an

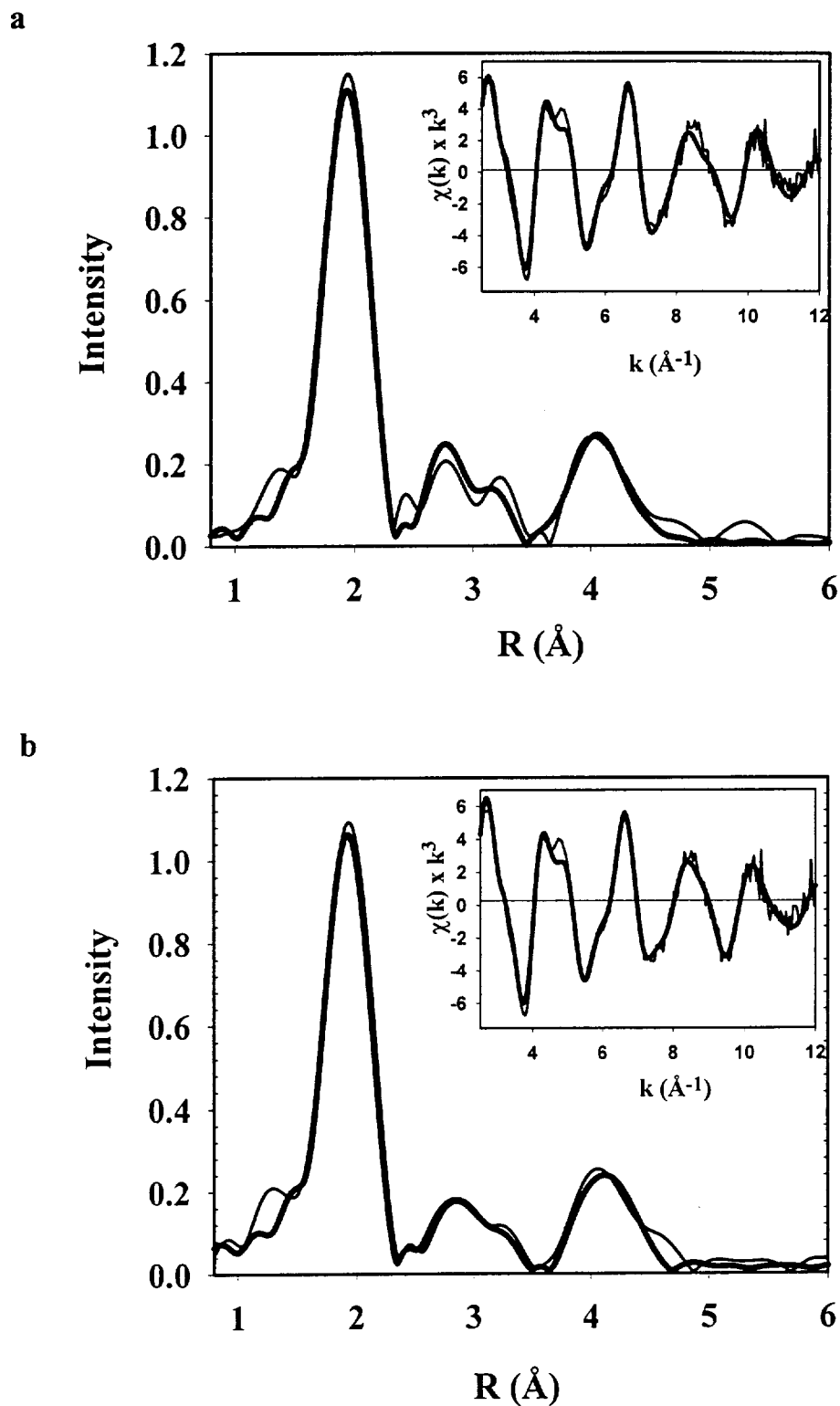


Fig. 5.2 X-ray absorption spectra of oxidized PHMcc at pH 5.5 collected on BL7.3. Thin lines are experimental data; thick lines represent the fit. (a) A fit of the data without including a sulfur shell; (b) simulation of data including a sulfur shell at 2.52 Å.

Table 5.2

EXAFS Parameters of Oxidized PHMcc at pH 5.5

First shell			Outer shells			
Shell	R (Å)	$2\sigma^2$	Shell	R (Å)	Cu- N_α -X (deg)	$2\sigma^2$
EXAFSPAK fit without coordinated S. Fit index = 0.33 $E_0 = -4.33$ eV						
2.5 N_α (imid)	1.97	0.010	2.5 C_β (imid)	2.97	125	0.017
			2.5 C_β (imid)	2.97	236	0.017
1.5 O_α (Solvent)	1.97	0.010	2.5 N_γ (imid)	4.13	165	0.021
			2.5 N_γ (imid)	4.13	203	0.021
EXAFSPAK fit with coordinated S. Fit index = 0.25 $E_0 = -0.80$ eV						
2.5 N_α (imid)	1.97	0.010	2.5 C_β (imid)	3.02	125	0.010
			2.5 C_β (imid)	2.91	237	0.010
			2.5 N_β (imid)	4.17	165	0.014
			2.5 C_β (imid)	4.06	203	0.014
1.5 O_α (Solvent)	1.97	0.010				
0.5 S_α (Met)	2.52	0.031				

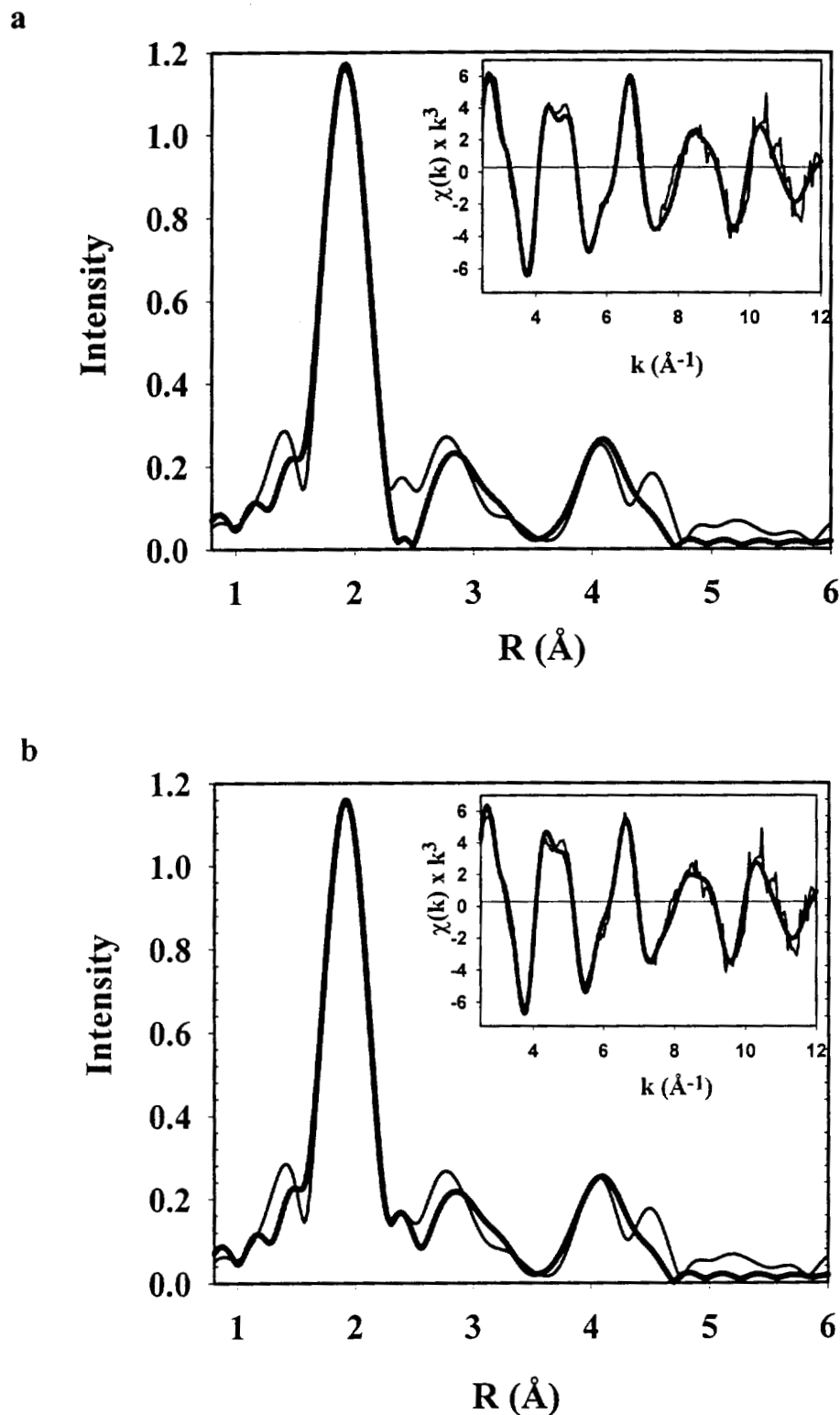


Fig. 5.3 X-ray absorption spectra of oxidized PHMcc with bound YVG at pH 5.5 collected on BL7.3. Thin lines are experimental data; thick lines represent the fit. (a) The best fit without inclusion of a sulfur shell; (b) the best fit including a sulfur shell at 2.34 Å.

Table 5.3

EXAFS Parameters of Oxidized PHMcc with Bound YVG at pH 5.5

First shell			Outer shells			
Shell	R (Å)	$2\sigma^2$	Shell	R (Å)	Cu- N_α -X (deg)	$2\sigma^2$
EXAFSPAK fit without coordinated S. Fit index = 0.35 $E_0 = -3.94$ eV						
2.5 N_α (imid)	1.96	0.008	2.5 C_β (imid)	2.98	124	0.008
			2.5 C_β (imid)	2.88	238	0.008
1.5 O_α (Solvent)	1.96	0.008	2.5 N_γ (imid)	4.12	161	0.015
			2.5 N_γ (imid)	4.05	213	0.015
EXAFSPAK fit with coordinated S. Fit index = 0.31 $E_0 = -4.60$ eV						
2.5 N_α (imid)	1.96	0.008	2.5 C_β (imid)	2.94	124	0.013
			2.5 C_β (imid)	2.94	235	0.013
			2.5 N_β (imid)	4.14	165	0.021
			2.5 C_β (imid)	4.12	201	0.021
1.5 O_α (Solvent)	1.97	0.008				
0.5 S_α (Met)	2.34	0.009				

acceptable parameter set. This resulted in a fit with 2.5 N(His) at 1.96 Å, 1.5 O(solvent) at 1.97 Å, and 0.5 S at 2.34 Å, with a decrease in the goodness of fit parameter of 12% (Fig. 5.3b and Table 5.3). Although the fit index is only slightly reduced, visual inspection of the EXAFS and FT spectra show a much closer fit when the sulfur is included. This likely represents a Cu-S(Met) interaction, and indicates that binding of substrate to oxidized enzyme causes a 0.079 Å shortening of the Cu-S(Met) bond length and a decrease in the Cu-S DW term. Furthermore, this suggests that there may be changes in the active site structure upon binding of peptidylgly substrates that affect the active site copper ligands but have not yet been identified.

5.3.4 Reduced PHMcc With and Without Bound Substrate, pH 5.5

The EXAFS and FT of reduced PHMcc at pH 5.5 are shown in Fig. 5.4. In fitting the reduced pH 5.5 data, the histidine shells were split to help distinguish between the two copper centers. This was previously shown to help accurately determine the average metal-His bond lengths at each copper site and additionally resulted in lower goodness of fit parameters [Blackburn et al., 2000; Jaron and Blackburn, 2001; this chapter]. The parameter set determined for reduced PHMcc at pH 7.5 was optimized to find a best fit for the pH 5.5 experimental data. The best fit using this ligand set resulted in a first shell of 1 N(His) at 1.97 Å, 1 N(His) at 1.84 Å, and 0.5 S(Met) at 2.26 Å; however, the FT simulation appeared to be lacking an interaction at ~2.5 Å (Fig. 5.4a). A second refinement was attempted, adding a third O/N ligand at a longer distance. This improved the fit by 25% and resulted in a structure with 1 N(His) at 1.98 Å, 1 N(His) at 1.85 Å, 0.5 S(Met) at 2.27 Å, and 0.5 N/O at 2.48 Å (Fig. 5.4b); the parameter sets for both simulations are shown in Table 5.4. The interaction of 0.5 N/O at 2.48 Å was not detected at higher pH, suggesting that lowering the pH of the reduced enzyme caused an additional active site ligand to move toward one of the copper sites. His172 was identified as the long Cu-N ligand in reduced PHMcc by X-ray crystallography. However, the crystal structure found a Cu_H-N(His172) bond length of 2.12 Å [Prigge et al., 1999]. EXAFS data at pH 7.5 suggested that His172 is not coordinated to Cu_H in the reduced

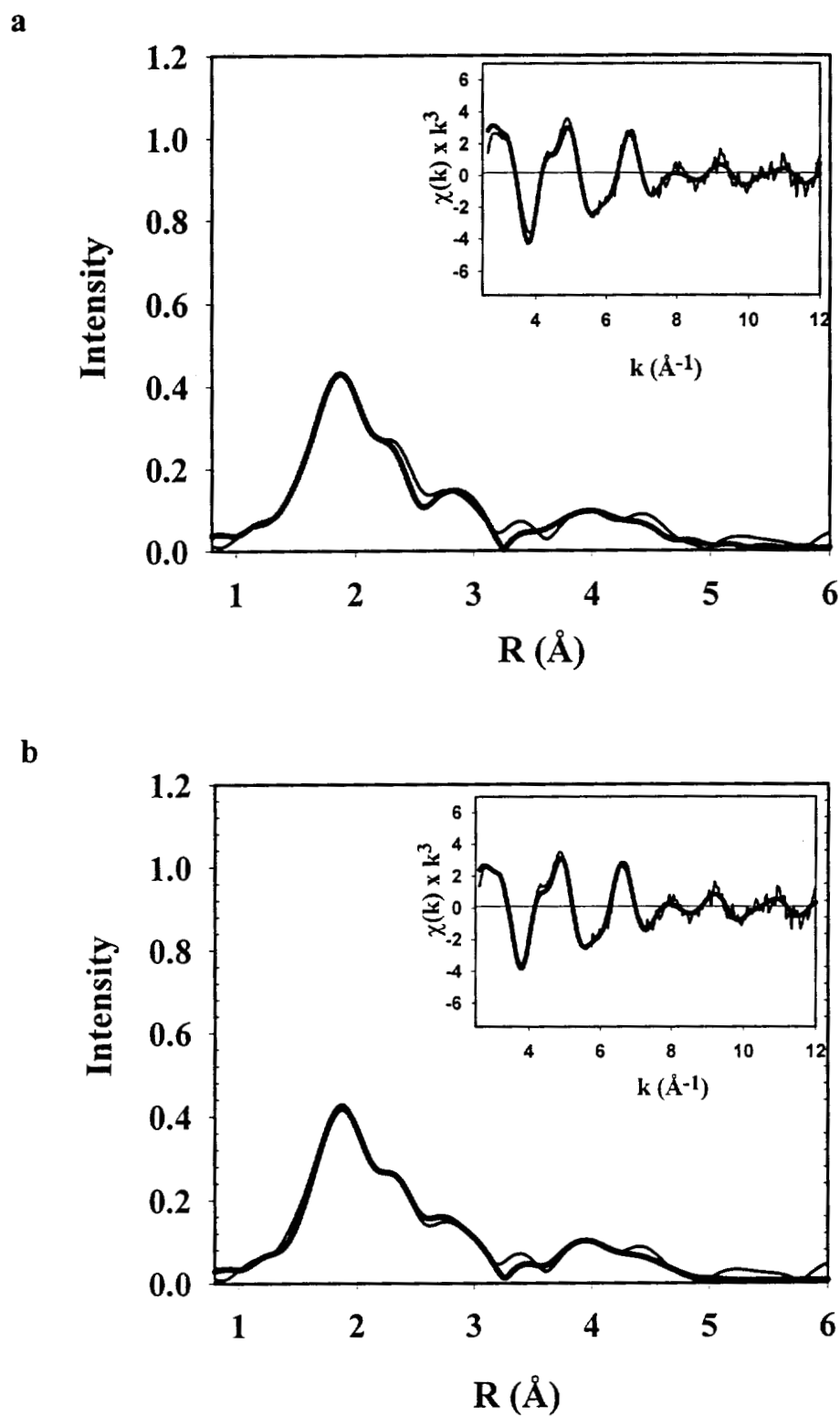


Fig. 5.4 X-ray absorption spectra of reduced PHMcc at pH 5.5 collected on BL7.3. Thin lines are experimental data; thick lines represent the fit. (a) Fit with 2 His and 0.5 S(Met); (b) an improved fit including 0.5 O/N atom at 2.46 Å.

Table 5.4
EXAFS Parameters of Reduced PHMcc at pH 5.5

First shell			Outer shells			
Shell	R (Å)	$2\sigma^2$	Shell	R (Å)	Cu- N_α -X (deg)	$2\sigma^2$
EXAFSPAK fit without additional N/O. Fit index = 0.48 $E_0 = -0.81$ eV						
1.0 N_α (imid)	1.97	0.001	1.0 C_β (imid)	3.01	236	0.007
			1.0 C_β (imid)	3.01	128	0.007
			1.0 N_γ (imid)	4.25	205	0.008
			1.0 N_γ (imid)	4.25	160	0.008
1.0 N_α (imid)	1.84	0.006	1.0 C_β (imid)	2.87	129	0.006
			1.0 C_β (imid)	2.87	233	0.006
			1.0 N_γ (imid)	4.07	160	0.008
			1.0 N_γ (imid)	4.07	202	0.008
0.5 S_α (Met)	2.26	0.007				
EXAFSPAK fit with additional N/O. Fit index = 0.36 $E_0 = -1.48$ eV						
1.0 N_α (imid A)	1.99	0.001	1.0 C_β (imid A)	3.01	237	0.006
			1.0 C_β (imid A)	3.01	134	0.006
			1.0 N_β (imid A)	4.26	202	0.010
			1.0 C_β (imid A)	4.26	161	0.010
1.0 N_α (imid B)	1.86	0.005	1.0 C_β (imid B)	2.88	131	0.006
			1.0 C_β (imid B)	2.88	240	0.006
			1.0 N_β (imid B)	4.08	162	0.007
			1.0 C_β (imid B)	4.08	216	0.007
0.5 S_α (Met)	2.29	0.010				
0.5 N/O_α	2.46	0.006				

enzyme [Blackburn et al., 2000], therefore defining His172 as a displaceable ligand. We previously suggested that His172 is coordinated in the oxidized form (Cu(II)) and uncoordinated or weakly bound in the reduced form (Cu(I)). If the atom at 2.48 Å in EXAFS is Cu-N(His172), then it may mean that at low pH (5.5), the uncoordinated His172 is more ordered.

Reduction of PHMcc at pH 5.5 also causes a decrease in the Cu-S(Met) bond length to 2.29 Å (-0.23 Å) and DW term to 0.010 (-0.021) from the oxidized structure at pH 5.5, suggesting that the Cu-S bond has strengthened. At pH 7.5, the Cu-S(Met) bond changed from undetectable in the oxidized spectrum to 2.24 Å in the reduced spectrum, also suggesting a strengthening of the Cu-S bond.

EXAFS and FT of reduced PHMcc+YVG are shown in Fig. 5.5, and the parameters used to fit these data are shown in Table 5.5. Parameters for reduced PHMcc were fit to this data with refinement until a best fit was obtained. The inclusion of a N/O ligand at 2.50 Å increased the goodness of fit by ~15% (Fig. 5.5b). Although this increase is fairly nominal, a visual inspection of the fit, with and without the extra atom, suggests its necessity. Most features in this spectrum are identical to reduced PHMcc without bound YVG at pH 5.5. However, there is a significant decrease in the DW term for the Cu-S bond. This indicates that the Cu-S bond has become stronger and/or more ordered upon binding of peptide substrate.

5.3.5 X-ray Absorption Edge

The X-ray absorption edge provides information about the coordination number and geometry of the absorbing atom(s), Cu(I) in the case of PHMcc. The edges of reduced PHMcc at each pH were considered, and Fig. 5.6 shows a comparison of these. There is no obvious difference in the edge features, either in their position, intensity or appearance, indicating that the coordination geometry likely does not change significantly upon changing pH.

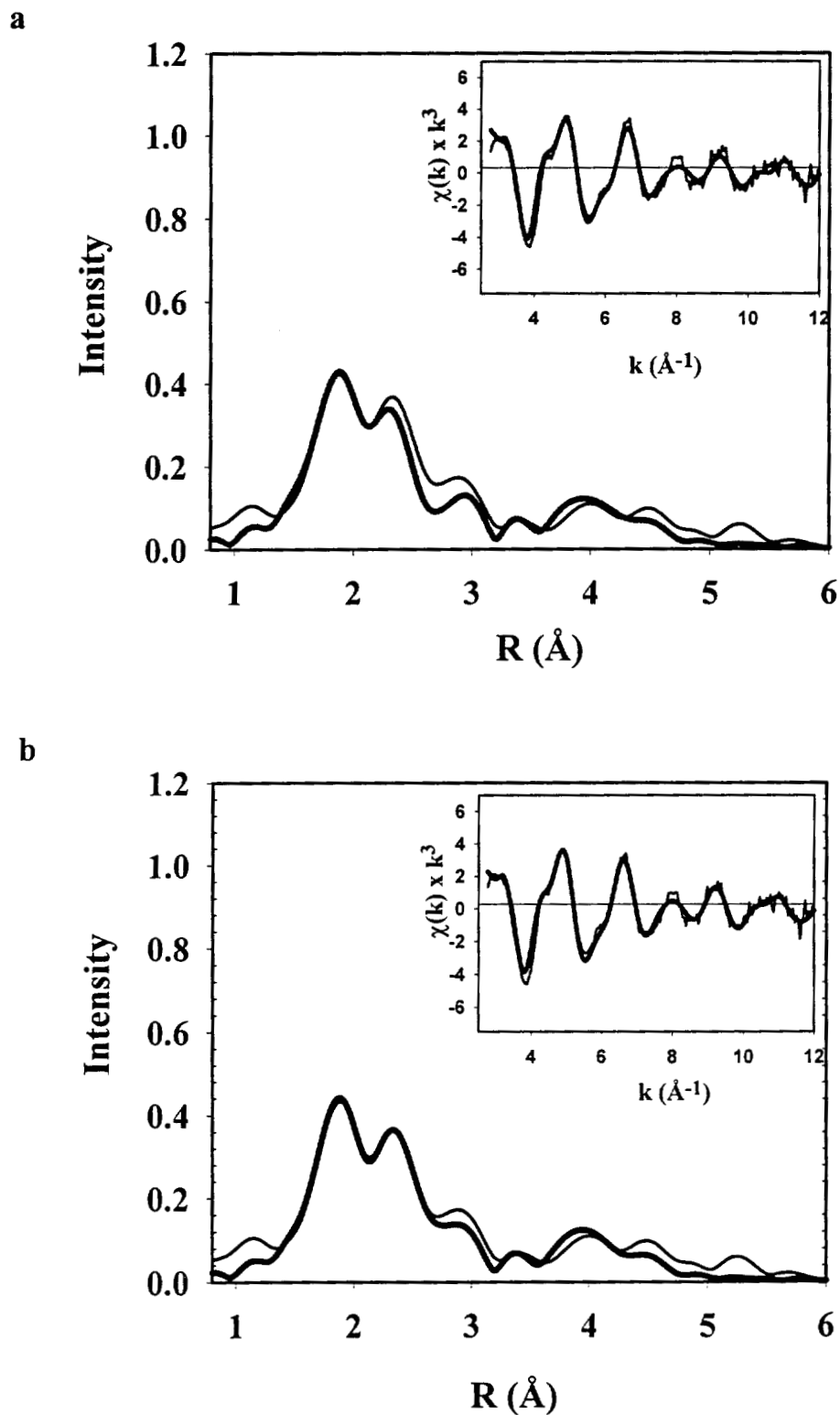


Fig. 5.5 X-ray absorption spectra of reduced PHMcc with bound YVG at pH 5.5 collected on BL9.3. Thin lines are experimental data; thick lines represent the fit. (a) A fit with 2 His and 0.5 S(Met) ligands; (b) an improved fit including 0.5 N/O at 2.5 Å.

Table 5.5

EXAFS Parameters of Reduced PHMcc with Bound YVG at pH 5.5

First shell			Outer shells			
Shell	R (Å)	2σ ²	Shell	R (Å)	Cu-N _α -X (deg)	2σ ²
EXAFSPAK fit without additional N/O. Fit index = 0.44 E ₀ = 1.12 eV						
1.0 N _α (imid)	1.98	0.001	1.0 C _β (imid)	3.02	228	0.008
			1.0 C _β (imid)	3.02	145	0.008
			1.0 N _γ (imid)	4.24	207	0.016
			1.0 N _γ (imid)	4.24	164	0.016
1.0 N _α (imid)	1.86	0.005	1.0 C _β (imid)	2.91	129	0.005
			1.0 C _β (imid)	2.91	240	0.005
			1.0 N _γ (imid)	4.08	171	0.006
			1.0 N _γ (imid)	4.08	210	0.006
0.5 S _α (Met)	2.27	0.003				
EXAFSPAK fit with additional N/O. Fit index = 0.39 E ₀ = 1.34 eV						
1.0 N _α (imid A)	1.99	0.002	1.0 C _β (imid A)	3.02	229	0.008
			1.0 C _β (imid A)	3.02	139	0.008
			1.0 N _β (imid A)	4.24	203	0.016
			1.0 C _β (imid A)	4.24	159	0.016
1.0 N _α (imid B)	1.86	0.005	1.0 C _β (imid B)	2.91	128	0.005
			1.0 C _β (imid B)	2.91	240	0.005
			1.0 N _β (imid B)	4.09	169	0.008
			1.0 C _β (imid B)	4.08	206	0.008
0.5 S _α (Met)	2.27	0.007				
0.5 N/O _α	2.50	0.001				

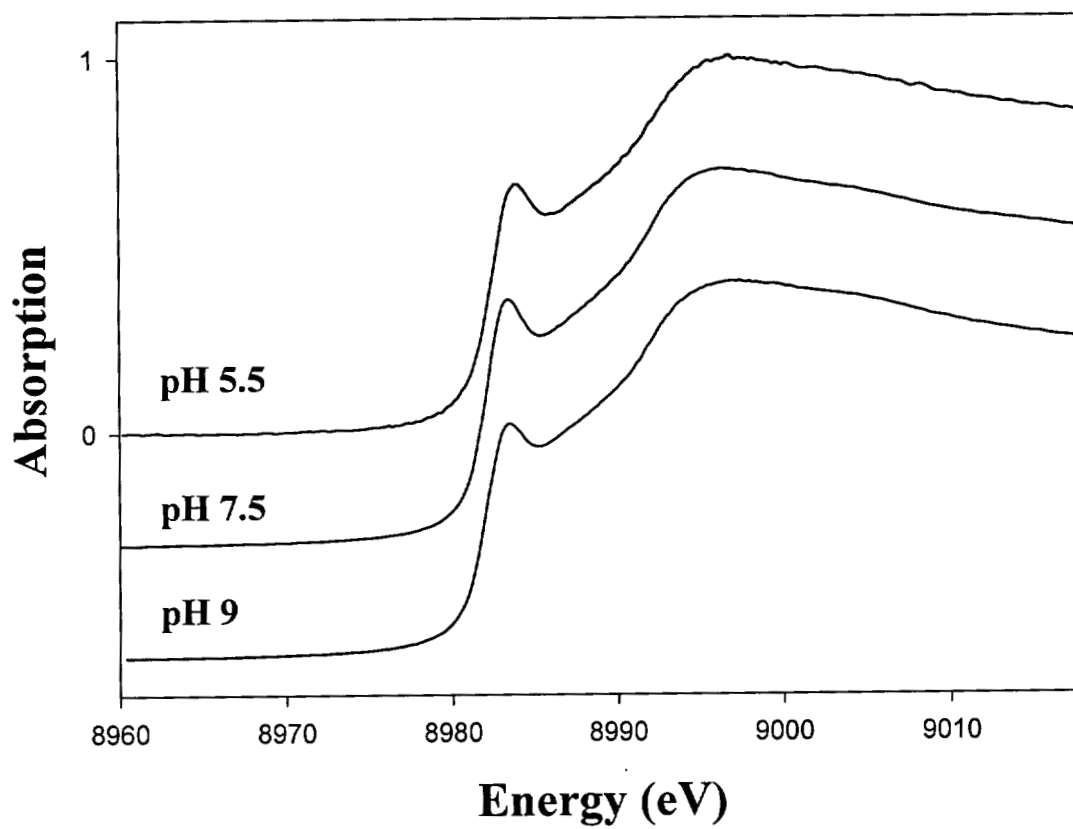


Fig. 5.6 X-ray absorption near edge structure (XANES) of reduced PHMcc at three different pHs. Data have been normalized to make the concentration of the sample irrelevant.

5.4 DISCUSSION

5.4.1 Structural Dependence on pH

In the main, there is very little difference in the overall EXAFS structures of PHMcc at the different pHs, suggesting that the disparity between EXAFS and crystallographic data is not based on pH differences. At each pH studied, PHM is composed of two unique copper centers that undergo significant structural changes during redox activity. The ligand coordination at these coppers is similar to what we published at pH 7.5 [Jaron and Blackburn, 1999]. In the oxidized enzyme, $\text{Cu}_M(\text{II})$ assumes a 4- or 5-coordinate distorted tetrahedral environment with two His ligands (H242, H244), two solvent molecules, and a possible weak interaction with M314. $\text{Cu}_H(\text{II})$ is held in either a square planar or square pyramidal geometry by three His ligands (H107, H108, H172) and a solvent molecule. Reduction of the enzyme causes $\text{Cu}_M(\text{I})$ to become 3- or 4-coordinate with a strong Cu-S(Met) bond, while $\text{Cu}_H(\text{I})$ becomes 2- or 3-coordinate, planar or T-shaped, with the loss of a solvent molecule and the weakening of one Cu-N(His) bond. At high pH (9.0), both oxidized and reduced structures are identical to that found at neutral (7.5) pH [Blackburn et al., 2000]. There are no obvious changes in the structure associated with increasing the pH from 7.5 to 9.0. The lack of subtle differences is likely due to the lack of groups in the active site that deprotonate over this range (the pKas of Arg and Tyr are above 10.0 and His is below 7.0).

At low pH (5.5), the overall coordination geometry for the copper sites is unchanged from neutral pH, and the copper ligand identities remain the same. The X-ray absorption-derived oxidized structure at pH 5.5 is identical to what was previously reported [Blackburn et al., 2000], with the exception that the S(Met) has become EXAFS detectable. This bond is still considered long, at 2.52 Å, and weak due to its high DW value (0.031), although lowering the pH causes a change that makes it detectable in the EXAFS.

Binding of substrate to the oxidized enzyme at low pH does not effect any of the copper-His bonds, although it appears to strengthen the copper-Met bond indicated by the substantial lowering of the DW value. A high DW term was

detected for the Cu-S(Met) bond in the H172A mutant and the half-apo derivative, and was proposed to be due to the presence of Met-on and Met-off conformers [Jaron and Blackburn, 2001; unpublished results]. However, it appears that, at low pH, binding of substrate in oxidized pHM favors the Met-on form. This is the first indication that substrate binding does have an effect on the copper ligation at Cu_M and suggests that the favored binding site for peptide substrate in oxidized PHM is close to Cu_M. This is supported by the X-ray crystal structure of oxidized PHMcc with bound YVG, which shows the peptide binding site close to Cu_M [Prigge et al., 1997, 1999].

Although the overall structure appears to be independent of pH, EXAFS spectroscopy detects subtle changes in the copper ligand environments of PHMcc upon lowering the pH. The Cu_M-S(Met) bond in oxidized PHMcc at pH 5.5 remains long and weak and is EXAFS detectable. Reduction of the enzyme causes the lengthening of one Cu-N(His) bond to 2.46 Å. Both of these EXAFS-detectable bonds were undetectable at higher pH.

5.4.2 Coordination of a New Ligand at Low pH in the Reduced Enzyme

In previous publications, the ligand environment at Cu_H(I) was described by EXAFS as 2- or 3-coordinate with a long, and undetectable, His ligand [Blackburn et al., 2000], which was later identified as His172 [Jaron and Blackburn, 2001]. Generally, weak metal-ligand interactions become completely EXAFS undetectable when there is bond disorder, for example, if there is movement in the ligand. At pH 5.5, however, there is evidence that this Cu_H(I)-His ligand begins to become ordered. The EXAFS structure of the reduced enzyme at low pH shows a long Cu-N/O bond at 2.46 Å with a low DW factor, indicative of stabilization of an atom. Lowering the pH to 5.5 is expected to cause the protonation of His residues, in particular the displaceable His172. In this case, we expect that protonated histidine would not be likely to ligate to Cu_H and would leave the site 2-coordinate, as was observed in the H172A mutant [Jaron and Blackburn, 2001]. The Cu-N/O distance is long and, therefore, probably not a direct ligand to the copper; however, it may indicate a different sort of interaction. The protonated histidine residue is likely to hydrogen-

bond to another site in the enzyme, which would suppress the movement of this side chain and allow it to interact with Cu_H. This could position the His172 proton toward the Cu_H-bound superoxide, proposed in the superoxide channeling mechanism, thus making His172 a candidate for proton donation.

5.4.3 Dependence of Methionine Coordination on pH and Peptidylgly Substrate Binding

The EXAFS spectra of both oxidized and reduced PHMcc at pH 5.5 detect the Cu-S(Met) bond. In the FT spectrum of the reduced enzyme, this sulfur shell is well resolved. These observations suggest that the Cu-S(Met) bond is stronger at pH 5.5 than at pH 7.5. At neutral pH, we suggested that the Cu-S(Met) bond was weak and long because it was undetectable by EXAFS [Blackburn et al., 2000]. Lowering the pH creates an interaction between copper and methionine in oxidized PHMcc, as indicated by the detection of the S(Met) bond at 2.52 Å in the EXAFS. However, the high (0.031) DW term for Cu-S suggests that this bond remains weak at pH 5.5. This is the first time EXAFS spectroscopy has detected an interaction between Cu_M and Met314 in the oxidized enzyme. Stabilization of Met314 appears to be linked to the low pH, suggesting that the protonation of a PHM residue organizes the Cu-S(Met) bond in the oxidized form. This fixing of the Met-off position may be important to the activity of PHM at low pH.

Large changes in the environmental pH have little effect on the active site structure in PHMcc. More importantly, the significant structural changes associated with redox activity of the metal sites observed in the EXAFS at pH 7.5 remain unchanged. Although X-ray crystallography does not detect these redox-induced structural changes, it is still apparent from the EXAFS spectra that these changes exist. The large reorganization of ligands during copper redox favors a mechanism of electron transfer similar to our superoxide channeling mechanism [Jaron and Blackburn, 1999].

CHAPTER 6

FUTURE DIRECTIONS

In this dissertation, we have provided evidence that the reaction mechanism of peptidylglycine α -hydroxylating monooxygenase (PHM) may occur through the shuttling of a superoxide molecule. A simple through-bond electron transfer appears unlikely due to the distance constraints and the oxygen reactivity of each copper. Transfer via a superoxide molecule is a viable alternative. There is no known monooxygenase, that transfers electrons via a superoxide channeling mechanism. However, it is known that superoxide can travel within an enzyme without being deleterious. Consider superoxide dismutase (SOD). Superoxide is a very powerful oxidant and is believed to be a factor in the formation of cancer [Totter, 1980]. SOD is responsible for the dismutation of superoxide into harmless products. In SOD, superoxide travels down a 14 Å active site channel where it docks at the copper atom responsible for its reduction to H_2O_2 and O_2 . Local positive charges along the channel guide superoxide to the copper [Getzoff et al., 1983]. Superoxide binds to the copper and H-bonds to Arg141, with a Cu-O distance of 2 Å and an O...Arg of 3 Å [Tainer et al., 1983]. The interaction between amino acid residues in the channel and the active site with the superoxide molecule demonstrates that superoxide channeling can occur. Whether this is, in fact, the mechanism occurring in PHM remains to be determined.

6.1 DIOXYGEN BINDING AT Cu_H

Our work has clearly identified open binding sites on both Cu(I) atoms in the active site of PHM. These sites are active toward the binding of CO. However, whether this translates into an O_2 binding site remains uncertain. Further insight can

be obtained through resonance Raman spectroscopy. Raman spectroscopy is able to detect the symmetric stretch of O-O, making it ideal for detecting dioxygen binding sites. A normal Raman spectrum, however, is usually very weak. Resonance enhancement of the vibrations produces a spectrum with sufficient intensity to be of use. This is accomplished by exciting with light that matches the absorption energy of a chromophore (charge transfer of $\pi\pi^*$ transitions) in the molecule. A peroxo-to-Cu(II) charge transfer band in PHM needs to be identified to take advantage of this technique.

6.2 SUPEROXIDE CHANNELING

Further evidence for superoxide channeling is necessary. This can be done using a number of methods: (1) inhibition by SOD; (2) addition of superoxide; (3) spin trapping of superoxide; (4) freeze trapping a Cu_H -superoxide intermediate.

6.2.1 Inhibition by Superoxide Dismutase

The reaction might be inhibited by the addition of SOD, indicating that the production of superoxide is an intermediate in the reaction. SOD is expected to scavenge any superoxide leaking out of the active site pocket. This assumes that the active site is leaky, however. In fact, we would expect the channeling of superoxide to be tightly controlled so that very little is lost. Experiments using the half-apo derivative of PHM suggested that other species, such as copper, might transfer between sites without being lost to bulk solvent. However, SOD efficiently attracts superoxide toward its active site and therefore may still inhibit PHM [Sines et al., 1990].

6.2.2 Addition of Superoxide

Enzyme turnover might be initiated by the addition of exogenous superoxide. Two methods for generating small quantities of superoxide for biochemical use are the xanthine oxidase-xanthine reaction or pulse radiolysis [Ingraham and Meyer, 1985]. The superoxide is expected to interact with $\text{Cu}_M(\text{I})$ to form the $\text{Cu}_M(\text{II})\text{-O-O-H}$

species. To be successful, this experiment must be carried out using the half-apo PHM derivative with only Cu_M present. Cu_H , in either the 1+ or 2+ form, could easily react with superoxide, forming either peroxide or $\text{Cu(I)} + \text{O}_2$ (as in a dismutase reaction), respectively. The dismutase reaction would then produce the necessary factors (O_2 and $\text{Cu}_H(\text{I})$) for a normal PHM turnover.

6.2.3 Spin Trapping Superoxide

It may be possible to spin trap superoxide using an EPR probe. Again, this requires that superoxide diffuse out of the active site pocket, which may not occur for the reasons describe above. Preliminary experiments using DEPMPO (5-diethoxyphosphoryl-5-methyl-1-pyrroline-n-oxide) have generated only negative results. In these experiments, the concentration of superoxide may have been too low to provide a detectable signal; therefore, these experiments should be repeated.

6.2.4 Freeze Trapping a Cu_H -Superoxide Intermediate

A $\text{Cu}_H(\text{I})\text{-O}_2$ or $\text{Cu}_H(\text{II})\text{-O}_2^{\cdot -}$ intermediate might be trapped using rapid freeze quench resonance Raman. This is a similar experiment to that described above for detecting O_2 binding sites.

6.3 IDENTIFYING RESIDUES INVOLVED IN SUPEROXIDE CHANNELING

The channeling of superoxide in the PHM active site requires the presence of a proton donor and/or residue(s) that assist in the channeling. We have already identified some candidate residues near the Cu_H site: Tyr79, Tyr318, and His172. Characterization of individual site-directed mutants should isolate the residue(s) involved in superoxide transfer. The H172A mutant has already been characterized, the results of which suggested this residue is ideally positioned to play the role of proton donor [Chapter 4]. However, the residues in the active site, which guide the translocation of superoxide, will need to be identified.

6.4 NMR SOLUTION STRUCTURES

Finally, we have suggested herein that there may be a second binding site for the peptidylgly substrate that is not seen by X-ray crystallography. The stretching frequency of the $\text{Cu}_H\text{-CO}$ was dependent on the identity of the peptide substrate [Chapter 2]. This indicated that peptide binding might occur in the vicinity of Cu_H . The crystallization process may generate a PHM-substrate complex that is structurally stable but inactive. The clear alternative is to determine the solution structure via NMR spectroscopy. Three species are of interest: (1) oxidized + substrate, (2) reduced + substrate, and (3) reduced + substrate + CO. The discovery of a second binding site will strengthen the proposed superoxide channeling mechanism. However, if the solution structure does not reveal a second peptide binding site, we will need to explore the question of how and why substrate binding activates ligand binding at a distant copper site.

The mechanism of electron transfer in the mononuclear copper monooxygenases is still unknown. However, we have proposed a reasonable, albeit unique, mechanism for the transfer in PHM. The unusual method involving superoxide transfer has, perhaps, invited scientists to think about electron transfer by methods other than the traditional through-bond or through-space mechanisms.

LITERATURE CITED

- Abudu, N., Banjaw, M. Y., and Ljones, T. (1998) Kinetic studies on the activation of dopamine β -monooxygenase by copper and vanadium ions. *Eur. J. Biochem.* **257**, 622-629.
- Acher, R. and Chauvet, J. (1953) La structure de la vasopressine de boeuf. *Biochim. Biophys. Acta* **12**, 487-488.
- Ahn, N., and Klinman, J. P. (1983) Mechanism of modulation of dopamine β -monooxygenase by pH and fumarate as deduced from initial rate and primary deuterium isotope effect studies. *Biochemistry* **22**, 3096-3106.
- Alben, J. O., Moh, P. P., Fiamingo, F. G., and Altschuld, R. A. (1981) Cytochrome oxidase (a_3) heme and copper observed by low-temperature Fourier transform infrared spectroscopy of the CO complex. *Proc. Natl. Acad. Sci. U.S.A.* **78**, 234-237.
- Ash, D. E., Papadopoulos, N. J., Colombo, G., and Villafranca, J. J. (1984) Kinetic and spectroscopic studies of the interaction of copper with dopamine β -hydroxylase. *J. Biol. Chem.* **259**, 3395-3398.
- Balogh-Hergovich, E., Speier, G., and Argay, G. (1991) The oxygenation of flavonol by copper(I) and copper (II) flavonolate complexes. The crystal and molecular structure of bis(flavonolato)copper(II). *J. Chem. Soc., Chem. Commun.* (8), 551-552.
- Beaudry, G. A., and Bertelsen, A. H. (1989) Secreted alpha amidating enzymes are generated by specific posttranslational processing of precursors containing transmembrane domains. *Biochem. Biophys. Res. Commun.* **163**, 959-966.
- Bell, J., Ash, D. E., Snyder, L. M., Kulathila, R., Blackburn, N. J., and Merkle, D. J. (1997) Structural and functional investigations on the role of zinc in bifunctional rat peptidylglycine α -amidating enzyme. *Biochemistry* **36**, 16239-16246.
- Beltramini, M., Ricchelli, F., Piazzesi, A., Barel, A., and Salvato, B. (1984) Removal of copper from *Octopus vulgaris* haemocyanin. Preparation of the half-apo and apo derivatives. *Biochem. J.* **221**, 911-914.
- Binsted, N., Gurman, S. J., and Campbell, J. W. (1988) Daresbury Laboratory EXCURV88 Program.

- Blackburn, N. J., Mason, H. S., and Knowles, P. F. (1980) Dopamine- β -hydroxylase: evidence for binuclear copper sites. *Biochem. Biophys. Res. Commun.* **95**, 1275-1281.
- Blackburn, N. J., Collison, D., Sutton, J., and Mabbs, F. E. (1984) Kinetic and e.p.r. studies of cyanide and azide binding to the copper sites of dopamine (3,4-dihydroxyphenethylamine) β -mono-oxygenase. *Biochem. J.* **220**, 447-454.
- Blackburn, N. J., Concannon, M., Shahiyan, S. K., Mabbs, F. E., and Collison, D. (1988) Active site of dopamine β -hydroxylase. Comparison of enzyme derivatives containing four and eight copper atoms per tetramer using potentiometry and EPR spectroscopy. *Biochemistry* **27**, 6001-6008.
- Blackburn, N. J., Strange, R. W., Reedijk, J., Volbeda, A., Farooq, A., Karlin, K. D., and Zubieta, J. (1989) X-ray absorption edge spectroscopy of copper(I) complexes. Coordination geometry of copper(I) in the reduced forms of copper proteins and their derivatives with carbon monoxide. *Inorg. Chem.* **28**, 1349-1357.
- Blackburn, N. J., Pettingill, T. M., Seagraves, K. S., and Shigeta, R. T. (1990) Characterization of a carbon monoxide complex of reduced dopamine β -hydroxylase. Evidence for inequivalence of the Cu(I) centers. *J. Biol. Chem.* **265**, 15383-15386.
- Blackburn, N. J., Hasnain, S. S., Pettingill, T. M., and Strange, R. W. (1991) Copper K-extended X-ray absorption fine structure studies of oxidized and reduced dopamine β -hydroxylase. Confirmation of a sulfur ligand to copper(I) in the reduced enzyme. *J. Biol. Chem.* **266**, 23120-23127.
- Blackburn, N. J., Barr, M. E., Woodruff, W. H., van der Oost, J., and de Vries, S. (1994) Metal-metal bonding in biology: EXAFS evidence for a 2.5 Å copper-copper bond in the CuA center of cytochrome oxidase. *Biochemistry* **33**, 10401-10407.
- Blackburn, N. J., Rhames, F. C., Ralle, M., and Jaron, S. (2000) Major changes in copper coordination accompany reduction of peptidylglycine monooxygenase: implications for electron transfer and the catalytic mechanism. *J. Biol. Inorg. Chem.* **5**, 341-353.
- Boswell, J. S., Reedy, B. J., Kulathila, R., Merkler, D., and Blackburn, N. J. (1996) Structural investigations on the coordination environment of the active-site copper centers of recombinant bifunctional peptidylglycine α -amidating enzyme. *Biochemistry* **35**, 12241-12250.
- Braas, K. M., Stoffers, D. A., Eipper, B. A., and May, V. (1989) Tissue specific expression of rat peptidylglycine α -amidating monooxygenase activity and mRNA. *Mol. Endocrinol.* **3**, 1387-1398.

- Bradbury, A. F., and Smyth, D. G. (1983) Substrate specificity of an amidating enzyme in porcine pituitary. *Biochem. Biophys. Res. Commun.* **112**, 372–377.
- Bradbury, A. F., and Smyth, D. G. (1987) Enzyme-catalysed peptide amidation. Isolation of a stable intermediate formed by reaction of the amidating enzyme with an imino acid. *Eur. J. Biochem.* **169**, 579–584.
- Bradbury, A. F., Finnie, M. D. A., and Smyth, D. G. (1982) Mechanism of C-terminal amide formation by pituitary enzymes. *Nature* **298**, 686–688.
- Brenner, M. C., and Klinman, J. P. (1989) Correlation of copper valency with product formation in single turnovers of dopamine β -monooxygenase. *Biochemistry* **28**, 4664–4670.
- Brenner, M. C., Murray, C. J., and Klinman, J. P. (1989) Rapid freeze- and chemical-quench studies of dopamine β -monooxygenase: comparison of pre-steady-state and steady-state parameters. *Biochemistry* **28**, 4656–4664.
- Bunker, G. (1997) *XAFS Tutorial Documents*. Revised: June 25, 1994. Illinois Institute of Technology. Available: <http://gbxafs.iit.edu/training/tutorials.html> [Viewed: January 8, 2000].
- Campbell, I. D., and Dwek, R. A. (1984) *Biological Spectroscopy*. Benjamin/Cummings Publishing Company, Menlo Park, CA.
- Christian, G. D., and Feldman, F. J. (1979) *Atomic Absorption Spectroscopy: Applications in Agriculture, Biology, and Medicine*. Robert E. Krieger Publishing Company, Huntington, NY.
- Clark, K., Penner-Hahn, J. E., Whittaker, M. M., Whittaker, J. W. (1990) Oxidation-state assignments for galactose oxidase complexes from X-ray absorption spectroscopy. Evidence for Cu(II) in the active enzyme. *J. Am. Chem. Soc.* **112**, 6433–6434.
- Clark, K., Penner-Hahn, J. E., Whittaker, M., and Whittaker, J. W. (1994) Structural characterization of the copper site in galactose oxidase using X-ray absorption spectroscopy. *Biochemistry* **33**, 12553–12557.
- Cuff, M. E., Miller, K. I., van Holde, K. E., and Hendrickson, W. A. (1998) Crystal structure of a functional unit from *Octopus* hemocyanin. *J. Mol. Biol.* **278**, 855–870.
- Decatur, S. M., DePillis, G. D., and Boxer, S. G. (1996) Modulation of protein function by exogenous ligands in protein cavities: CO binding to a myoglobin cavity mutant containing unnatural proximal ligands. *Biochemistry* **35**, 3925–3932.

du Vigneaud, V., Ressler, C., and Trippet, S. (1953) The sequence of amino acids in oxytocin, with a proposal for the structure of oxytocin. *J. Biol. Chem.* **205**, 949–957.

Dunn, B. C., Ochrymowycz, L. A., and Rorabacher, D. B. (1995) Electron-transfer kinetics of the copper(II/I) complex with 1,4,8,11-tetrathiacyclotetradecane in acetonitrile. *Inorg. Chem.* **34**, 1954–1956.

Dunn, B. C., Ochrymowycz, L. A., and Rorabacher, D. B. (1997a) Effect of conformational constraints on gated electron transfer kinetics. 2. Copper(II/I) complexes with phenyl-substituted [14]aneS₄ ligands in acetonitrile. *Inorg. Chem.* **36**, 3253–3257.

Dunn, B. C., Wijetunge, P., Vyvyan, J. R., Howard, T. A., Grall, A. J., Ochrymowycz, L. A., and Rorabacher, D. B. (1997b) Electron-transfer kinetics and thermodynamic characterization of copper(II/I) complexes with acyclic tetrathiaethers in aqueous solution. *Inorg. Chem.* **36**, 4484–4489.

Dyer, R. B., Einarsdóttir, Ó., Killough, P. M., López-Garriga, J. J., and Woodruff, W. H. (1989) Transient binding of photodissociated CO to Cu_B⁺ of eukaryotic cytochrome oxidase at ambient temperature. Direct evidence from time-resolved infrared spectroscopy. *J. Am. Chem. Soc.* **111**, 7657–7659.

Ebsworth, E. A. V., Rankin, D. W. H., and Cradock, S. (1991) Vibrational spectroscopy. In *Structural Methods in Inorganic Chemistry*, 2nd Ed., CRC Press, Boca Raton, FL, pp. 173–254.

Eickman, N. C., Himmelwright, R. S., and Solomon, E. I. (1979) Geometric and electronic structure of oxyhemocyanin: spectral and chemical correlations to met apo, half met, met, and dimer active sites. *Proc. Natl. Acad. Sci. U.S.A.* **76**, 2094–2098.

Eipper, B. A., and Mains, R. E. (1988) Peptide α -amidation. *Annu. Rev. Physiol.* **50**, 333–344.

Eipper, B. A., and Mains, R. E. (1991) The role of ascorbate in the biosynthesis of neuroendocrine peptides. *Am. J. Clin. Nutr.* **54**, 1153S–1156S.

Eipper, B. A., Mains, R. E. and Glembotski, C. C. (1983) Identification in pituitary tissue of a peptide α -amidation activity that acts on glycine-extended peptides and requires molecular oxygen, copper, and ascorbic acid. *Proc. Natl. Acad. Sci. U.S.A.* **80**, 5144–5148.

Eipper, B. A., Perkins, S. N., Husten, E. J., Johnson, R. C., Keutmann, H. T., and Mains, R. E. (1991) Peptidyl- α -hydroxyglycine α -amidating lyase. Purification, characterization, and expression. *J. Biol. Chem.* **266**, 7827–7833.

- Eipper, B. A., Stoffers, D. A., and Mains, R. E. (1992) The biosynthesis of neuropeptides: peptide α -amidation. *Annu. Rev. Neurosci.* **15**, 57–85.
- Eipper, B. A., Quon, A. S. W., Mains, R. E., Boswell, J. S., and Blackburn, N. J. (1995) The catalytic core of peptidylglycine α -hydroxylating monooxygenase: investigation by site-directed mutagenesis, Cu X-ray absorption spectroscopy, and electron paramagnetic resonance. *Biochemistry* **34**, 2857–2865.
- Eisses, J. F., Stasser, J. P., Ralle, M., Kaplan, J. H., and Blackburn, N. J. (2000) Domains I and III of the human copper chaperone for superoxide dismutase interact via a cysteine-bridged dicopper(I) cluster. *Biochemistry* **39**, 7337–7342.
- Emeson, R. B. (1984) Hypothalamic peptidyl-glycine α -amidating monooxygenase: preliminary characterization. *J. Neurosci.* **4**, 2604–2613.
- Fager, L. Y., and Alben, J. O. (1972) Structure of the carbon monoxide binding site of hemocyanins studied by Fourier transform infrared spectroscopy. *Biochemistry* **11**, 4786–4792.
- Fitzpatrick, P. F., Flory, D. R., Jr., and Villafranca, J. J. (1985) 3-Phenylpropenes as mechanism-based inhibitors of dopamine β -hydroxylase: evidence for a radical mechanism. *Biochemistry* **24**, 2108–2114.
- Francisco, W. A., Merkler, D. J., Blackburn, N. J., and Klinman, J. P. (1998) Kinetic mechanism and intrinsic isotope effects for the peptidylglycine α -amidating enzyme reaction. *Biochemistry* **37**, 8244–8252.
- Freedman, T. B., Loehr, J. S., and Loehr, T. M. (1976) A resonance Raman study of the copper protein, hemocyanin. New evidence for the structure of the oxygen-binding site. *J. Am. Chem. Soc.* **98**, 2809–2815.
- Freeman, J. C., Villafranca, J. J., and Merkler, D. J. (1993) Redox cycling of enzyme-bound copper during peptide amidation. *J. Am. Chem. Soc.* **115**, 4923–4924.
- Gans, P. (1980) Vibrational spectroscopy. In *An Introduction to Spectroscopy for Biochemists* (Brown, S. B., Ed.), Academic Press, New York, pp. 115–147.
- George, G. N. (1990) EXAFSPAK. Stanford Synchrotron Radiation Laboratory, Stanford Linear Accelerator Center. Revised: April 20, 2001. Available: <http://ssrl.slac.stanford.edu/exafspak.html> [Viewed: October 23, 2000].
- Getzoff, E. D., Tainer, J. A., Weiner, P. K., Kollman, P. A., Richardson, J. S., and Richardson, D. C. (1983) Electrostatic recognition between superoxide and copper, zinc superoxide dismutase. *Nature* **306**, 287–290.

- Gilligan, J. P., Lovato, S. J., Mehta, N. M., Bertelsen, A. H., Jeng, A. Y., and Tamburini, P. P. (1989) Multiple forms of peptidyl α -amidating enzyme: purification from rat medullary thyroid carcinoma CA-77 cell-conditioned medium. *Endocrinology* **124**, 2729–2736.
- Gray, H. B., and Winkler, J. R. (1996) Electron transfer in proteins. *Annu. Rev. Biochem.* **65**, 537–561.
- Gurman, S. J. (1989) Structural information in extended X-ray absorption fine structure (EXAFS). In *Synchrotron Radiation and Biophysics* (Hasnain, S. S., Ed.), Ellis Horwood Limited, Chichester, pp. 9–42.
- Gurman, S. J., Binsted, N. and Ross, I. (1984) A rapid, exact curved-wave theory for EXAFS calculations. *J. Phys. C: Solid State Phys.* **17**, 143–151.
- Gurman, S. J., Binsted, N., and Ross, I. (1986) A rapid, exact, curved-wave theory for EXAFS calculations. II. The multiple-scattering contributions. *J. Phys. C: Solid State Phys.* **19**, 1845–1861.
- Guss, J. M., Harrowell, P. R., Murata, M., Norris, V. A., and Freeman, H. C. (1986) Crystal structure analyses of reduced (Cu^{I}) poplar plastocyanin at six pH values. *J. Mol. Biol.* **192**, 361–387.
- Hauser, F., Williamson, M., and Grimmelikhuijzen, C. J. (1997) Molecular cloning of a peptidylglycine α -hydroxylating monooxygenase from sea anemones. *Biochem. Biophys. Res. Commun.* **241**, 509–512.
- Hazes, B., Magnus, K. A., Bonaventura, C., Bonaventura, J., Dauter, Z., Kalk, K. H., and Hol, W. G. (1993) Crystal structure of deoxygenated *Limulus polyphemus* subunit II hemocyanin at 2.18 Å resolution: clues for a mechanism for allosteric regulation. *Protein Sci.* **2**, 597–619.
- Hirota, S., Iwamoto, T., Tanizawa, K., Adachi, O., and Yamauchi, O. (1999) Spectroscopic characterization of carbon monoxide complexes generated for copper/topa quinone-containing amine oxidases. *Biochemistry* **38**, 14256–14263.
- Holm, R. H., Kennepohl, P., and Solomon, E. I. (1996) Structural and functional aspects of metal sites in biology. *Chem. Rev.* **96**, 2239–2314.
- Hosler, J. P., Kim, Y., Shapleigh, J., Gennis, R., Alben, J., Ferguson-Miller, S., and Babcock, G. (1994) Vibrational characteristics of mutant and wild-type carbon monoxy cytochrome *c* oxidase: evidence for a linear arrangement of heme *a*, *a*₃, and Cu_B . *J. Am. Chem. Soc.* **116**, 5515–5516.

- Husten, E. J., and Eipper, B. A. (1991) The membrane-bound bifunctional peptidylglycine α -amidating monooxygenase protein. Exploration of its domain structure through limited proteolysis. *J. Biol. Chem.* **266**, 17004–17010.
- Husten, E. J., Tausk, F. A., Keutmann, H. T., and Eipper, B. A. (1993) Use of endoproteases to identify catalytic domains, linker regions, and functional interactions in soluble peptidylglycine α -amidating monooxygenase. *J. Biol. Chem.* **268**, 9709–9717.
- Ingraham, L. L., and Meyer, D. L. (1985) *Biochemistry of Dioxygen*. Plenum Publishing Corporation, New York.
- Isied, S. S., Ogawa, M. Y., and Wishart, J. F. (1992) Peptide-mediated intramolecular electron transfer: long-range distance dependence. *Chem. Rev.* **92**, 381–394.
- Jacobson, R. R., Tyeklár, Z., Farooq, A., Karlin, K. D., Liu, S., and Zubieta, J. (1988) A $\text{Cu}_2\text{-O}_2$ complex. Crystal structure and characterization of a reversible dioxygen binding system. *J. Am. Chem. Soc.* **110**, 3690–3692.
- Jameson, R. F. (1981) Coordination chemistry of copper with regard to biological systems. In *Properties of Copper* (Sigel, H., (Ed.), Marcel Dekker, New York, pp. 1–30.
- Jaron, S., and Blackburn, N. J. (1999) Does superoxide channel between the copper centers in peptidylglycine monooxygenase? A new mechanism based on carbon monoxide reactivity. *Biochemistry* **38**, 15086–15096.
- Jaron, S., and Blackburn, N. J. (2001) Characterization of a half-apo derivative of peptidylglycine monooxygenase. Insight into the reactivity of each active site copper. *Biochemistry* **40**, 6867–6875.
- Karlin, K. D., Cruse, R. W., Gultneh, Y., Farooq, A., Hayes, J. C., and Zubieta, J. (1987) Dioxygen–copper reactivity. Reversible binding of O_2 and CO to a phenoxo-bridged dicopper(I) complex. *J. Am. Chem. Soc.* **109**, 2668–2679.
- Karlin, K. D., Tyeklár, Z., and Zuberbühler, A. D. (1993) Formation, structure, and reactivity of copper dioxygen complexes. In *Bioinorganic Catalysis* (Reedijk, J., Ed.), Marcel Dekker, New York, pp. 261–315.
- Kato, I., Yonekura, H., Tajima, M., Yanagi, M., Yamamoto, H., and Okamoto, H. (1990) Two enzymes concerned in peptide hormone α -amidation are synthesized from a single mRNA. *Biochem. Biophys. Res. Commun.* **172**, 197–203.

Katopodis, A. G., Ping, D. and May, S. W. (1990) A novel enzyme from bovine neurointermediate pituitary catalyzes dealkylation of α -hydroxyglycine derivatives, thereby functioning sequentially with peptidylglycine α -amidating monooxygenase in peptide amidation. *Biochemistry* **29**, 6115–6120.

Kau, L.-S., Spira-Solomon, D. J., Penner-Hahn, J. E., Hodgson, K. O., and Solomon, E. I. (1987) X-ray absorption edge determination of the oxidation state and coordination number of copper: application to the type 3 site in *Rhus vernicifera* laccase and its reaction with oxygen. *J. Am. Chem. Soc.* **109**, 6433–6442.

Kennedy, J. H. (1990) Spectrochemical methods. In *Analytical Chemistry: Principles*, 2nd Ed. (Kennedy, J. H., Ed.), Saunders College Publishing, New York, pp. 388–495.

Kitajima, N., Fujisawa, K., Moro-oka, Y., and Toriumi, K. (1989) μ - η^2 : η^2 -Peroxo binuclear copper complex, $[\text{Cu}(\text{HB}(3,5\text{-iPr}_2\text{pz})_3)]_2(\text{O}_2)$. *J. Am. Chem. Soc.* **111**, 8975–8976.

Kizer, J. S., Bateman, R. C., Jr., Miller, C. R., Humm, J., Busby, W. H., Jr., and Youngblood, W. W. (1986) Purification and characterization of a peptidyl glycine monooxygenase from porcine pituitary. *Endocrinology* **118**, 2262–2267.

Klabunde, T., Eicken, C., Sacchettini, J. C., and Krebs, B. (1998) Crystal structure of a plant catechol oxidase containing a dicopper center. *Nat. Struct. Biol.* **5**, 1084–1090.

Klinman, J. P. (1996) Mechanisms whereby mononuclear copper proteins functionalize organic substrates. *Chem. Rev.* **96**, 2541–2561.

Kolhekar, A. S., Keutmann, H. T., Mains, R. E., Quon, A. S. W., and Eipper, B. A. (1997a) Peptidylglycine α -hydroxylating monooxygenase: active site residues, disulfide linkages, and a two-domain model of the catalytic core. *Biochemistry* **36**, 10901–10909.

Kolhekar, A. S., Roberts, M. S., Jiang, N., Johnson, R. C., Mains, R. E., Eipper, B. A., and Taghert, P. H. (1997b). Neuropeptide amidation in *Drosophila*: separate genes encode the two enzymes catalyzing amidation. *J. Neurosci.* **17**, 1363–1376.

Kulathila, R., Consalvo, A. P., Fitzpatrick, P. F., Freeman, J. C., Snyder, L. M., Villafranca, J. J., and Merkler, D. J. (1994) Bifunctional peptidylglycine α -amidating enzyme requires two copper atoms for maximum activity. *Arch. Biochem. Biophys.* **311**, 191–195.

- Landymore-Lim, A. E. N., Bradbury, A. F., and Smyth, D. G. (1983) The amidating enzyme in pituitary will accept a peptide with C-terminal D-alanine as substrate. *Biochem. Biophys. Res. Commun.* **117**, 289-293.
- Lee, P. A. (1981) Theory of extended X-Ray absorption fine structure. In *EXAFS Spectroscopy. Techniques and Applications* (Teo, B. K., and Joy, D. C., Eds.), Plenum Press, New York, pp. 5-12.
- Longa, S. D., Ascone, I., Bianconi, A., Bonfigli, A., Castellano, A. C., Zarivi, O., and Miranda, M. (1996) The dinuclear copper site structure of *Agaricus bisporus* tyrosinase in solution probed by X-ray absorption spectroscopy. *J. Biol. Chem.* **271**, 21025-21030.
- Mackin, R. B., Flacker, J. M., Mackin, J. A., and Noe, B. D. (1987) Peptidyl-glycine α -amidating monooxygenase is present in islet secretory granules of the anglerfish, *Lophius americanus*. *Gen. Comp. Endocrinol.* **67**, 263-269.
- Magnus, K. A., Hazes, B., Ton-That, H., Bonaventura, C., Bonaventura, J., and Hol, W. G. (1994) Crystallographic analysis of oxygenated and deoxygenated states of arthropod hemocyanin shows unusual differences. *Proteins* **19**, 302-309.
- Marcus, R., and Sutin, N. (1985) Electron transfers in chemistry and biology. *Biochim. Biophys. Acta* **811**, 265-322.
- Merkler, D. J. (1994) C-terminal amidated peptides: production by the *in vitro* enzymatic amidation of glycine-extended peptides and the importance of the amide to bioactivity. *Enzyme Microb. Technol.* **16**, 450-456.
- Merkler, D. J., and Young, S. D. (1991) Recombinant type A rat 75-kDa α -amidating enzyme catalyzes the conversion of glycine-extended peptides to peptide amides via an α -hydroxyglycine intermediate. *Arch. Biochem. Biophys.* **289**, 192-196.
- Merkler, D. J., Kulathila, R., Consalvo, A. P., Young, S. D., and Ash, D. E. (1992) ^{18}O isotopic ^{13}C NMR shift as proof that bifunctional peptidylglycine α -amidating enzyme is a monooxygenase. *Biochemistry* **31**, 7282-7288.
- Merkler, D. J., Kulathila, R., Young, S. D., Freeman, J., and Villafranca, J. J. (1993) The enzymology of peptide amidation. In *Bioinorganic Chemistry of Copper* (Karlin, K. D., and Tyeklár, Z., Eds.), Chapman and Hall, New York, pp. 196-209.
- Miller, D. A., Sayad, K. U., Kulathila, R., Beaudry, G. A., Merkler, D. J., and Bertelsen, A. H. (1992) Characterization of a bifunctional peptidylglycine α -amidating enzyme expressed in Chinese hamster ovary cells. *Arch. Biochem. Biophys.* **298**, 380-388.

- Miller, S. M., and Klinman, J. P. (1985) Secondary isotope effects and structure-reactivity correlations in the dopamine β -monooxygenase reaction: evidence for a chemical mechanism. *Biochemistry* **24**, 2114–2127.
- Morley, J. S. (1968) Structure-function relationships in gastrin-like peptides. *Proc. R. Soc. Lond. B Biol. Sci.* **170**, 97–111.
- Nakamoto, K. (1986) *Infrared and Raman Spectra of Inorganic and Coordination Compounds*, 4th Ed., John Wiley & Sons, New York.
- Noguchi, M., Seino, H., Kochi, H., Okamoto, H., Tanaka, T., and Hiramata, M. (1992) The source of the oxygen atom in the α -hydroxyglycine intermediate of the peptidylglycine α -amidating reaction. *Biochem. J.* **283**, 883–888.
- Obata, A., Tanaka, H., and Kawazura, H. (1987) Magnetic resonance studies on the copper site of dopamine β -monooxygenase in the presence of cyanide and azide anions. *Biochemistry* **26**, 4962–4968.
- Pasquali, M., and Floriani, C. (1983) Copper(I)-carbon monoxide chemistry: recent advances and perspectives. In *Copper Coordination Chemistry: Biochemical and Inorganic Perspectives* (Karlin, K. D., and Zubieta, J., Eds.), Adenine Press, Guilderland, NY, pp. 311–330.
- Patch, M. G., Choi, H.-k., Chapman, D. R., Bau, R., McKee, V., and Reed, C. A. (1990) Copper(I) hemocyanin models: variable coordination number and distorted geometries in benzimidazole chelates. *Inorg. Chem.* **29**, 110–119.
- Pate, J. E., Cruse, R. W., Karlin, K. D., and Solomon, E. I. (1987) Vibrational, electronic, and resonance Raman spectral studies of $[\text{Cu}_2(\text{XYL}-\text{O}-\text{O})_2]^+$, a copper(II) peroxide model complex of oxyhemocyanin. *J. Am. Chem. Soc.* **109**, 2624–2630.
- Perkins, S. N., Husten, E. J., and Eipper, B. A. (1990) The 108-kDa peptidylglycine α -amidating monooxygenase precursor contains two separable enzymatic activities involved in peptide amidation. *Biochem. Biophys. Res. Commun.* **171**, 926–932.
- Pettingill, T. M., Strange, R. W., and Blackburn, N. J. (1991) Carbonmonoxy dopamine β -hydroxylase. Structural characterization by Fourier transform infrared, fluorescence, and \AA -ray absorption spectroscopy. *J. Biol. Chem.* **266**, 16996–17003.
- Ping, D., Katopodis, A. G., and May, S. W. (1992) Tandem stereochemistry of peptidylglycine α -monooxygenase and peptidylamidoglycolate lyase, the two enzymes involved in peptide amidation. *J. Am. Chem. Soc.* **114**, 3998–4000.

- Pratt, G. E., Farnsworth, D. E., Siegel, N. R., Fok, K. F., and Feyereisen, R. (1989) Identification of an allatostatin from adult *Diploptera punctata*. *Biochem. Biophys. Res. Commun.* **163**, 1243–1247.
- Prigge, S. T., Kolhekar, A. S., Eipper, B. A., Mains, R. E., and Amzel, L. M. (1997) Amidation of bioactive peptides: the structure of peptidylglycine α -hydroxylating monooxygenase. *Science* **278**, 1300–1305.
- Prigge, S. T., Kolhekar, A. S., Eipper, B. A., Mains, R. E., and Amzel, L. M. (1999) Substrate-mediated electron transfer in peptidylglycine α -hydroxylating monooxygenase. *Nat. Struct. Biol.* **6**, 976–983.
- Prigge, S. T., Mains, R. E., Eipper, B. A., and Amzel, L. M. (2000) New insights into copper monooxygenases and peptide amidation: structure, mechanism and function. *Cell. Mol. Life Sci.* **57**, 1236–1259.
- Puustinen, A., Bailey, J. A., Dyer, R. B., Mecklenburg, S. L., Wikstrom, M., and Woodruff, W. H. (1997) Fourier transform infrared evidence for connectivity between CuB and glutamic acid 286 in cytochrome *bo*₃ from *Escherichia coli*. *Biochemistry* **36**, 13195–13200.
- Ramer, S. E., Cheng, H., Palcic, M. M., and Vederas, J. C. (1988) Formation of peptide amides by peptidylglycine α -amidating monooxygenase: a new assay and stereochemistry of hydrogen loss. *J. Am. Chem. Soc.* **110**, 8526–8532.
- Reedy, B. J., and Blackburn, N. J. (1994) Preparation and characterization of half-apo dopamine- β -hydroxylase by selective removal of CuA. Identification of a sulfur ligand at the dioxygen binding site by EXAFS and FTIR spectroscopy. *J. Am. Chem. Soc.* **116**, 1924–1931.
- Rittel, W., Maier, R., Brugger, M., Kamber, B., Riniker, B., and Sieber, P. (1976) Structure-activity relationship of human calcitonin. III. Biological activity of synthetic analogues with shortened or terminally modified peptide chains. *Experientia* **32**, 246–248.
- Rosenzweig, A. C., Nordlund, P., Takahara, P. M., Frederick, C. A., and Lippard, S. J. (1995) Geometry of the soluble methane monooxygenase catalytic diiron center in two oxidation states. *Chem. Biol.* **2**, 409–418.
- Ross, P. K., and Solomon, E. I. (1991) An electronic structural comparison of copper-peroxide complexes of relevance to hemocyanin and tyrosinase active sites. *J. Am. Chem. Soc.* **113**, 3246–3259.

- Sanyal, I., Karlin, K. D., Strange, R. W., and Blackburn, N. J. (1993) Chemistry and structural studies on the dioxygen-binding copper-1,2-dimethylimidazole system. *J. Am. Chem. Soc.* **115**, 11259–11270.
- Sharp, K. A. (1998) Calculation of electron transfer reorganization energies using the finite difference Poisson-Boltzmann model. *Biophys. J.* **74**, 1241–1250.
- Sines, J. J., Allison, S. A., and McCammon, J. A. (1990) Point charge distributions and electrostatic steering in enzyme/substrate encounter: Brownian dynamics of modified copper/zinc superoxide dismutases. *Biochemistry* **29**, 9403–9412.
- Sisley, M. J., and Jordan, R. B. (1992) Kinetics of the reaction of copper(II) with cobalt(II) sepulchrate: catalysis by chloride ion and imidazole. *Inorg. Chem.* **31**, 2880–2884.
- Solomon, E. I., Hemming, B. L., and Root, D. E. (1993) Electronic structures of active sites in copper proteins: coupled binuclear and trinuclear cluster sites. In *Bioinorganic Chemistry of Copper* (Karlin, K. D. and Tyeklár, Z., Eds.), Chapman & Hall, New York, pp. 3–20.
- Solomon, E. I., Sundaram, U. M., and Machonkin, T. E. (1996) Multicopper oxidases and oxygenases. *Chem. Rev.* **96**, 2563–2605.
- Sorrell, T. N., and Borovik, A. S. (1987) Synthesis, structure, and spectroscopic properties of an unusual copper(I) dimer having imidazole ligands. A model for the carbonyl derivative of hemocyanin and implications for the structure of deoxyhemocyanin. *J. Am. Chem. Soc.* **109**, 4255–4260.
- Sorrell, T. N., and Jameson, D. L. (1983) Synthesis, structure, and reactivity of monomeric two-coordinate copper(I) complexes. *J. Am. Chem. Soc.* **105**, 6013–6018.
- Sorrell, T. N., and Malachowski, M. R. (1983) Mononuclear three-coordinate copper(I) complexes: synthesis, structure, and reaction with carbon monoxide. *Inorg. Chem.* **22**, 1883–1887.
- Southan, C., and Kruse, L. I. (1989) Sequence similarity between dopamine β -hydroxylase and peptide α -amidating enzyme: evidence for a conserved catalytic domain. *FEBS Lett.* **255**, 116–120.
- Stern, E. A. (1988) Theory of EXAFS. In *X-Ray Absorption: Principles, Applications, Techniques of EXAFS, SEXAFS, and XANES* (Koningsberger, D. C., and Prins, R., Eds.), John Wiley & Sons, New York, pp. 3–52.

- Stewart, L. C., and Klinman, J. P. (1987) Characterization of alternate reductant binding and electron transfer in the dopamine β -monooxygenase reaction. *Biochemistry* **26**, 5302-5209.
- Stewart, L. C., and Klinman, J. P. (1988) Dopamine β -hydroxylase of adrenal chromaffin granules: structure and function. *Annu. Rev. Biochem.* **57**, 551-592.
- Stoffers, D. A., Green, C. B.-R., and Eipper, B. A. (1989) Alternative mRNA splicing generates multiple forms of peptidyl-glycine α -amidating monooxygenase in rat atrium. *Proc. Natl. Acad. Sci. U.S.A.* **86**, 735-739.
- Stoffers, D. A., Ouafik, L., and Eipper, B. A. (1991) Characterization of novel mRNAs encoding enzymes involved in peptide α -amidation. *J. Biol. Chem.* **266**, 1701-1707.
- Strange, R. W., Blackburn, N. J., Knowles, P. F., and Hasnain, S. S. (1987) X-ray absorption spectroscopy of metal-histidine coordination in metalloproteins. Exact simulation of the EXAFS of tetrakis(imidazole)copper(II) nitrate and other copper-imidazole complexes by the use of a multiple-scattering treatment. *J. Am. Chem. Soc.* **109**, 7157-7162.
- Stryer, L. (1995) *Biochemistry*, 4th Ed., W. H. Freeman and Company, New York.
- Tainer, J. A., Getzoff, E. D., Richardson, J. S., and Richardson, D. C. (1983) Structure and mechanism of copper, zinc superoxide dismutase. *Nature* **306**, 284-287.
- Tajima, M., Iida, T., Yoshida, S., Komatsu, K., Namba, R., Yanagi, M., Noguchi, M., and Okamoto, H. (1990) The reaction product of peptidylglycine α -amidating enzyme is a hydroxyl derivative at α -carbon of the carboxyl-terminal glycine. *J. Biol. Chem.* **265**, 9602-9605.
- Takahashi, K., Okamoto, H., Seino, H., and Noguchi, M. (1990) Peptidylglycine α -amidating reaction: evidence for a two-step mechanism involving a stable intermediate at neutral pH. *Biochem. Biophys. Res. Commun.* **169**, 524-530.
- Tamburini, P. P., Jones, B. N., Consalvo, A. P., Young, S. D., Lovato, S. J., Gilligan, J. P., Wennogle, L. P., Erion, M., and Jeng, A. Y. (1988) Structure-activity relationships for glycine-extended peptides and the α -amidating enzyme derived from medullary thyroid CA-77 cells. *Arch. Biochem. Biophys.* **267**, 623-631.
- Tamburini, P. P., Young, S. D., Jones, B. N., Palmesino, R. A., and Consalvo, A. P. (1990) Peptide substrate specificity of the α -amidating enzyme isolated from rat medullary thyroid CA-77 cells. *Int. J. Pept. Protein Res.* **35**, 153-156.

Tian, G., Berry, J. A., and Klinman, J. P. (1994) Oxygen-18 kinetic isotope effects in the dopamine β -monooxygenase reaction: evidence for a new chemical mechanism in non-heme metallomonooxygenases. *Biochemistry* **33**, 226–234.

Totter, J. R. (1980) Spontaneous cancer and its possible relationship to oxygen metabolism. *Proc. Natl. Acad. Sci. U.S.A.* **77**, 1763–1767.

Tyeklár, Z., and Karlin, K. D. (1993) Functional models for hemocyanin and copper monooxygenases. In *Bioinorganic Chemistry of Copper* (Karlin, K. D. and Tyeklár, Z., Eds.), Chapman & Hall, New York, pp. 277–291.

Vale, W., Spiess, J., Rivier, C., and Rivier, J. (1981) Characterization of a 41-residue ovine hypothalamic peptide that stimulates secretion of corticotropin and β -endorphin. *Science* **213**, 1394–1397.

van Gastel, M., Coremans, J. W. A., Mol, J., Jeuken, L. J. C., Canters, G. W., and Groenen, E. J. J. (1999) The binding of imidazole in an azurin-like blue-copper site. *J. Biol. Inorg. Chem.* **4**, 257–265.

van Gastel, M., Bubacco, L., Groenen, E. J., Vijgenboom, E., and Canters, G. W. (2000) EPR study of the dinuclear active copper site of tyrosinase from *Streptomyces antibioticus*. *FEBS Lett.* **474**, 228–232.

Villacorta, G. M., and Lippard, S. J. (1987) Dicopper(I) carbonyl tropocoronands. Preparation, structural characteristics, and reactivity of neutral binuclear Cu–CO macrocyclic compounds. *Inorg. Chem.* **26**, 3672–3676.

Volbeda, A., and Hol, W. G. (1989) Crystal structure of hexameric haemocyanin from *Panulirus interruptus* refined at 3.2 Å resolution. *J. Mol. Biol.* **209**, 249–279.

Walker, G. A., Kon, H., and Lovenberg, W. (1977) An investigation of the copper site(s) of dopamine- β -hydroxylase by electron paramagnetic resonance. *Biochim. Biophys. Acta* **482**, 309–322.

Wand, G. S., Ney, R. L., Baylin, S., Eipper, B., and Mains, R. E. (1985a) Characterization of a peptide α -amidation activity in human plasma and tissues. *Metabolism* **34**, 1044–1052.

Wand, G. S., Ney, R. L., Mains, R. E., and Eipper, B. A. (1985b) Characterization of peptide α -amidation activity in human cerebrospinal fluid and central nervous system tissue. *Neuroendocrinology* **41**, 482–489.

Williams, R. J. P. (1990) Overview of biological electron transfer. In *Electron Transfer in Biology and the Solid State: Inorganic Compounds with Unusual*

Properties (Johnson, M. K., King, R. B., Kurtz, J. D. M., Kutal, C., Norton, M. L. and Scott, R. A., Eds.), American Chemical Society, Washington, DC, pp. 1-23.

Wimalasena, K., and May, S. W. (1987) Mechanistic studies on dopamine β -monooxygenase catalysis: N-dealkylation and mechanism-based inhibition by benzylic-nitrogen-containing compounds. Evidence for a single-electron-transfer mechanism. *J. Am. Chem. Soc.* **109**, 4036-4046.

Winkler, J. R., and Gray, H. B. (1992) Electron transfer in ruthenium-modified proteins. *Chem. Rev.* **92**, 369-379.

Woolery, G. L., Powers, L., Winkler, M., Solomon, E. I., Lerch, K., and Spiro, T. G. (1984) Extended X-ray absorption fine structure study of the coupled binuclear copper active site of tyrosinase from *Neurospora crassa*. *Biochim. Biophys. Acta* **788**, 155-161.

Xie, B., Elder, T., Wilson, L. J., and Stanbury, D. M. (1999) Internal reorganization energies for copper redox couples: the slow electron-transfer reactions of the $[\text{Cu}^{\text{III}}(\text{bib})_2]^{2+/+}$ couple. *Inorg. Chem.* **38**, 12-19.

Yonekura, H., Anzai, T., Kato, I., Furuya, Y., Shizuta, S., Takasawa, S., and Okamoto, H. (1996) Identification of the five essential histidine residues for peptidylglycine monooxygenase. *Biochem. Biophys. Res. Commun.* **218**, 495-499.

Young, S. D., and Tamburini, P. P. (1989) Enzymatic peptidyl α -amidation proceeds through formation of an α -hydroxyglycine intermediate. *J. Am. Chem. Soc.* **111**, 1933-1934.

Zabriskie, T. M., Cheng, H., and Vederas, J. C. (1991) Incorporation of aerobic oxygen into the hydroxyglycyl intermediate during formation of C-terminal peptide amides by peptidylglycine α -amidating monooxygenase (PAM). *J. Chem. Soc., Chem. Commun.* 571-572.

Zolla, L., Calabrese, L., and Brunori, M. (1984) Distribution of copper atoms and binding of carbon monoxide in partially copper-depleted hemocyanin. *Biochim. Biophys. Acta* **788**, 206-213.

Zuberbuhler, A. D. (1983) Copper(I), dioxygen, and catalysis. In *Copper Coordination Chemistry: Biochemical and Inorganic Perspectives* (Karlin, K. D., and Zubieta, J., Eds.). Adenine Press, New York, pp. 237-258.

BIOGRAPHICAL SKETCH

Shulamit Jaron was born in Detroit, Michigan, on November 16, 1971. She attended South Kingstown High School in South Kingstown, Rhode Island, from 1985 to 1989, graduating with honors. She received a B.S. degree in Chemistry in 1994 from the University of Rhode Island. During her studies at U.R.I., Shula was recognized as the 1993 Analytical Chemist of the Year by the Department of Chemistry. After graduation, she worked for one year for Philip Environmental in Washougal, Washington, as an Environmental Specialist. She began her graduate studies in the Department of Biochemistry and Molecular Biology at the Oregon Graduate Institute of Science and Technology in the fall of 1995. During her graduate career, Shula participated in student government, and was elected Student Council President in the spring of 2000. In 1999, she was the recipient of the Student Achievement Award, awarded by the Oregon Graduate Institute for excellence in scholarship, leadership, and community service. She began her postdoctoral appointment in January 2001, in the laboratory of Dr. Dennis Winge at the University of Utah.

Publications:

Jaron, S., and Blackburn, N. J. (1999) Does superoxide channel between the copper centers in peptidylglycine monooxygenase? A new mechanism based on carbon monoxide reactivity. *Biochemistry* **38**, 15086-15096.

Blackburn, N. J., Rhames, F. C., Ralle, M., and Jaron, S. (2000) Major changes in copper coordination accompany reduction of peptidylglycine monooxygenase: implications for electron transfer and the catalytic mechanism. *J. Biol. Inorg. Chem.* **5**, 341-353.

Jaron, S., and Blackburn, N. J. (2001) Characterization of a half-apo derivative of peptidylglycine monooxygenase. Insight into the reactivity of each active site copper. *Biochemistry* **40**, 6867-6875.